Aus dem Institut für Prophylaxe und Epidemiologie der Kreislaufkrankheiten (IPEK) -
Institut der Ludwig-Maximilians-Universität München

Dissertation

zum Erwerb des Doctor of Philosophy (Ph.D.)

an der Medizinischen Fakultät der

Ludwig-Maximilians-Universität München

Role of peripheral CB1 cannabinoid receptors in atherosclerosis and metabolism

vorgelegt von:

Bingni Chen

aus:

Shenzhen

Jahr:

2024

Mit Genehmigung der Medizinischen Fakultät der
Ludwig-Maximilians-Universität München

Erstes Gutachten von:	Prof. Dr. Sabine Marten-Steffens
Zweites Gutachten von:	Prof. Dr. Stephan Herzig
Drittes Gutachten von:	Priv. Doz. Dr. Kristina Adorjan
Viertes Gutachtes:	Priv. Doz. Dr. Tobias Petzold

Dekan: **Prof. Dr. med. Thomas Gudermann**

Datum der Verteidigung:

07.05.2024

The results of this work were presented at the following conferences:

ORAL PRESENTATIONS

09/2021	**44th Annual ELC Scientific Meeting,** Tutzing, Germany
05/2022	**90th EAS Congress**, Milan, Italy
09/2022	**IRTG 1123 Annual Retreat,** Tutzing, Germany
04/2023	**CRC1123 Atherosclerosis Annual Retreat**, Grainau, Germany
06/2023	**IRTG1123 Annual Retreat**, Venice, Italy

POSTER PRESENTATIONS

10/2019	**IRTG1123 Annual Retreat**, Grainau, Germany
10/2021	**IRTG1123 Annual Retreat**, Venice, Italy
04/2022	**88th Annual DGK Meeting**, Mannheim, Germany
10/2022	**CRC1123 Atherosclerosis International Symposium**, Munich, Germany
04/2023	**89th Annual DGK Meeting**, Mannheim, Germany

List of Publications:

Yong Wang, Guo Li, Bingni Chen, George Shakir, Mario Volz, Emiel P.C. van der Vorst, Sanne L. Maas, Carolin Muley, Alexander Bartelt, Zhaolong Li, Nadja Sachs, Lars Maegdefessel, Maliheh Nazari Jahantigh, Michael Hristov, Michael Lacy, Beat Lutz, Christian Weber, Stephan Herzig, Raquel Guillamat Prats, Sabine Steffens

bioRxiv preprint doi: https://doi.org/10.1101/2023.04.06.535832

Bingni Chen, Aishvaryaa Prabhu, Guo Li, Anna Kaltenbach, Yong Wang, George Shakir, Lucia Natarelli, Yvonne Jansen, Remco Megens, Valentina Paloschi, Zhaolong Li, Nadja Sachs, Lars Maegdefessel, Michael Hristov, Xinyu Di, Mario van der Stelt, Alexander Faussner, Beat Lutz, Christian Weber, Stephan Herzig, Raquel Guillamat Prats and Sabine Steffens. Endothelial cannabinoid CB1 receptor deficiency reduces arterial inflammation and lipid uptake in response to atheroprone shear stress.

bioRxiv preprint doi: https://doi.org/10.1101/2024.05.15.594375

TABLE OF CONTENT

LIST OF FIGURES

LIST OF TABLES

ABBREVIATIONS

2-AG	2-arachidonoylglycerol
3-alpha-HSD	3-alpha-hydroxysteroid dehydrogenase
ABCA1	ATP-binding cassette transporter A1
ABCG1	ATP-binding cassette sub-family G member 1
ACK	Ammonium chloride potassium
AEA	Anandamide
AF	AlexaFluor
ALK1	Activin-like kinase 1
ANOVA	Analysis of variance
AP	Atheroprone
ApoE	Apolipoprotein E
AR	Atheroresistance
ATLO	Artery tertiary lymphoid organs
ATP	Adenosine triphosphate
AUC	Area under the curve
BAT	Brown adipose tissue
BMP4	Bone morphogenetic protein 4
BMPER	BMP binding endothelial regulator
BMX-Cre ERT2	Transgenic mice carrying the bone marrow x (Bmx) promoter to drive the expression of a tamoxifen-inducible Cre-oestrogen receptor (ERT2) fusion protein
BSA	Bovine serum albumin
cAMP	Cyclic adenosine monophosphate
Cav1	Caveolin 1
CB1	Cannabinoid receptor type 1
Ccr	C-C motif chemokine receptor
CD36	Cluster of differentiation 36
cDNA	Complementary DNA
CNS	Central nervous system
CVD	Cardiovascular disease
Cxcr	Chemokine receptor type
DAGL	Diacylglycerol lipase
DAMPs	Damage-associated molecular pattern molecules
ddH2O	Double distilled water
ddPCR	Droplet digital PCR

DEGs	Differentially expressed genes
DHR	Dihydrorhodamine 123
DIO	Diet-induced obesity model
DMSO	Dimethyl sulfoxide
DNA	Deoxyribonucleic acid
DNase	Deoxyribonuclease
DOCK4	Dedicator of cytokinesis protein 4
EC	Endothelial cell
ECM	Extracellular matrix
EDTA	Ethylenediaminetetraacetic acid
ELISA	Enzyme-linked immunosorbent assay
EndoMT	Endothelial-to-mesenchymal transition
eNOS	Endothelial nitric oxide synthase
EVB	Evans blue
FAAH	Fatty acid amide hydrolase
FACS	Fluorescence-activated cell sorting
FDR	False discovery rate
FISH	Fluorescence *in situ* hybridization
Fwd	Forward
GO	Gene ontology
GPCR	G-protein-coupled receptor
GPIHBP1	Glycosylphosphatidylinositol anchored high density lipoprotein binding protein 1
GSEA	Gene set enrichment analysis
h	Hour
H&E	Hematoxylin and eosin
HAoECs	Human aortic endothelial cells
HDL	High density lipoproteins
Hprt	Hypoxanthine-guanine phosphoribosyltransferase
HUVECs	Human umbilical vein endothelial cells
i.p.	Intraperitoneal
IBMX	3-Isobutyl-1-methylxanthine
ICAM1	Intercellular adhesion molecule 1
IgG	Immunoglobulin G
IL	Interleukin
JIR	Jackson Immuno Research

KLF	Kruppel-like factor
LDL	Low-density lipoprotein
LDLR	Low-density lipoprotein receptors
LPL	Lipoprotein Lipase
LSS	Laminar shear stress
MAGL	Monoacylglycerol lipase
MFI	Mean fluorescence intensity
min	Minute
MMP	Matrix metallopeptidase
mRNA	Messenger RNA
NF-κB	Nuclear factor kappa-light-chain-enhancer of activated B cells
OEA	Oleoylethanolamide
ORO	Oil Red O
OSS	Oscillatory shear stress
PAMPs	Pathogen-associated molecular patterns
PBS	Phosphate buffered saline 3
PCR	Polymerase chain reaction
PE	Phycoerythrin
PEA	Palmitoylethanolamide
PECAM	Platelet endothelial cell adhesion molecule
PerCP	Peridinin chlorophyll
PFA	Paraformaldehyde
PFKFB3	6-Phosphofructo-2-kinase/fructose-2,6-bisphosphatases
PKA	Protein kinase A
PPAR	Peroxisome proliferator-activated receptors
Prdm16	PR domain containing 16
qPCR	Quantitative PCR
RAC1	Ras-related C3 botulinum toxin substrate 1
Rev	Reverse
RM	Repeated measures
RNA	Ribonucleic acid
RNase	Ribonuclease
ROI	Region of interest
ROS	Reactive oxygen species
RT	Reverse transcription

RT	Room temperature
Sec	Second
SMAD	Suppressor of mothers against decapentaplegic
SR-A1	Macrophage scavenger receptor 1
SR-B1	Scavenger receptor class B type 1
TG	Triglyceride
TGFβ	Transforming growth factor- β
THC	Delta-9-tetrahydrocannabinol
THP-1	Human monocytic cell line
TIMP3	Tissue inhibitors of metalloproteinases 3
TLR	Toll-like receptor
TNFα	Tumor necrosis factor alpha
TRPV1	Transient receptor potential vanilloid 1
t-SNE	t-distributed stochastic neighbor embedding
UCP1	Uncoupling Protein 1
VCAM1	Vascular cell adhesion molecule 1
VE-cadherin	Vascular endothelial (VE)-cadherin
VEGF	Vascular endothelial growth factor
VLDL	Very low density lipopoteine
vWF	von Willebrand factor
WAT	White adipose tissue
WD	Western diet
WHO	World health organization
wks	weeks

1. SUMMARY

Atherosclerosis is a chronic immune disease fueled by a complex interplay of lipid, inflammatory, and biomechanical factors. Previous studies demonstrated that the cannabinoid CB1 receptor plays a detrimental role in metabolic and cardiovascular diseases. While the development of peripherally restricted CB1 antagonists, which are devoid of central side effects, hold promise in treating metabolic disorders such as diabetes and obesity, their potential benefit in atherosclerosis is unknown. The aim of this thesis was to clarify the endothelial cell-specific effects of CB1 and underlying mechanisms in the pathophysiology of atherosclerosis. It was found that endothelial *Cnr1* expression was upregulated upon oscillatory shear stress (OSS) in human aortic endothelial cells (HAoECs) and preferentially expressed in atheroprone areas of mouse aortic endothelium. Endothelial *Cnr1* deficiency (*Cnr1*$^{EC\text{-}KO}$) in female mice on atherogenic apolipoprotein E (*Apoe*) deficiency background reduced plaque formation, particularly in atheroprone sites. Only moderate effects were observed in male mice, which may hint to a sex-specific difference in endothelial CB1 signalling. Moreover, aortic endothelial cells of female *Cnr1*$^{EC\text{-}KO}$ mice exhibited a less pro-inflammatory phenotype with decreased adhesion molecule ICAM1 and VCAM1 expression. Interestingly, *ex vivo* imaging of carotid arteries via two-photon microscopy revealed less endothelial DIL-LDL uptake in female *Cnr1*$^{EC\text{-}KO}$ mice endothelial cells along with a significantly reduced aortic endothelial expression of caveolin-1 (CAV1), a key structural protein involved in lipid transcytosis. RNA sequencing of aortic endothelial cells further supported the role of CB1 in regulating caveolar signalling. *In vitro*, pharmacological blocking with CB1 antagonist AM281 in HAoECs under OSS resulted in a decreased LDL uptake, which was mediated through a cAMP-PKA-dependent regulation of CAV1 expression. *Vice versa*, the stimulation of HAoECs with the CB1 agonist ACEA increased DIL-LDL uptake and enhanced CAV1 expression. Notably, endothelial CB1 deficiency protected against metabolic dysfunction in adipose tissue and liver, while improving insulin sensitivity. Finally, treating mice with the peripherally active CB1 antagonist JD5037 reduced plaque progression, CAV1 expression, and endothelial adhesion molecule expression, which was only observed in females. Collectively, impaired CB1 signalling in endothelial cells inhibits endothelial LDL uptake, attenuates vascular inflammation, and improves metabolic function, leading to protection against atherosclerosis.

2. ZUSAMMENFASSUNG

Atherosklerose ist eine chronische Immunerkrankung, die durch ein komplexes Zusammenspiel von Lipid-, Entzündungs- und biomechanischen Faktoren verursacht wird. Frühere Studien haben gezeigt, dass der Cannabinoid-CB1-Rezeptor eine schädliche Rolle bei Stoffwechsel- und Herz-Kreislauf-Erkrankungen spielt. Während die Entwicklung selektiv peripher wirksamer CB1-Antagonisten, die keine zentralen Nebenwirkungen haben, bei der Behandlung von Stoffwechselstörungen wie Diabetes und Fettleibigkeit vielversprechend erscheint, ist ein potentieller therapeutischer Nutzen dieser peripher wirkenden Antagonisten in der Atherosklerose bislang unerforscht. Ziel dieser Arbeit war es, die endothelzellspezifische Rolle von CB1 und die zugrundeliegenden liegenden intrazellulären Mechanismen in der Pathophysiologie der Atherosklerose zu untersuchen. Die Ergebnisse zeigen, dass die endotheliale *Cnr1*-Expression durch oszillatorischen Scherstress (OSS) in menschlichen Aortenendothelzellen (HAoECs) hochreguliert und bevorzugt in Atherosklerose-anfälligen Bereichen der Mausaorta exprimiert ist. Ein endothelialer *Cnr1*-Knockout ($Cnr1^{EC\text{-}KO}$) bei weiblichen Mäusen mit atherogenem Apolipoprotein-E-Knockout (*Apoe*) Hintergrund führte zu reduzierter Plaquebildung. Bei männlichen Mäusen wurden nur geringe Effekte beobachtet, was auf einen geschlechtsspezifischen Unterschied in der endothelialen CB1-Signalisierung hinweisen könnte. Darüber hinaus zeigten die Endothelzellen weiblicher $Cnr1^{EC\text{-}KO}$-Mäuse einen weniger proinflammatorischen Phänotyp mit einer verringerten Expression der Adhäsionsmoleküle ICAM1 und VCAM1. Interessanterweise zeigte die Ex-vivo-Bildgebung von Halsschlagadern mittels Zwei-Photonen-Mikroskopie eine geringere endotheliale DIL-LDL-Aufnahme in Endothelzellen weiblicher $Cnr1^{EC\text{-}KO}$-Mäuse zusammen mit einer deutlich verringerten endothelialen Expression von Caveolin-1 (CAV1), einem Schlüsselstrukturprotein der Lipidtranszytose. Die RNA Sequenzierung von murinen Aortenendothelzellen bestätigte eine CB1-vermittelte Regulierung von Caveolae-abhängigen Signalwegen. *In vitro* führte die pharmakologische Blockierung mit dem CB1-Antagonisten AM281 in HAoECs unter OSS-Bedingungen zu einer Verringerung der LDL-Aufnahme und CAV1 Expression, was auf einen cAMP-PKA-abhängigen Signalweg zurückgeführt werden konnte. Umgekehrt führte die Stimulation von HAoECs mit dem CB1-Agonisten ACEA zu einer erhöhten Aufnahme von DIL-LDL mit verstärkter CAV1-Expression. Weiterhin führte der endotheliale CB1-Knockout zu einer verbesserten Stoffwechselfunktion sowohl im Fettgewebe als auch in der Leber, was mit verbesserter Insulinsensitivität einherging. Darüber hinaus reduzierte die Behandlung mit dem peripheren CB1-Antagonisten JD5037 die Zunahme der Plaquegröße sowie die Expression von CAV1 und der endothelialen Adhäsionsmoleküle. Der Effekt war wiederum nur bei weiblichen Mäusen zu beobachten. Daraus lässt sich schlussfolgern, dass die genetische Defizienz oder pharmakologische Inhibierung der CB1-Signalübertragung im Endothel die

LDL-Aufnahme hemmt und Gefäßentzündungen reduziert, was neben einer verbesserten Stoffwechselfunktion zum Schutz vor Atherosklerose führt.

3. INTRODUCTION

3.1 Cardiovascular diseases

Cardiovascular diseases (CVDs) are the leading cause of death worldwide, which still stands as the primary cause of mortality, accounting for 17.9 million lives lost each year.[1] Ischemic heart disease and stroke, complications of atherosclerosis, are the predominant drivers of mortality in CVD, encompassing 84.9% of all cardiovascular-related fatalities.[2] Numerous contributing factors, including a sedentary lifestyle, tobacco smoking, alcohol usage, high perceived stress level, physical inactivity, obesity and hypertension altogether, play a role in the rising prevalence of CVDs.[3] CVD risk factors may present as heightened blood pressure (hypertension), elevated blood glucose levels (diabetes mellitus), as well as conditions like overweight, increased cholesterol levels (dyslipidaemia) and obesity. Notably, inflammation has recently been acknowledged as a pivotal risk factor for CVD.[4] Conventional therapies targeting inflammation in CVD have displayed protective advantages in various models of cardiovascular disease.[5] Several inflammatory markers of vascular disease showed a positive correlation with endothelial dysfunction, highlighting its crucial role in CVD.[6] Traditional lipid-lowering medications, antihypertensive agents, antidiabetic drugs, as well as novel interventions like proprotein convertase subtilisin/kexin type 9 inhibitors and interleukin 1β monoclonal antibodies, collectively address endothelial dysfunction as part of their clinical advantages.[7]

3.2 Atherosclerosis

As one of the major causes of CVD, atherosclerosis is characterized by the buildup of plaque through an intricate interplay between lipids, immune cells, and the vascular endothelium within the inner layer of arteries. The initial records about human atherosclerosis pathology go back around 500 years. Atherosclerosis is composed of the words “athero” and “sclerosis”, which means gruel and hardening. This composite term signifies the lipid deposition process and blood vessel hardening.[8] It is generally believed that atherosclerosis is a chronic inflammatory process, and numerous risk factors contribute to this process during the progression of the disease. Conventional risk factors include the build-up of cholesterol due to the retention of low-density lipoprotein (LDL) within the arterial intima, which is subsequently taken up by immune cells infiltrating the atherosclerotic plaque. In addition to these traditional factors, non-traditional contributors such as environmental stress, alterations in the microbiome, air pollution, physical inactivity, and disrupted sleep have also received significant attention.[9] In the initial phases of atherosclerosis, dysfunctional endothelial cells (ECs) respond to abnormal lipid metabolism and hemodynamic damage by releasing pro-inflammatory signals. This triggers the adherence of blood monocytes to the vessel wall, which contributes

to foam cell formation and lesion progression.[10, 11] The unique environment of atherosclerosis, including hypoxia, inflammatory aggregation, and oxidative stress, triggers the production of pro-angiogenic factors. This, in turn, triggers the generation of fresh blood vessels within atherosclerotic plaques. The emergence of these new blood vessels enhances the supply of nutrients and facilitates the localized hypoxic environment, thereby fostering the continued advancement of the plaque. Advanced atherosclerosis is a complex process involving multiple contributors that lead to the formation of cholesterol crystals, fibrous caps, and necrotic cores, ultimately resulting in processes such as calcification, stenosis, surface erosion, and rupture (Figure 1). After an atherosclerotic plaque rupture, the prothrombotic plaque content is exposed, and it can trigger a series of reactions involving platelet receptors and coagulation factors. This results in the activation and clustering of platelets, eventually forming a superimposed thrombus - a condition commonly referred to as atherothrombosis.[8, 12] Vascular inflammation plays a crucial role during this process and can induce vascular hyperplasia independently of conventional cardiovascular risk factors, contributing to complications in advanced atherosclerosis.[13] Canakinumab, one of the anti-inflammatory therapies, specifically targeting the central pro-inflammatory mediator interleukin (IL)-1β that drives the interleukin-6 signalling pathway, has shown positive effects in reducing the recurrence of cardiovascular events, independent of lipid-lowering.[14, 15] However, it has encountered limitations due to the high cost, elevated infection risk, and the necessity for injection administration. Future research should help to gain a deeper understanding of the disease's mechanisms and develop safer, more affordable, and widely accessible therapies with low risk of side effects.

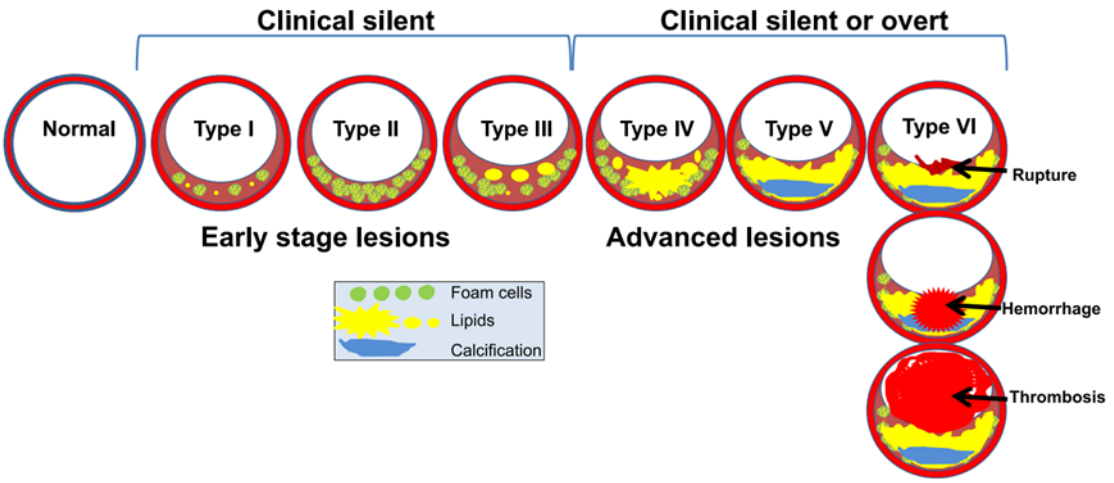

Figure 1.The risk factors for cardiovascular disease.
Schematic histological characteristics of human atherosclerosis are categorized based on the American Heart Association's classification. Adapted from Jianglin Fane *et al.*[8]

3.2.1 The immune system in atherosclerosis

In the past, atherosclerosis was thought to arise from the passive accumulation of lipids in the vessel wall. However, today's picture is far more complex, as numerous studies have illuminated the dynamic interplay of multiple factors, including inflammation, genetics, and lifestyle choices, contributing to atheroprogression. Cells from both the innate and adaptive immune systems play pivotal roles during this process.[10, 16-18] The immune cells secrete both pro-inflammatory and anti-inflammatory chemokines and cytokines while also coordinating interactions among different immune cells. This orchestration by the immune system profoundly influences the likelihood of plaque rupture, ultimately contributing to the clinical symptoms of myocardial infarction and stroke.

3.2.1.1 Pathophysiology of atherosclerosis

The initial step of atherosclerosis involves the activation and dysfunction of EC, resulting in leukocyte infiltration and lipid accumulation, especially low-density lipoprotein (LDL), beneath the endothelial layer. Within this subendothelial environment, lipids are susceptible to modification by oxidative radicals, including reactive oxygen species (ROS), thereby promoting the inflammatory cascade.[19] EC activation by pro-inflammatory stimuli induces the expression of pro-inflammatory adhesion molecules and chemokines (such as E-selectin, ICAM1, and VCAM1, CXCL8, CCL2),[20] which recruits leukocytes and activated platelets to adhere to the endothelium (Figure 2). These recruited immune cells release additional cytokines and chemokines (such as CXCL4 and CCL5),[21, 22] which further promotes a positive feedback loop that facilitates inflammation and lesion development. Within early atherosclerotic lesions, the initial cellular components comprise dendritic cells (DCs), monocytes, and T cells. After entering the artery wall, monocytes, the predominant white blood cells in plaques, undergo differentiation into tissue macrophages. These phagocytic cells subsequently initiate the process of engulfing (modified) lipids, transitioning into the distinctive “foam cell” phenotype.[23] T cells are then recruited alongside macrophages and play a role as atherogenic mediators. Although DCs are naturally present in healthy arteries, their active recruitment becomes a notable hallmark during the progression of atherosclerosis.[24]

Mechanistic studies are mostly carried out in two atherosclerotic mouse models: The *Apoe*$^{-/-}$ mice, which exhibit a spontaneous hyperlipidemic phenotype leading to atherosclerosis development without dietary intervention, whereas *Ldlr*$^{-/-}$ mice only develop atherosclerosis under high-fat diet conditions.[25] Modulating atherosclerotic plaque progression in mouse models is possible by manipulating their cholesterol and fat intake. Therefore, atherosclerotic plaque burden, immune system activation, and lipid levels also depend on the specific experimental conditions and chosen model. Additionally, given the heterogeneous nature of atherosclerotic development, data obtained from one region may not necessarily apply to other

regions of the artery.

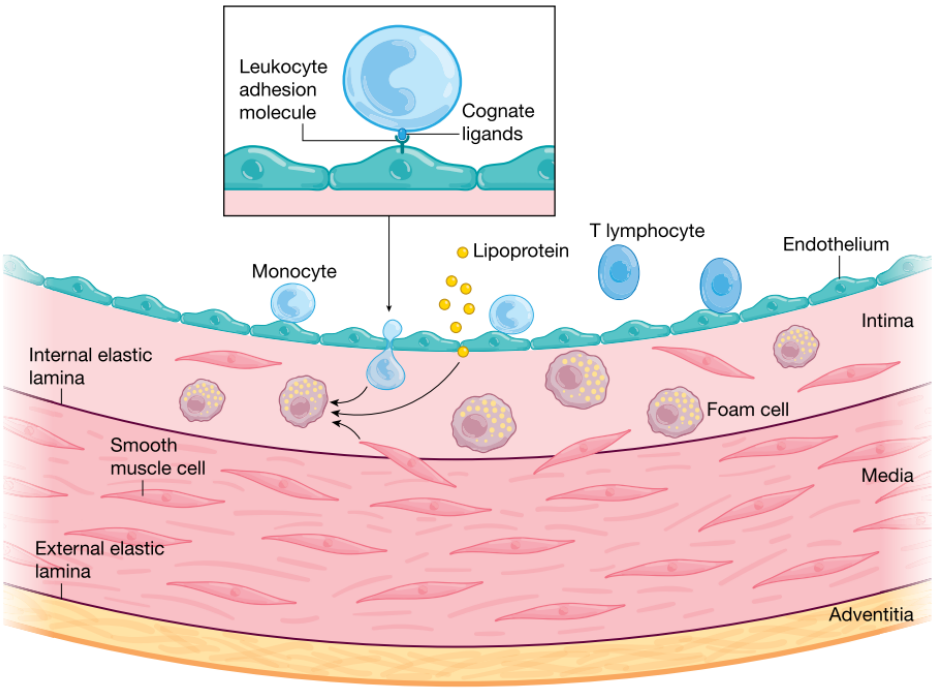

Figure 2. Initiation of atherosclerosis.
A typical artery consists of three layers: the innermost layer, called the intima, which directly interfaces with the bloodstream; the middle layer, known as the tunica media; and the outermost layer, referred to as adventitia. Under physiological conditions, the endothelial monolayer lining the intima maintains a non-attractive barrier for blood leukocytes. However, upon activation by proinflammatory cytokines or other cardiovascular risk factors, EC can trigger the expression of leukocyte adhesion molecules, such as VCAM1. These molecules interact with their corresponding ligands, like VLA4, facilitating the initial rolling and subsequent adherence of blood monocytes and lymphocytes to the endothelial layer. Within the intima, lipid-rich foam cells, derived from monocytes differentiating into macrophages, contribute to atherosclerosis. Adapted from Peter Libby *et al.*[9]

3.2.1.2 Immune cell interaction during atheroprogression

Atherosclerosis is a complex disease involving both innate and adaptive immune responses (Figure 3). In recent decades, advanced techniques such as flow cytometry, real-time fluorescence imaging, mass cytometry, and sequencing-based molecular profiling approaches have unveiled the intricate cellular compositions and their interaction within atherosclerotic plaques.[26-28] This extensive exploration not only sheds light on the dynamic landscape of immune cells but also emphasizes the significance of deciphering the underlying pathways that govern their behaviours. Understanding the underlying pathway of these immune cells and their regulation will be crucial for the development of clinical interventions for atherosclerosis, including pharmacological treatment and potentially vaccination-based therapeutic strategies.

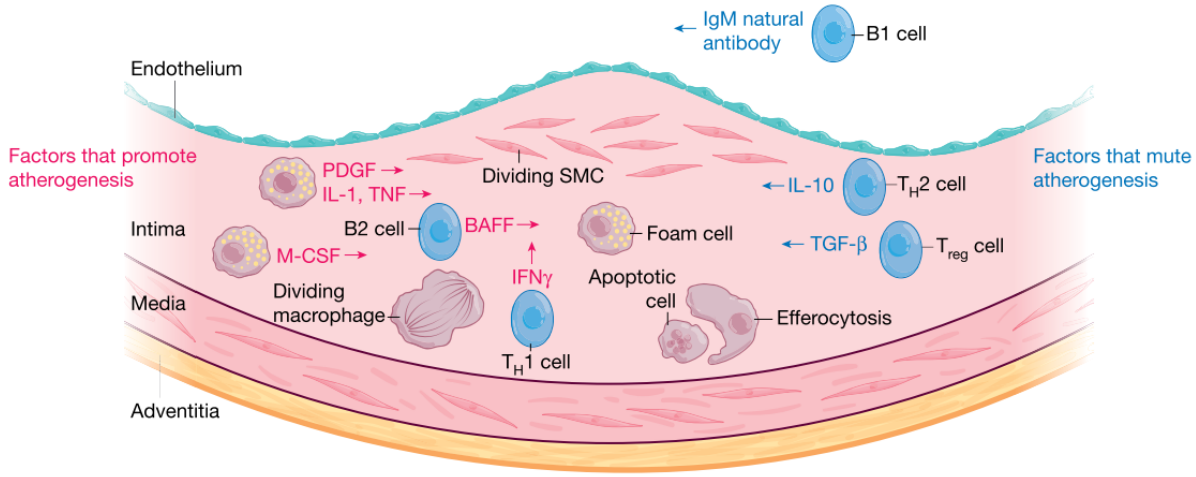

Figure 3. The interplay of inflammatory factors in atherosclerosis.
Pathways are believed to promote plaque formation (shown in red), and potential mechanisms dampening atherosclerosis (shown in blue). Several immune cells within the plaque can release cytokines, including IL-1, TNF, and M-CSF. Activated T-helper 1 (T_H1) lymphocytes release IFNγ, stimulating mononuclear phagocytes and worsen atherosclerosis. Other cell types produce opposing substances. B1 lymphocytes produce IgM natural antibodies, T-helper 2 (T_H2) lymphocytes release the anti-inflammatory cytokine IL-10, and regulatory T (Treg) cells secrete TGFβ, inhibiting inflammatory cell growth, promoting extracellular matrix synthesis, and reducing inflammation. Adapted from Peter Libby *et al.*[9]

Monocytes and macrophages: Monocytes, which are short-lived mononuclear phagocytes originating from myeloid cells, make up approximately 3-8% of the total leukocytes circulating in the bloodstream. Monocytes are typically infrequent in healthy arteries. However, hypercholesterolemia induces monocytosis by enhancing the proliferation of hematopoietic stem and progenitor cells.[29] In mice, researchers have identified two distinct monocyte subsets: the classical monocyte, which expresses $Ly6C^{high}CX3CR1^{low}CCR2^{+}$, and is recruited to atherosclerotic plaques, thereby playing a proatherogenic role. On the other hand, the nonclassical $Ly6C^{low}CX3CR1^{high}CCR2^{-}$ monocytes, devoid of CCR2 expression, patrol blood vessels and are considered to play an atheroprotective role in atherosclerosis.[30] [31] Still, recent high-dimensional mass cytometry data showed enrichment of nonclassical monocytes expressing the carbohydrate marker 6-sulfo LacNAc in the blood of patients with cardiovascular disease.[32] CCR2 and its primary ligand, CCL2, have been demonstrated to play a role in monocyte migration into the arterial wall.[33] Targeting CCR2 through antagonists has been shown to effectively reduce the number of circulating classical monocytes and reduce lesion size in murine models.[34] Although blocking CCR2 or its ligand in preclinical trials has shown successful improvements in atherosclerosis, the challenges remain due to the complex molecular structures of CCL2 and CCR2, along with issues related to their presumed binding interface and the effective delivery of drugs to the desired tissues.[35, 36]

In the intima, monocyte-derived macrophages possess phagocytic capabilities and additionally

serve as instructors for other immune cells, producing a range of immune effector molecules and serving as antigen-presenting cells (APCs).[37] They initiate the uptake and clearance of lipoproteins. When the rate of LDL uptake exceeds the efflux, or if efflux is impaired, lipids accumulate within these macrophages, turning macrophages into “foam cells”.[38] The primary uptake of LDL is through scavenger receptors like SRA and CD36, but a recent study indicated that the deficiency of SRA and CD36 does not completely abolish foam cell formation, suggesting that additional classes of scavenger receptors might be involved in this process.[39] While foam cells are traditionally considered contributors to atherosclerosis, certain subsets of foam cells have been associated with anti-inflammatory and tissue-repair functions.[40, 41] Identifying the precise role of aortic macrophage subsets in modulating atherosclerosis and their interaction with other immune cells will be crucial for understanding their relevance to atherosclerosis progression.

Neutrophils: Neutrophils, initial responders to microbial invasion or tissue damage, rapidly neutralize and remove pathogens by endocytosis of foreign materials and produce myeloperoxidase (MPO), ROS and proteolytic enzymes.[42] In humans, there exists a notable association between the quantity of intra-plaque neutrophils and the characteristics of unstable plaques, which often exhibit a larger lipid core, diminished presence of smooth muscle cells, and reduced collagen content.[43] In *Apoe*$^{-/-}$ mice, neutrophils actively interact with EC and contribute to inflammatory activity. During the early stages of atherosclerotic mouse plaques, neutrophils are primarily localized in the sub-endothelial space.[44] However, in more advanced and rupture-prone plaques, they are observed in diverse regions, including the shoulder area of the plaque, adventitia, and intra-plaque haemorrhage.

T and B cells in atherosclerosis: T cells were first identified within human plaques in 1985. They are recruited to the vessel wall along with macrophages, but in smaller amounts.[45] Inside the arterial wall, T cells undergo activation in response to antigens, triggering the production of pro-inflammatory mediators like IFNγ. These mediators subsequently amplify the inflammatory response, promoting the progression of the disease. Various subsets of T cells are involved in atherosclerosis at different stages, ranging from its initial plaque formation to advanced lesions.[46] Atherosclerotic mice exhibit the presence of CD4$^+$ T cells and, to a lesser extent, CD8$^+$ and γδ T cells within plaques. Results from knockout and depletion experiments in mice suggest a primarily pro-atherogenic role for CD4$^+$ T cells, particularly in the early phases of atherosclerotic disease progression.[47, 48] However, other studies indicated that an increased burden of atherosclerosis in *CD4*$^{-/-}$*Apoe*$^{-/-}$ female mice might be linked to the absence of CD4$^+$ Tregs and a compensatory rise in CD8$^+$ cells within this specific mouse model.[49] The role of CD8$^+$ T cells in atherogenesis remains a topic of ongoing debate.

B cells, originating from the bone marrow and characterized by the B cell receptor (BCR), play a pivotal role in humoral immune responses in atherosclerosis through the production of

antibodies essential for eliminating antigens.[50] Beyond their antibody-producing function, B cells exhibit antigen-presenting capabilities, engaging in both $CD4^+$ and $CD8^+$ T cell activation.[51] These multifaceted functions play a pivotal role in the regulation of chronic immune responses by facilitating the recruitment of leukocytes and influencing the polarization of T cells.[52] Mature B cells comprise two primary cellular subsets, named B1 and B2 cells, distinguished by their unique localization characteristics and activation prerequisites. B-1 cells are further categorized into B1a and B1b subsets, while B2 cells include both follicular B cells and marginal zone B cells.[53] Although the technical contamination of circulating B cells cannot be ruled out, recent data obtained by mass-cytometry analysis revealed a substantial portion of B cells in human carotid atherosclerotic plaques, highlighting the involvement of B cells in atherosclerosis.[53] Consistent with this, early experimental evidence presented by Caligiuri *et al.* showed exacerbated atherosclerosis in *Apoe*$^{-/-}$ mice upon spleen removal. However, when B cells were transferred to these mice after spleen removal, it alleviated the progression of the disease.[54] B1 cells exert an atheroprotective effect by secreting natural IgM, which diminishes oxidized low-density lipoprotein (OxLDL) uptake by macrophages within lesions.[55, 56] Lewis *et al.* observed that *Ldlr*$^{-/-}$ mice lacking IgM in their serum exhibited accelerated formation of atherosclerotic lesions, providing evidence for the atheroprotective role of IgM.[57] On the other hand, injecting a CD20-specific monoclonal antibody, which selectively targets B2 cells, reduced atherosclerosis in *Apoe*$^{-/-}$ or *Ldlr*$^{-/-}$ mice.[58, 59] Nonetheless, Meritxell Nus *et al.* reported that marginal zone B cells limit atherosclerosis in a $CD4^+$ T cell-dependent manner.[60] This suggests that therapeutic approaches directed at the entire B-2 cell compartment may not be optimal. Therefore, it is crucial to better understand the roles of B cell responses in order to design precise therapies for atherosclerosis.

3.2.2 Role of endothelial cells in atherosclerosis

Although the link between cardiovascular risk factors and atherosclerotic disease is well described, the precise mechanisms through which these risk factors trigger plaque development and result in atherosclerosis remain not fully elucidated. The vascular endothelium, which lines the cardiovascular system, is likely a critical factor in translating risk factors into adverse vascular changes due to its unique location and biological characteristics.[61] A healthy endothelium plays a significant role in maintaining vascular homeostasis by releasing various factors, such as nitric oxide (NO) and prostacyclin, to establish an anti-thrombotic environment.[62] However, the disruption of the balance between NO and ROS leads to a vicious pathogenic cycle causing oxidative damage and EC dysfunction.[19] This, in turn, can trigger chronic inflammation, adhesion of leukocytes and increased permeability in EC, contributing to atherosclerotic plaque formation.[7] While elevated oxidative stress is acknowledged as a primary mechanism in the development of EC

dysfunction, various other factors also contribute to this process.[63] The local factors, hemodynamic forces like shear stress, have also been acknowledged as important regulators of endothelial function, influencing local endothelial homeostasis.[64] Lipotoxicity, another factor of EC dysfunction, is triggered by overnutrition and metabolic disorder, leading to EC inflammation, enhanced endoplasmic reticulum stress, and mitochondrial dysfunction.[65] Given the variable endothelial susceptibility among individual patients, there are additional factors, including genetic predisposition, that need to be considered as driving or protective factors of endothelial dysfunction (Figure 4).[66]

Collectively, endothelial function status reflects overall cardiovascular risk. The dysfunction of EC is the leading risk factor for atherosclerosis, creating an atherogenic vascular environment.[67] Targeting endothelial dysfunction, which serves as the primary pathological event in atherosclerosis, is pivotal in preventing the onset of atherosclerotic cardiovascular diseases.

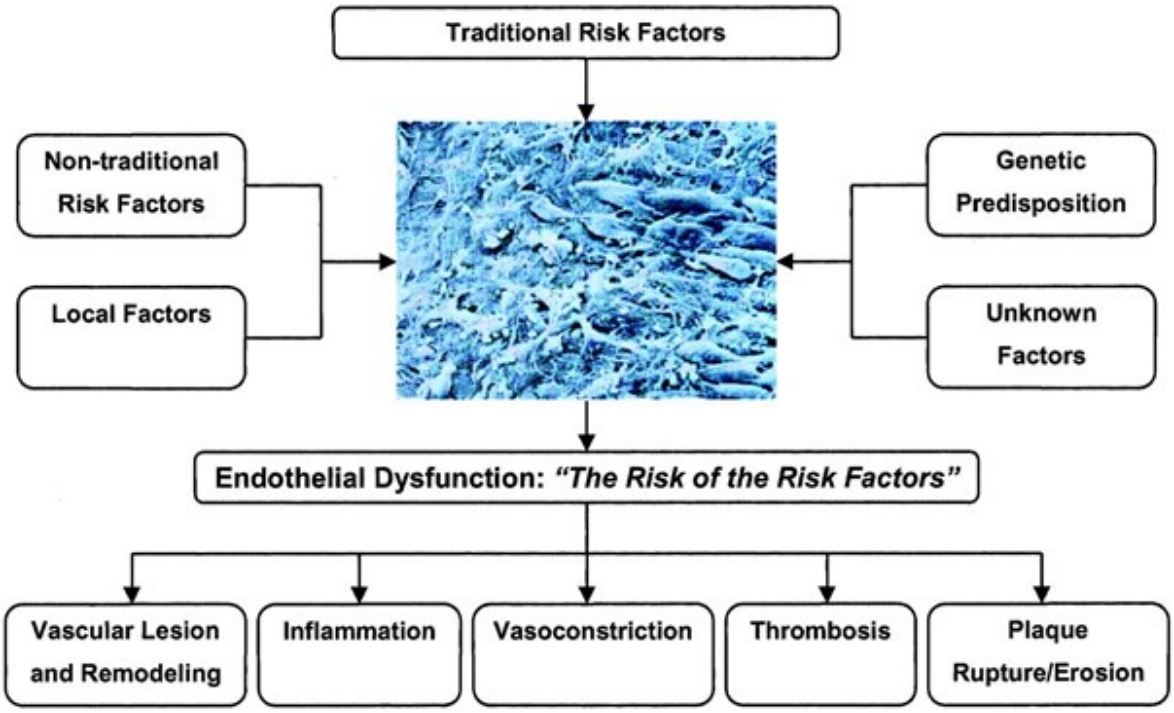

Figure 4. The risk factors of endothelial dysfunction.
Endothelial function is affected by a combination of traditional and non-traditional risk factors, including local factors like shear stress, genetic factors, and unidentified factors that could exert either protective or harmful effects. The endothelial dysfunction reflects the atherogenic environment within the blood vessels, initiating the cardiovascular events. Adapted from Piero O. Bonetti *et al.*[67]

3.2.2.1 Endothelial responses to shear stress in atherosclerosis

An intriguing aspect of atherosclerosis is that the susceptibility of plaque development varies within the same artery. Clinical studies demonstrated that plaques are often observed in disturbed flow regions within the thoracic aorta, coronary arteries, cerebral arteries, carotid arteries, and renal arteries, while the laminar flow regions in the internal thoracic artery, hepatic

arteries, and radial arteries generally remain unaffected by atherosclerosis in the same patient (Figure 5).[68] EC play a pivotal role as the blood flow sensor governing both physiological and pathophysiological reactions, yet the underling mechanisms how they decode shear stress landscapes remain not fully understood. Shear stress refers to the frictional force generated by the flow of liquids (such as blood, urine, and lymphatic fluid) on EC (including vascular EC, urinary tract epithelial cells, and lymphatic vessel EC, among others), and depends on the velocity within the blood boundary layer (Figure 6).[69]

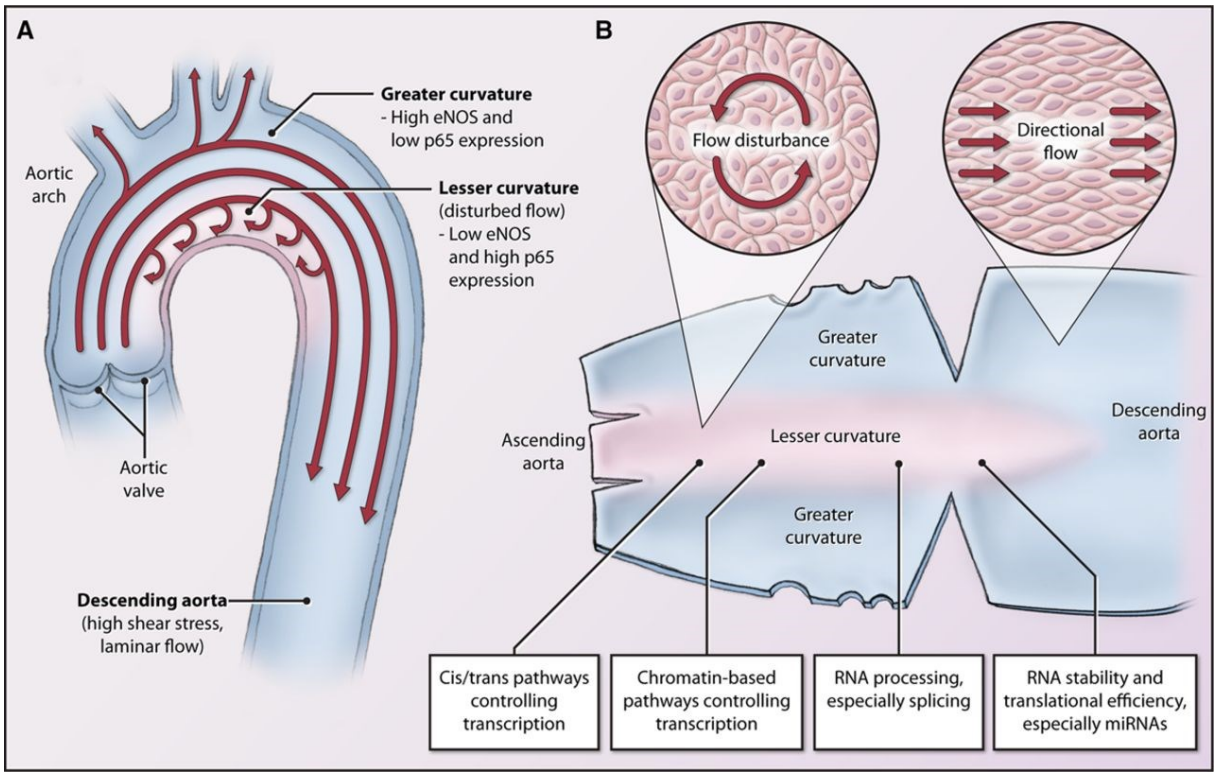

Figure 5. Impact of disturbed blood flow patterns on the gene expression of EC.
(**A**) In straight segments of arteries, like those in the descending aorta, blood flow maintains a consistent and smooth laminar pattern, subjecting EC to laminar shear stress (LSS). These regions are often referred to as atheroresistant sites. In contrast, disturbed laminar flow is observed at branch points and inner curvatures, exposing EC in these areas to oscillatory shear stress (OSS). These regions are often designated as atheroprone sites and are highly susceptible to plaque formation. (**B**) Several mechanisms have been identified to explain the influence of disturbed flow on endothelial gene expression, involving the regulation of transcription, mRNA processing and post-transcriptional processes. (Adapted from Myron I. Cybulsky *et al.*)[70]

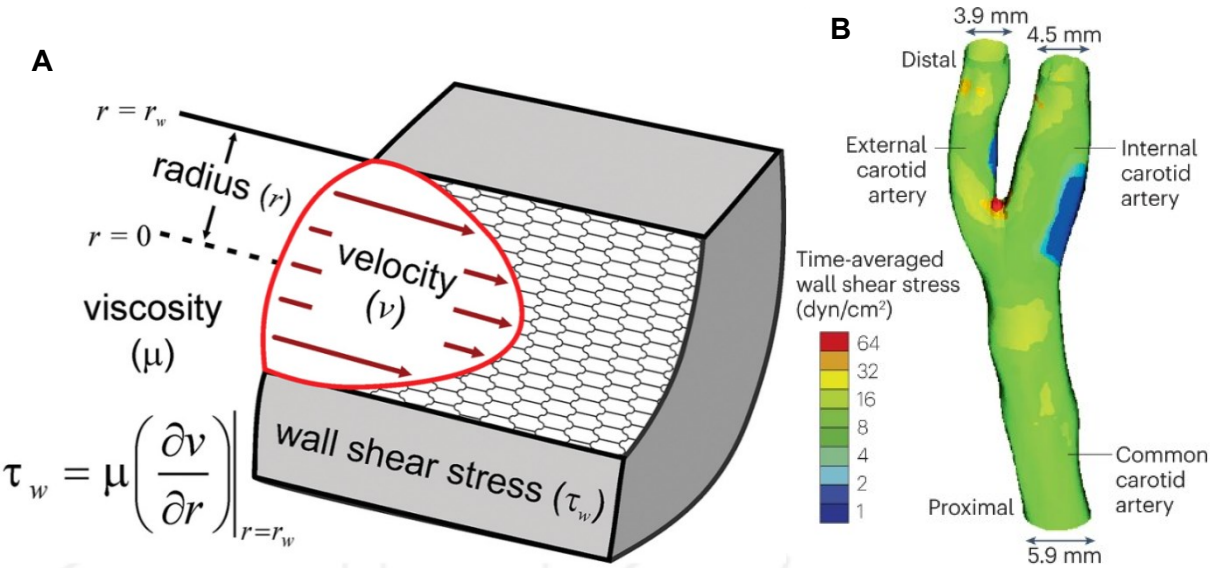

Figure 6. Impact of shear stress to arterial wall.
(**A**) Wall shear stress (WSS). The schematic depicts the influence of blood velocity and viscosity on shear stress by EC. (**B**) The time-averaged shear stress observed in the left carotid artery of a healthy human reveals that the site of the internal carotid is exposed to low and oscillating shear stress as a result of disturbed flow, rendering it highly susceptible to plaque formation. (Figure adapted from Margaret M. Samyn and Ian A. Tamargo *et al.*) [71, 72]

ECs perceive changes in fluid shear stress through mechanosensitive signalling molecules on their surface and convert them into biochemical signals, guiding endothelial cells to execute corresponding physiological functions. *In vitro* and *in vivo* studies using vascular endothelial cells under different flow conditions for RNA sequencing revealed transcriptomic changes involved in mechanosensitive signalling.[73-76] Most fluid shear-sensitive genes are protein-encoding genes, including atheroprotective factors *KLF2*,[77] *KLF4*,[78, 79] *TIMP3*,[80] and endothelial NO synthase (eNOS encoding gene *NOS3*),[81] which is upregulated by stable laminar shear stress (LSS). In contrast, oscillatory shear stress (OSS) upregulates the expression of many atherosclerosis-related genes, including *VCAM1*,[82] *MMP9*,[83] and *BMP4*,[84] which can induce adverse events in vascular endothelial cells such as inflammation, proliferation, and apoptosis.

Recent research revealed long noncoding RNA (LncRNA) could also respond to the blood flow and mediate the shear stress-associated gene.[85] The data indicated that the knockdown of a lncRNA AF131217.1, which is upregulated by LSS in HUVEC, prevented the flow-mediated reduction of monocyte adhesion, specifically VCAM1 and ICAM1; it also prevented the flow-mediated enhancement of flow-responsive expression of KLF2 and eNOS. Other investigations employing a carotid partial ligation model in mice (Figure 7) revealed altered gene expression patterns regulated by shear stress. These gene programs are associated with the control of cell morphology, proliferation, and inflammation. The mechanosensitive molecules encompass the transcription factor hypoxia-inducible factor 1α (HIF1α),

transforming growth factor-β (TGFβ), genes related to endothelial to-mesenchymal transition (EndMT) and its targets, vascular endothelial growth factor (VEGF) and glycolysis- related genes *PFKFB3*.[86, 87] Omics studies in EC consistently revealed a strong connection between adult arteries blood flow patterns and genes related to angiogenesis and embryonic development.

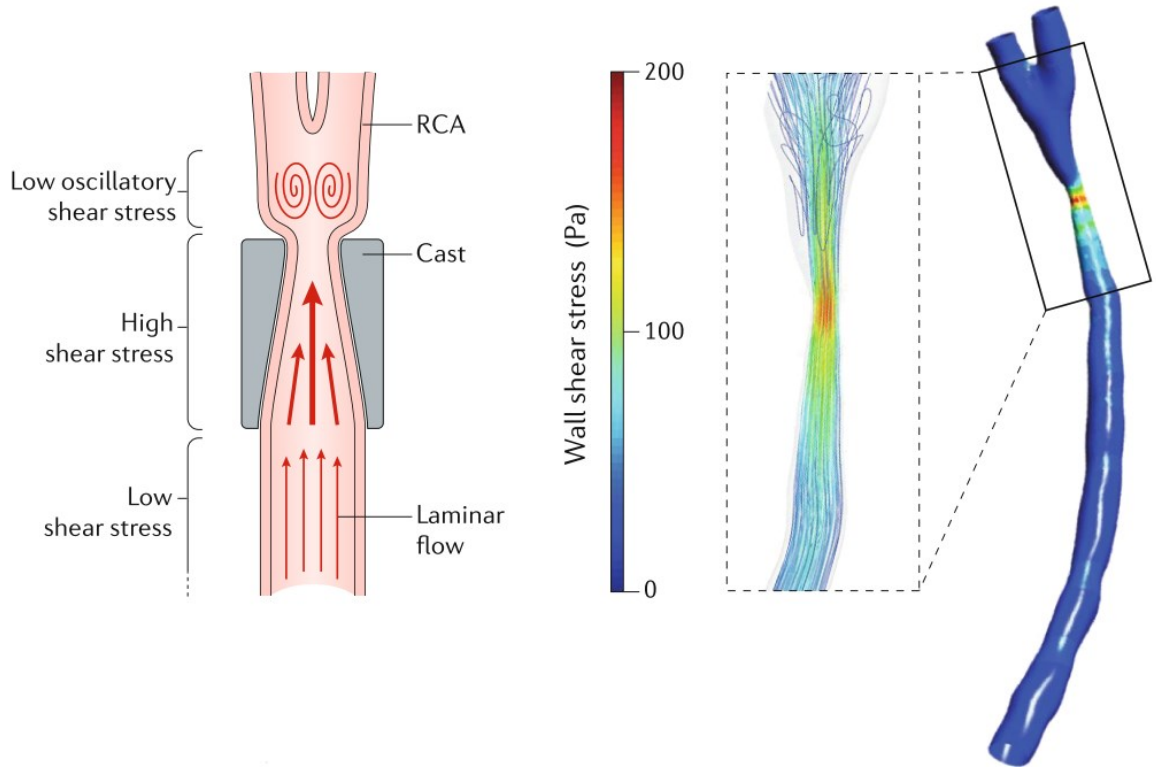

Figure 7. Modulation of shear stress *in vivo.*
In the left panel, the cast model displays a constriction cuff strategically positioned around hypercholesterolemic mice's right carotid artery (RCA) to manipulate blood flow dynamics. This manipulation is further elucidated through computational fluid dynamics modelling, illustrating the intricacy of blood flow. (Adapted from Celine Souilhol *et al.*).[64]

BMP signalling: As part of the TGFβ superfamily, BMPs were known as initiators of bone formation but were later found to play a role in regulating tissue homeostasis and embryogenesis. In the microarray analysis of mouse adult aortic endothelial cells, *Bmp4* emerged as a mechanically sensitive gene, with its expression being triggered by OSS. Consistently, in atheroprone areas, where the ECs are exposed to OSS in mouse and rat aorta, *Bmp4* expression levels were higher compared to the atheroresistant areas where endothelial cells are subjected to LSS.[88] Furthermore, in an aortic stenosis rat model, low oscillatory shear stress directly induced the expression of *Bmp4*,[89] indicating a potential association between shear stress-dependent BMP activation and the development of disease.

KLF2: Krüppel-like factor 2 (KLF2) was initially discovered in mouse embryos as an essential factor for tissue development, such as the lung.[90] Later, KLF2 emerged as a shear stress-

regulated factor, playing a pivotal role in promoting an anti-inflammatory and cytoprotective response to laminar shear stress (Figure 8). KLF2 is regulated by local shear stress to maintain arterial homeostasis and serves as an important factor for blood vessel stabilization.[90-92]

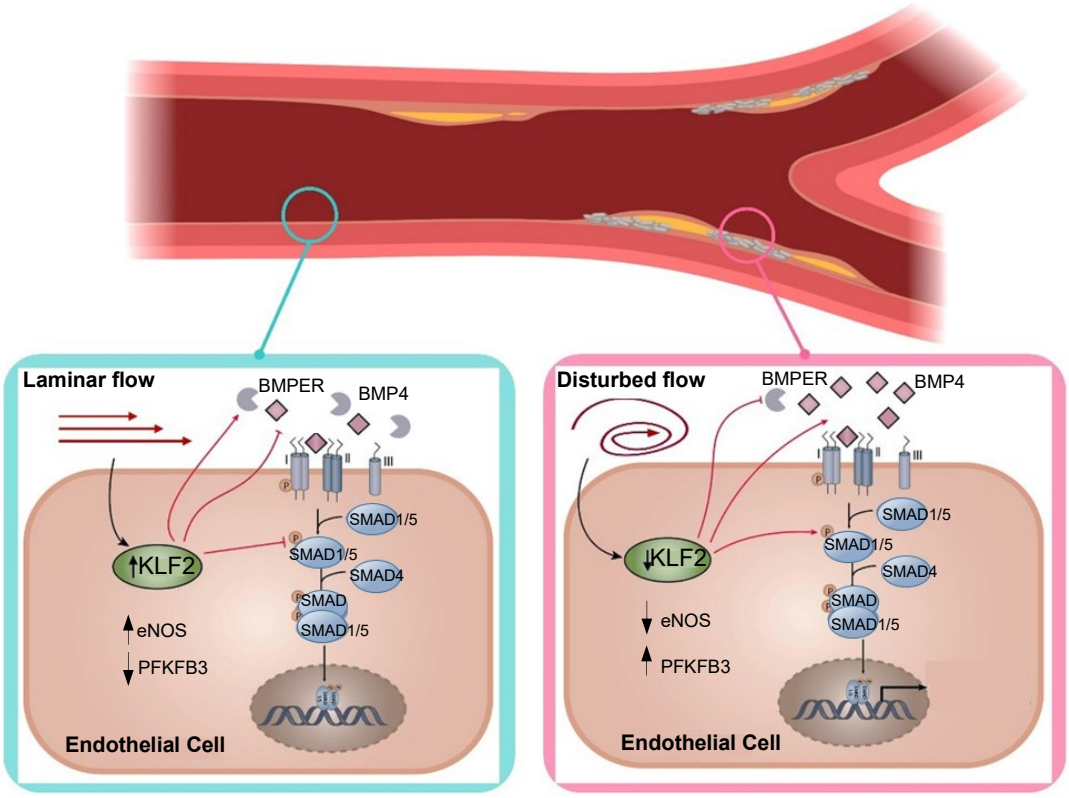

Figure 8. Endothelial cells sense blood flow and respond to mechanical force.
Laminar flow promotes an atheroresistance phenotype in ECs protective against atherosclerosis, while disturbed flow exerts an atheroprone phenotype. (Adapted from Juan Huang *et al.*)[93]

HIF1α: Hypoxia-inducible factor (HIF)-1 are transcription factors regulating angiogenesis, which gets activated under hypoxia conditions. Microarray studies revealed increased HIF1α expression in atheroprone regions of the aorta, where ECs experience low shear stress.[94] Other investigators showed that NF-κB signalling upregulated *HIF1α* transcription under low shear stress,[95] whereas deletion of *Hif1*α in EC mitigated the atherosclerotic lesion size in a mouse model triggered by the disturbed flow.[96]

Endothelial-to-mesenchymal transition (EndMT)*:* TWIST1, which is highly expressed by atheroprone endothelial cells, has been found to act as a regulator of EndMT in atherosclerosis.[74] EndMT is characterized by endothelial cells undergoing a series of cellular transformations, including the disruption of intercellular junctions, loss of cell polarity, increased proliferation, and the potential for cells to detach and migrate into surrounding tissues. TGFβ signalling is a driving factor during this process, which triggers the activation of transcription factors SMAD2, SMAD3, and SMAD4. Furthermore, BMPs can also induce

EndMT through pathways dependent on activin receptor type 1 (ALK2) and/or BMP receptor type 1A (ALK3).[97] Notably, endothelial cells display mesenchymal markers, and the extent of this marker expression aligns with plaque progression in human coronary arteries and carotid arteries, indicating the involvement of EndMT in atherosclerosis.[98]

Collectively, these studies suggest the flow-associated genes involved in endothelial function and targeting these mechanosensitive molecules could be a promising strategy for atherosclerosis.

3.2.2.2 Endothelial inflammation and oxidative stress

Endothelial impairment represents a complex pathophysiological event involving both increased EC activation and dysfunction. EC activation is characterized by an inflammatory and procoagulant state of EC, featuring an elevated expression of cell surface adhesion molecules essential for recruiting and attaching inflammatory cells.[20] Many studies have revealed that oxidants play a significant role in initiating inflammation.[99] ROS are dynamic molecular oxygen intermediates that are physiologically generated within cells as natural products of cellular metabolism, mainly through the mitochondria's electron transport chain (ETC). However, one of the major causes of endothelial dysfunction is the imbalance between antioxidant defence systems and reactive ROS generation, resulting in vascular damage and EC dysfunction. A multitude of sources exist within cells for ROS production (Figure 9). The free radical superoxide anion ($O_2^{\cdot-}$) plays a pivotal role in orchestrating the generation of other physiologically relevant reactive species in the vascular endothelium, such as peroxynitrite ($ONOO^-$), hydroxyl radical ($OH^{\cdot}$), and hydrogen peroxide (H_2O_2). Additionally, NADPH oxidases, present in EC and various other cell types, serve as another source for superoxide production, playing a pivotal position in initiating the inflammatory response.

Under physiological conditions, blood vessels are maintained in a quiescent and dilated state through nitric oxide (NO). However, under pathological conditions, NO is quenched by excess ROS, primarily generated within blood vessels by vascular NADPH oxidase. In this case, eNOS "uncoupling" will generate superoxide instead of NO and further react with remaining NO to produce peroxynitrite, which is another potent oxidant contributing to ROS production.[100] It has been shown that BMP4 is upregulated in endothelial cells exposed to OSS, which stimulates the release of ROS from NOX1, ultimately leading to monocyte adhesion and the onset of inflammation.[101] Overall, ROS is intricately associated with inflammatory signalling, ultimately leading to endothelial dysfunction.

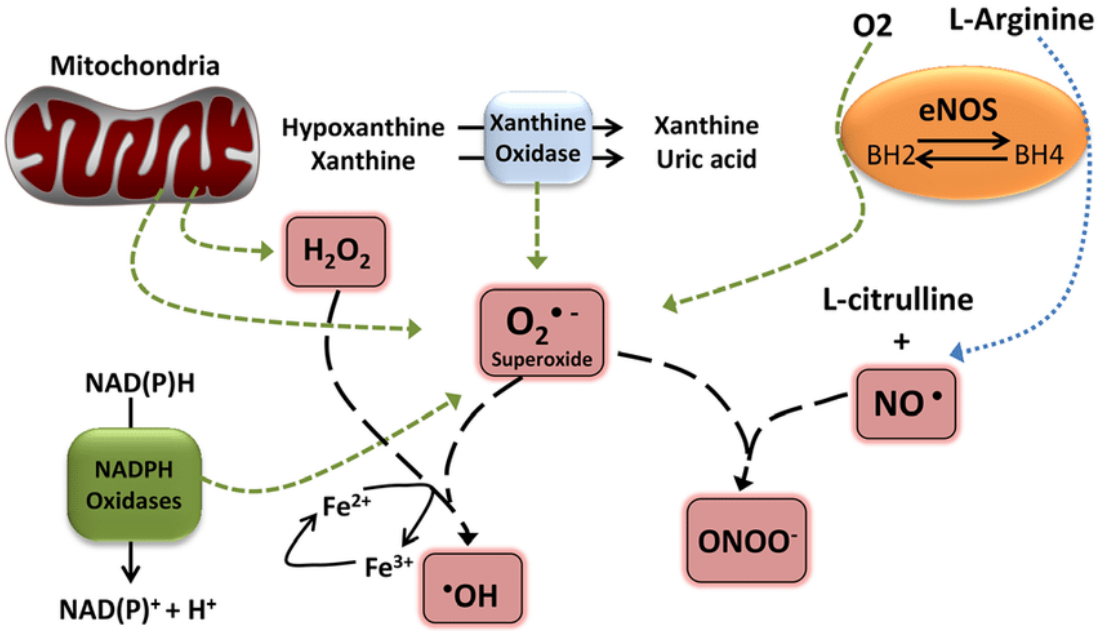

Figure 9. Major ROS generation pathways.
Schematic of ROS production from mitochondria. Mitochondrial dismutase O2•⁻ into H_2O_2, which can be converted to •OH by transitioning to Fe^{2+}. Superoxide can also be formed through (1) NAD(P)H oxidases, which oxidize NADH/NADPH to NAD^+/$NADP^+$, (2) xanthine oxidase, converting hypoxanthine to uric acid, and (3) eNOS, switching from NO• production to O_2•⁻ when L-arginine is reduced, BH4 is deficient, or eNOS is glutathionylated. Superoxide can react with NO• to produce peroxynitrite $ONOO^-$. Adapted from Kai-Chien Yang *et al.*[102]

3.2.2.3 Endothelial interaction with lipids and plaque formation

ECs form a thin monolayer that covers the inner surface of blood vessels and hold a crucial function in maintaining the entire organism's metabolism. They rely on their metabolic processes to support their own cellular functions, including important processes such as angiogenesis. ECs predominantly rely on glucose as their primary energy source,[103, 104] and extensive studies have been dedicated to understanding the mechanisms of glucose transport and glucose metabolism together with others.[103, 105, 106] However, there has been comparatively limited research unravelling the mechanisms of lipid transport and the role of lipids in normal endothelial cell function. The accumulation of excess lipids directly impairs the barrier function of ECs, contributing to chronic vascular endothelial inflammation in atherosclerosis and metabolic disorders like obesity and diabetes.[107] Several recent studies have shed light on caveolae, a subset of lipid rafts, which serve as organizing centres for cellular signal transduction.[108, 109] Gaining a more comprehensive insight into the mechanisms of endothelial lipid transfer is pivotal for advancing the development of therapies that specifically target the early stages of atherosclerosis.

Endothelial LDL transcytosis: Low-density lipoprotein (LDL) particles are lipid-protein complexes with diameters ranging from 22 nm to 28 nm.[110] Macromolecules are transported across endothelial cells through either the paracellular or transcellular pathways. However, the paracellular transfer of lipoproteins with diameters exceeding 6 nm encounters limitations due

to inter-endothelial junctions, including tight junctions, gap junctions, and adherent junctions.[111] Conventional endothelial LDL endocytosis occurs through the LDL receptor (LDLR) by recognizing ApoB in LDL particles, facilitating the internalization of LDL into cells. After internalization, LDL undergoes degradation through lysosomal enzymes, while LDLR is recycled back to the plasma membrane. Intriguingly, systemic endothelial LDL transcytosis does not depend on the LDLR, as indicated by the absence of discernible effect observed in nonhepatic tissue following either genetic depletion or PCSK9-mediated degradation of LDLR.[112, 113]

Caveolae-mediated LDL transcytosis: Caveolae are flask-shaped structural features found on the plasma membranes in various cell types, with particularly high abundance in endothelial cells and adipocytes.[114] Caveolin-1 (Cav1) is the major protein component of the plasma membrane (PM) caveolae structure, yet they have also been identified within intracellular compartments, such as the lipid bodies and Golgi complex, contributing to caveolae-associated functions in endothelial cells. Carlos Fernández-Hernando´s research group revealed that genetic depletion of *Cav1* significantly decreases plaque formation in atherosclerotic mouse models by reducing LDL infiltration independent of eNOS production, whereas selective overexpression of *Cav1* in the endothelium reversed the observed phenotypes.[115] Moreover, the authors observed higher *Cav1* expression in the atherosclerotic arteries and increased basolateral and intracellular caveolae structures located within atheroprone regions (lower curvature of the aortic arch) compared to the atheroresistant areas (greater curvature of the aortic arch) (Figure 10). These findings suggest that hemodynamic and mechanical forces play a role in shaping caveolae in the aortic endothelium, subsequently influencing LDL transport into the arterial wall and the development of atherosclerotic lesions. In subsequent studies, the same research group further described that genetic depletion of *Cav1* enhances EC autophagy within atheroprone regions of *Ldlr*$^{-/-}$ mice. However, the pharmacological autophagy inhibitor 3-methyladenine reduced vascular inflammation in *Cav1*$^{-/-}$ mice without affecting lipid content in atherosclerotic plaques, suggesting that CAV1-mediated autophagy may not be involved in the LDL transcytosis process.[116, 117]

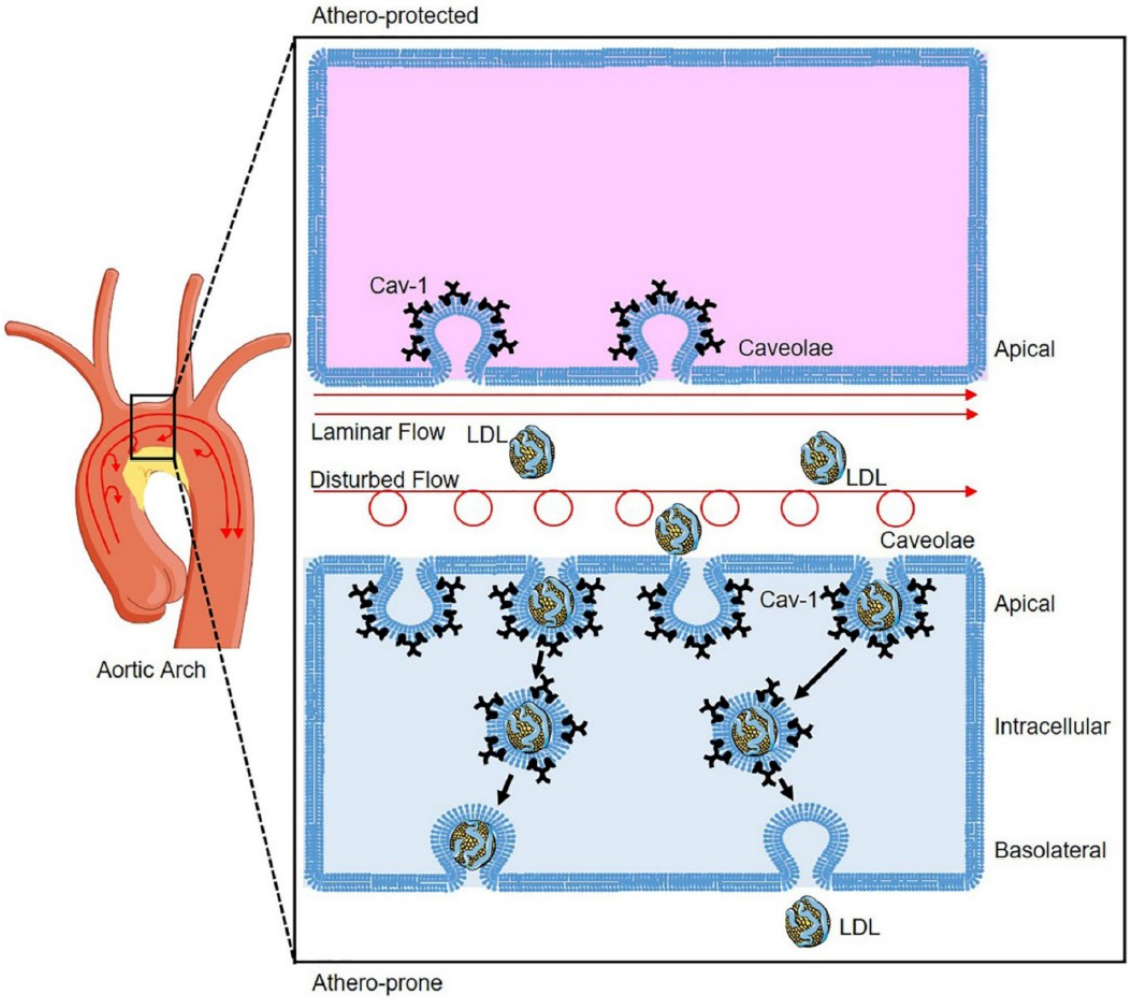

Figure 10. LDL transcytosis through caveolae in EC.
Atherosclerosis preferentially develops at the atheroprone regions of the artery. A higher number of caveolae structures and Cav1 expression are found in this region and promote LDL infiltration. Adapted from Xinbo Zhang *et al.*[113]

Regulation of endothelial LDL transcytosis: Several receptors and transporters like activin receptor-like kinase 1 (ALK1),[118] scavenger receptor B1 (SR-B1),[119] and CD36, ABCA1, and ABCG1 are localized in caveolae, thereby contributing to the uptake or efflux of cholesterol within these lipid-rich subcellular microdomains (Figure 11).[120] SR-B1 is widely recognized as a prominent receptor for HDL that plays an important role in the reverse cholesterol transport (RCT) process, facilitating cholesterol efflux from peripheral tissues to HDL particles, thereby enabling the specific transfer of cholesteryl esters to the liver. A recent study by Warren L. Lee´s group uncovered an unexpected role of endothelial SR- B1 in mediating LDL transcytosis in human coronary artery ECs (HCAECs). In their study, they employed total internal reflection fluorescence (TIRF) microscopy to demonstrate that SR-B1 mediates LDL transcytosis in competition with HDL binding.[112] Notably, Philip W. Shaul's group demonstrated that endothelial-specific depletion of SR-B1 in *Apoe*$^{-/-}$ mice results in less aortic LDL uptake and reduced atherosclerotic plaque progression.[119] They uncovered that the process of LDL transcytosis engages direct binding of SR-B1, accompanied by the recruitment of guanine

nucleotide exchange factor DOCK4 (dedicator of cytokinesis 4). The interaction of DOCK4 with SR-B1 enhances the internalization of SR-B1, contributing to the coupling of LDL binding to SR-B1. This process is driven by the activation of RAC1 (Rac Family Small GTPase 1). A recent genome-wide siRNA screen pinpointed ALK1 as a new LDL receptor characterized by its high capacity to bind LDL.[118] Remarkably, ALK1 facilitates LDL transcytosis independent of its kinase activity *in vitro*. In addition, it has been found that the absence of ALK1 in endothelial cells attenuates aortic endothelium LDL uptake and inhibits atherosclerosis progression in mice.[121] ALK1 is widely recognized as a receptor for TGFß-1, with the capability to bind to BMP9 and BMP10. Together, these findings uncovered the pivotal role of Cav1, SR-B1, and ALK1 in regulating LDL transcytosis within the arterial wall. This provides the opportunity to limit atherosclerosis progression by targeting caveolae-associated molecules.

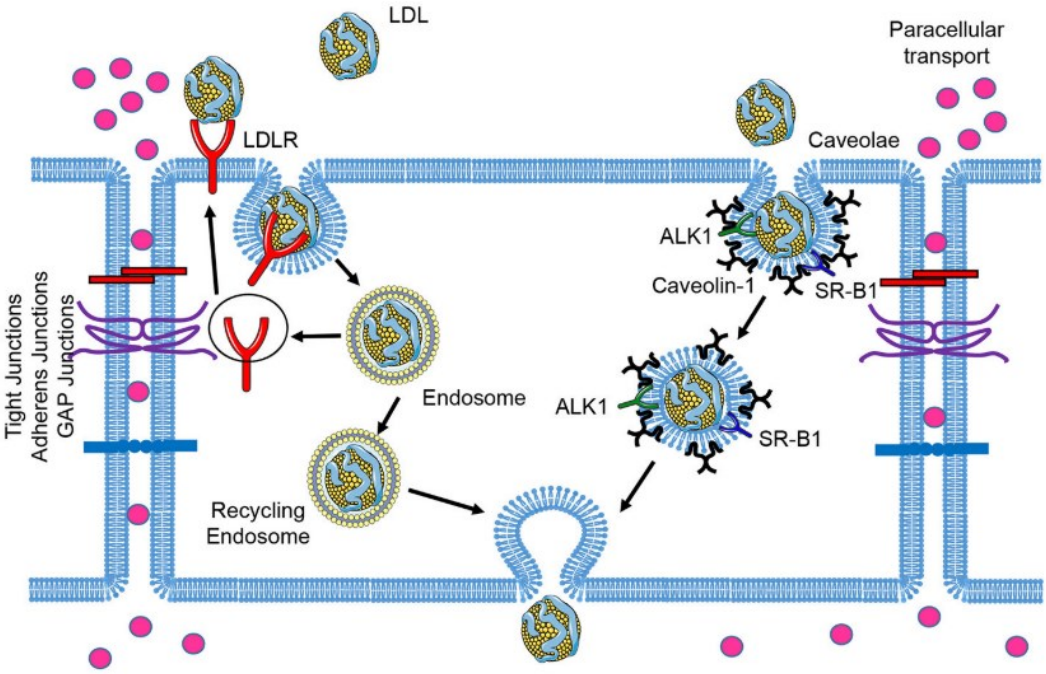

Figure 11. EC LDL transcytosis.
Water and molecules less than 6 nm traverse EC through the paracellular pathway. The LDLR pathway mediates LDL uptake and degradation in lysosomes, but it is not required for transcytosis. LDL can cross EC via receptor-mediated transcytosis involving SR-B1 and ALK1. It can also use caveolae-mediated direct transcytosis before exocytosis into the subendothelial space. Adapted from Xinbo Zhang *et al.*[117]

3.2.3 Tissue lipid uptake and metabolism in atherosclerosis

3.2.3.1 Brown and white adipose tissue

Lipids have a central role in supporting cellular structure and growth by generating and sorting energy. Adipose tissues, including white adipose tissue (WAT), brown adipose tissue (BAT), and perivascular adipose tissue (PVAT), function as central energy storage sites found in diverse regions of the body.[122] WAT, a key player in energy regulation, serves as a primary repository by storing excess dietary fatty acids such as triglycerides within adipocytes. These

stored lipids can be released on demand through intracellular lipolysis, providing energy supplies for the other organs. Spherical adipocytes in WAT are characterized by the presence of a singular, large lipid droplet, accompanied by a sparse distribution of mitochondria forming a thin layer around the cytoplasm (Figure 12). BAT is found in the neck, above the collarbone, and along the spinal cord in humans. Unlike WAT's traditional role, which stores energy, BAT has a distinct function of utilizing fatty acids not for storage but to generate heat through a specialized process called non-shivering thermogenesis, a critical mechanism for maintaining and regulating body temperature. Therefore, brown adipocytes have smaller lipid droplets with an abundance of mitochondria, which are important components for efficient thermogenesis. Thermogenesis in BAT relies on intracellular lipolysis, a process facilitated by the presence of uncoupling protein 1 (UCP1), which produces fatty acids serving as substrates for heat production.[123] Apart from classical brown adipocytes exhibiting high UCP1 expression, there exist brown-like cells residing in WAT, referred to as beige adipocytes, with low basal UCP1 but showing a high responsiveness for UCP1 upregulation.[124] Under physiological conditions, WAT functions as a lipid reservoir, efficiently storing lipids. This role is essential in preventing the excessive accumulation of lipids in the bloodstream, which contributes to its anti-atherogenic properties. However, in the condition of obesity, a reduced turnover of triglycerides in white adipocytes leads to heightened lipid storage and impaired removal. Meanwhile, BAT displays a whitened phenotype with less fatty acid consumption.[125] This intricate interplay underscores the multifaceted role of lipids in maintaining energy homeostasis and metabolic equilibrium in the body.

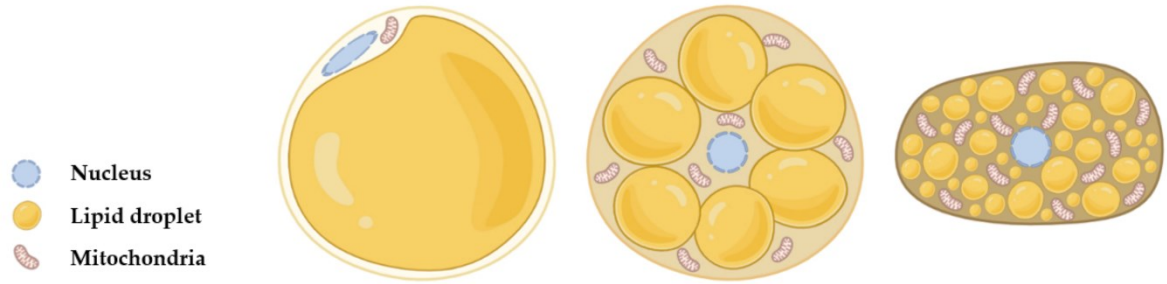

	White adipocyte	Beige/brite adipocyte	Brown adipocyte
UCP1 expression	Negative	Positive	Positive
Mitochondria density	Low	Medium	High
LD morphology	One large lipid droplet	Small multiple droplet	Small multiple droplet
Function	Store excess energy as fat	Heat generation	Heat generation

Figure 12. Adipocyte characteristics.
The figure illustrates unique features of white, beige, and brown adipocytes, including UCP1 and LD (lipid droplet). Adapted from Min-Kyeong Lee *et al.*[126]

In 2011, Alexander Bartelt and colleagues demonstrated that activation of BAT by cold could efficiently lower plasma triglyceride levels in *Apoa5*$^{-/-}$ mice.[127] In a subsequent study, Khedoe *et al.* revealed that BAT actively takes up plasma triglycerides following the lipolysis process, highlighting the critical roles of lipoprotein lipase (LPL) activity and the presence of CD36 in facilitating triglyceride clearance by BAT.[128] Recently, Berbée *et al*. showed that activation of BAT through the stimulation of β3-adrenergic receptors protects against atherosclerosis development in *E3L.CETP* mice.[129] In human studies, it has been demonstrated that six weeks of cold exposure (17°C for 2 h/day) leads to a reduction in body fat mass.[130] Collectively, activating brown adipocytes to enhance the combustion of fatty acids within BAT emerges as a therapeutic approach for targeting adipose tissue depots to reduce atherosclerosis.

3.2.3.2 GPIHBP1 facilitates the transportation of LPL to the capillary lumen

The uptake of lipids from the bloodstream by tissues requires that lipids cross the EC barrier, which involves lipoprotein lipase (LpL) and its binding protein GPIHBP1 (glycosylphosphatidylinositol-anchored HDL binding protein 1).[131] GPIHBP1 can be detected in almost every peripheral tissue, with notably elevated levels observed in BAT and the heart, corresponding to the abundance of LPL in these tissues. LpL is produced by adipocytes and subsequently secreted into the intercellular space. Released LPL sticks to heparan sulfate proteoglycan (HSPG) and shifts to GPIHBP1 on the surface of capillary endothelial cells. GPIHBP1 shuttles lipoprotein lipase (LPL) to its functional location within the capillary lumen. The GPIHBP1-LPL complex is essential for the lipid uptake from triglyceride-rich lipoproteins (TRL) in the bloodstream, as the positioning on the capillary endothelium enables LPL to break down triglycerides into lipoprotein particles (called ‘remnants’).[132] In contrast, the dysfunction of GPIHBP1 results in chylomicronaemia or hypertriglyceridemia, as observed in patients with autoantibodies against GPIHBP1, which block the binding of LPL to GPIHBP1 and thereby limit the transport of LPL, resulting in circulating lipid accumulation (Figure 13).[133]

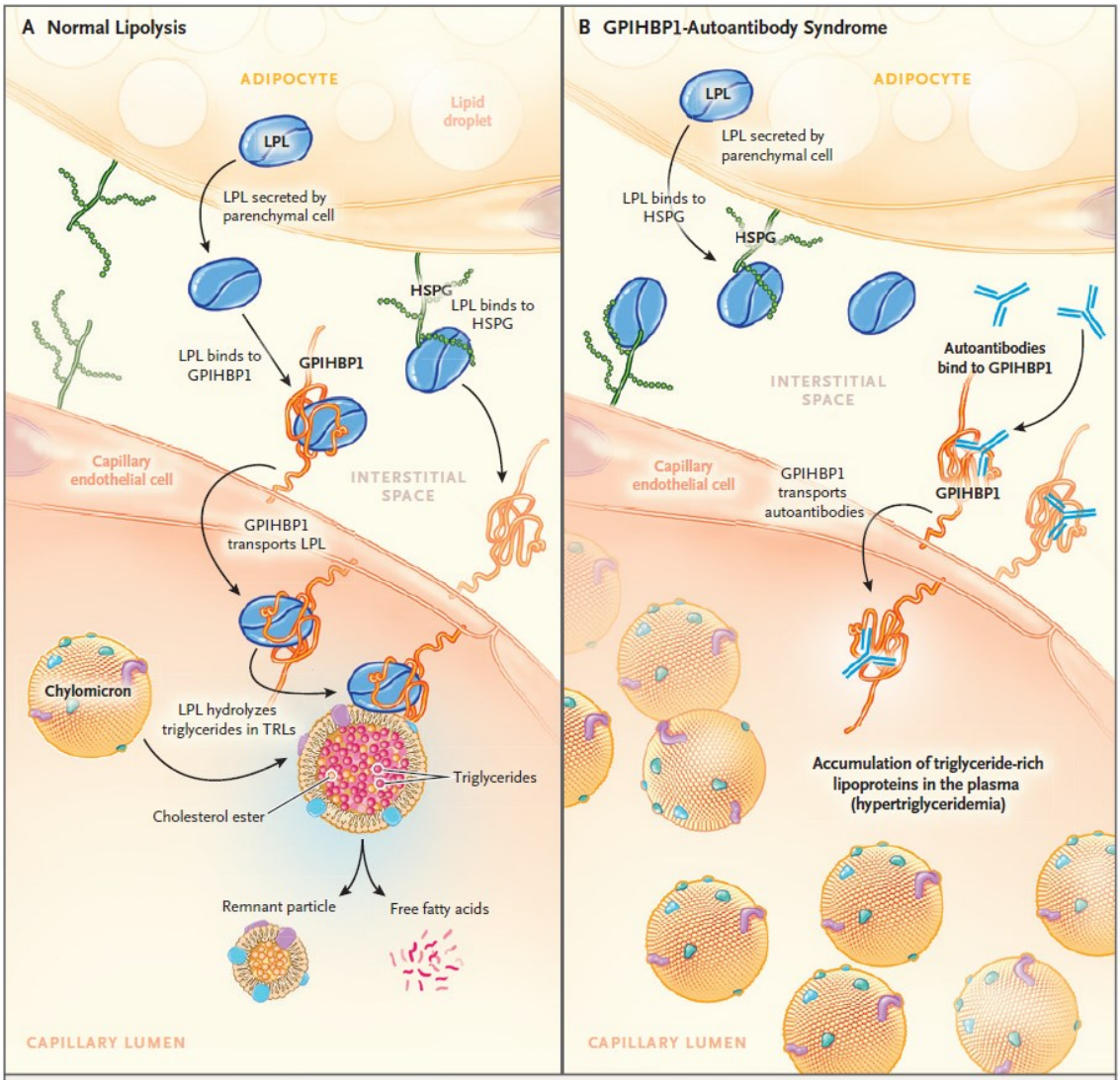

Figure 13. GPIHBP1 function and GPIHBP1-autoantibody syndrome.
Panel A illustrates the intravascular triglyceride processing under normal physiological condition, while panel B highlights the impaired triglyceride processing in patients afflicted by GPIHBP1-autoantibody syndrome. In a healthy state, lipoprotein lipase (LPL), secreted by parenchymal cells like myocytes and adipocytes, binds to GPIHBP1 on the basolateral surface of EC. GPIHBP1 facilitates the translocation of LPL across EC to capillary lumen, where it breaks down triglycerides within triglyceride-rich lipoproteins. GPIHBP1 autoantibodies disrupt the interaction between LPL and GPIHBP1, thereby impeding the transport of LPL. (HSPG stands for heparan sulphate proteoglycan, and TRL represents triglyceride-rich lipoprotein.) Adapted from A.P. Beigneux *et al.* [133]

3.3 Endocannabinoid system

Cannabis, commonly called marijuana, is a psychoactive drug extracted from the Cannabis plant. It has been used for medicinal purposes for centuries, particularly for pain relief and appetite stimulation.[134] In the 1960s, scientists made significant progress in comprehending Cannabis. They successfully identified THC, the psychoactive component of Cannabis, and elucidated its pharmacology and mechanism.[135] The endogenous endocannabinoid ligands, including 2-arachidonoylglycerol (2-AG) and anandamide (AEA), were subsequently discovered. Endocannabinoids are locally acting lipid hormones, exerting effects in an autocrine or paracrine manner. The endogenous ligands, along with plant-derived or synthetic

cannabinoids, bind to G-protein-coupled receptors(GPCRs), specifically cannabinoid (CB) receptors 1 and 2.[136, 137] While CB1 receptors are more abundant found in the central nervous system (CNS), CB2 receptors are predominantly expressed in the periphery, particularly by cells of the immune system.[138] The CB1 receptor is associated with pro-inflammatory and pro-oxidative stress responses, which are linked to CVD.[139, 140] Unlike CB1, the activation of the CB2 receptor seems to inhibit and regulate various pro-inflammatory effects, indicating divergent downstream signalling pathways.[141, 142] Apart from the traditional cannabinoid receptors, cannabinoids also exert their effects on other receptors. These include GPCRs like GPR55,[143] GPR18[144] and GPR119,[145] or the transient receptor potential cation channel subfamily V member 1 (TRPV1),[146] and peroxisome proliferator-activated receptors (PPARs).

3.3.1 Endogenous ligands of the endocannabinoid system

The endocannabinoid system constitutes a complex network, including cannabinoid receptors, endogenous ligands, and enzymes integral to the biosynthesis and degradation of endocannabinoids. These bioactive lipids, N-arachidonoylethanolamine (anandamide, AEA) and 2-arachidonylglycerol (2-AG), are fatty acids that are generated in response to specific physiological demands from lipid precursors and subsequently released into the extracellular space (Figure 14). N-arachidonoyl phosphatidylethanolamine (NAPE) serves as the substrate for AEA synthesis through NAPE-specific phospholipase D (NAPE-PLD). For the 2-AG synthesis, phospholipase C-β (PLC-β) facilitates the hydrolysis of phosphatidylinositol 4,5-bisphosphate (PIP_2) to produce diacylglycerol (DAG), which is subsequently hydrolysed by diacylglycerol lipases (DAGL) α and β to generate 2-AG. Fatty acid amide hydrolase (FAAH) mediates the termination of AEA, whereas monoacylglycerol lipase (MAGL) orchestrates the degradation of 2-AG.[147]

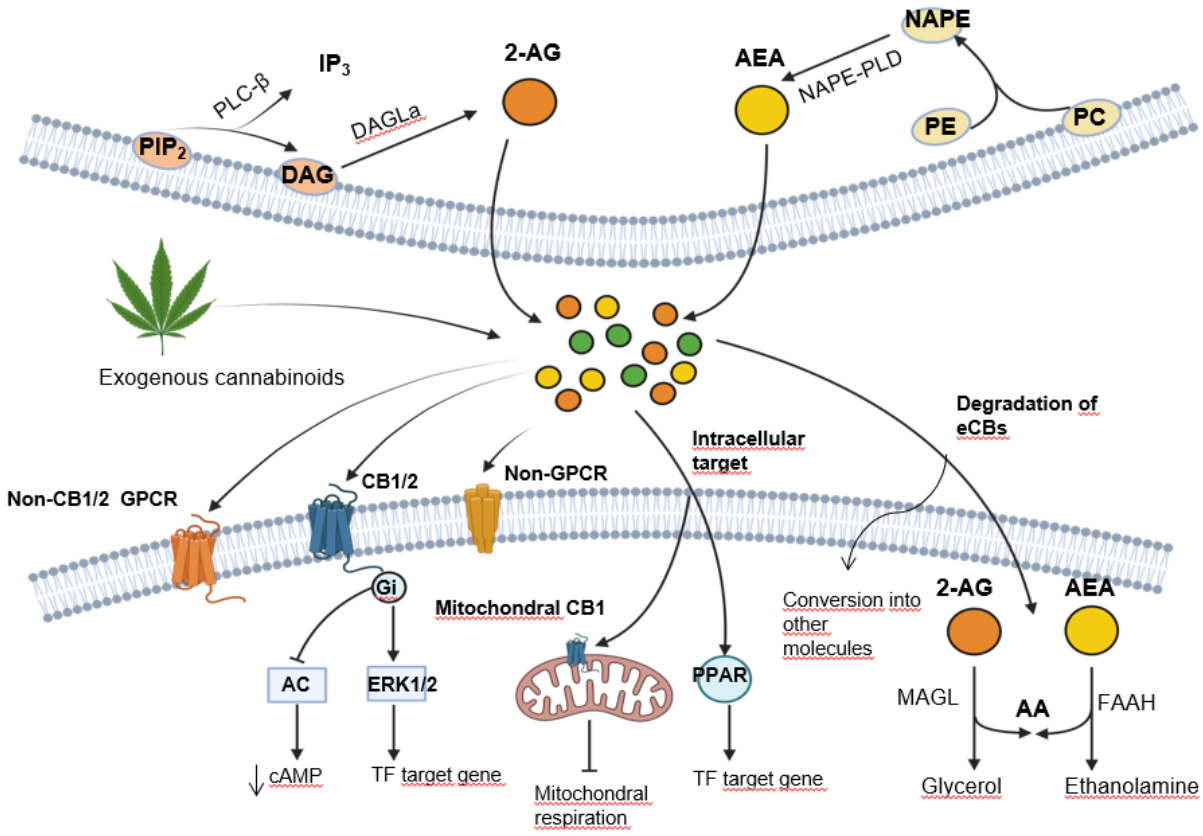

Figure 14. The endocannabinoid system.
The endogenously synthesized endocannabinoids AEA and 2-AG, are dynamically generated from lipid precursors. Both exogenous or endogenous cannabinoids bind to Gi-coupled receptors CB1 or CB2 to induce intracellular pathways. This modulation extends to the inhibition of adenylyl cyclase (AC) and the orchestration of transcriptional regulation mediated via extracellular signal-regulated kinases (ERKs). Beyond the canonical CB1 and CB2, there are other cannabinoid receptors, such as non-GPCRs like TRPV1 and non-CB1/2 GPCRs. Furthermore, intracellular receptors like mitochondrial CB1 (mtCB1) and peroxisome proliferator-activated receptors (PPARs) were recently reported. Adapted from Henrike Horn *et al.*[147]

3.3.2 Cannabinoid receptors in atherosclerosis

The two major cannabinoid receptors are CB1 and CB2, which are GPCRs coupled to Gi/o protein alpha-subunits, thereby inhibiting adenylyl cyclase activity. Several studies have provided evidence that cannabinoid receptor signalling affects the progression of plaque formation in atherosclerotic models. Low doses of THC were reported to show anti-atherosclerotic properties, as it effectively reduced the pro-inflammatory cytokine production and macrophage migration, leading to a smaller plaque formation.[148] However, the antiatherogenic effect was inhibited by CB2 antagonism treatment, indicating a athero-protective role via CB2 receptor signalling.[148, 149] Another study has unveiled that THC induces cytotoxicity and inflammation in human endothelial cells, which is likely mediated via CB1.[150] In liver macrophages, CB1 activation with ACEA stimulates NLRP3 inflammasome activation, leading to the release of the pro-inflammatory cytokine interleukin (IL)-1β.[151] Together, these findings suggest a pro-inflammatory role of CB1. In the cardiovascular system, CB1 can be

found in cardiomyocytes, endothelial cells, and smooth muscle cells.[152, 153] AEA induces CB1-mediated changes in heart rate and blood pressure, indicating that the endocannabinoid system is involved in the regulation of heart and vascular function.[154] In cultured primary human cardiomyocytes and umbilical vein endothelial cells, the activation of CB1 receptors triggered p38 and JNK MAPK signalling cascades, and induced cellular apoptosis.[155, 156] Upregulated CB1 receptors were found in epicardial fat from human ischemic hearts,[157] as well as in atherosclerotic plaques of patients with unstable angina [158]. Additionally, adipocyte-specific deletion of the CB1 improved metabolic function and protected adult mice from diet-induced obesity.[159] These observations suggest that CB1 plays a proatherogenic role in cardiovascular disease. Recent studies have indicated that pharmacological antagonism of CB1 with rimonabant not only effectively reduces body weight and improves the cardiometabolic profile [160-162, 163] but also reduces plaque formation in mice.[164] In other studies, the researchers did not detect plaque size changes in mice treated with CB1 antagonist but reported an improvement in aortic endothelium-dependent vasodilation with decreased ROS production.[165] Nevertheless, the beneficial application of the CB1 antagonist rimonabant is hampered by serious side effects, notably depression and anxiety, primarily resulting from the drug's impact on the brain. Peripherally restricted CB1 antagonists such as JD5037 or TM38837 have recently been developed to minimize undesired psychotropic side effects.[166] JD5037 has so far been tested in diet-induced obese (DIO) mice, demonstrating improvements in hepatic steatosis, dyslipidaemia and insulin resistance in a leptin-dependent manner.[167] These findings emphasize the critical role of endocannabinoid signalling in the development of obesity and cardiovascular disease and its potential impact on fundamental pathways associated with atherosclerosis. Therefore, exploring interventions that target the endocannabinoid system could be a promising approach for patients suffering from atherosclerosis and its related complications.

3.4 Aims of the study

Peripherally restricted CB1 antagonists, which do not penetrate the blood-brain barrier and thereby mitigate central side effects, show promise in treating metabolic disorders such as diabetes and obesity.[159, 167, 168] This provides a rationale for further exploring the role of the endocannabinoid system in atherosclerosis and the therapeutic benefits of peripheral CB1 receptor targeting in this context. Our preliminary findings generated from single-cell RNA sequencing data of human atherosclerotic plaques from the Munich Vascular Biobank (collaboration with Prof. Lars Maegdefessel, TUM) revealed a predominant expression of the CB1 encoding gene *CNR1* in human plaque endothelial cells (Figure 15).

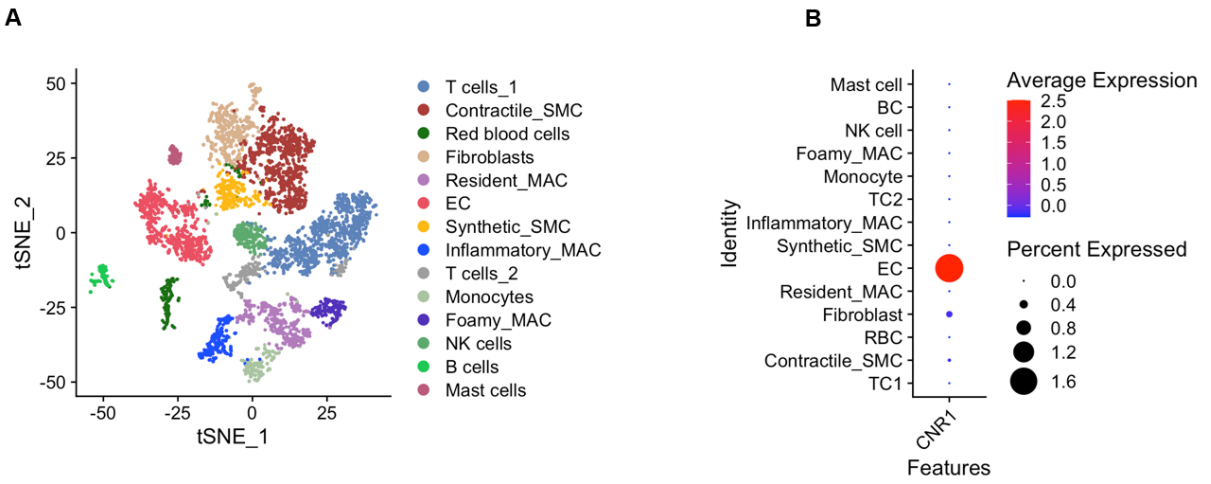

Figure 15. *CNR1* expression in human atherosclerotic plaques.
(A) t-distributed Stochastic Neighbor Embedding (t-SNE) reveals cell clusters in human atherosclerosis single-cell sequencing (scSeq) data provided by the Munich Vascular Biobank. **(B)** The dot plot displays the *CNR1* expression patterns within each cell cluster, with the colour gradient from blue to red indicating the average expression level (low to high) and the point size reflecting the percentage of gene expression within each cluster. (SMC: Smooth muscle cells, MAC: Macrophage, EC: Endothelial cells, NK cell: Natural killer cells)

Based on these findings, the critical role of endothelial dysfunction during atherosclerosis progression and the pro-atherogenic role of CB1 in this disease, the overarching aim of this thesis was to investigate the endothelial cell-specific role of CB1 in atherosclerosis.

The following specific objectives were studied in this thesis:

1. Effect of shear stress on CB1 signalling in ECs.
2. Generation of endothelial cell-specific CB1 knockout mice on an atherogenic background to study the impact of endothelial CB1 deficiency on vascular and barrier function, lipid uptake, vascular inflammation and whole-body metabolism.
3. Mechanisms underlying the metabolic effects in the absence of endothelial CB1 signalling.
4. Therapeutic potential of the peripheral CB1 antagonist JD5037 in atherosclerosis.

4. MATERIALS AND METHODS

4.1 Materials

4.1.1 Chemicals and reagents

Table 1*:* Chemicals and reagents

Chemical /Reagents	Supplier
0.2% Gelatin solution	Sciencell, United States
Accutase	Sigma-Aldrich Chemie GmbH, Munich, Germany
ACEA	Tocris Bioscience, Bristol, United Kingdom
Acetic acid (glacial) 100% anhydrous	Merck KGaA, Darmstadt, Germany
Acetone	Sigma-Aldrich Chemie GmbH, Munich, Germany
AM281	Sigma-Aldrich Chemie GmbH, Munich, Germany
Aniline blue	Sigma-Aldrich Chemie GmbH, Munich, Germany
Antifade mounting medium	Vector Laboratories, Newark, United States
Biebrich Scarlet-Acid Fuchsin Solution	Sigma-Aldrich Chemie GmbH, Munich, Germany
Bouin's solution	Sigma-Aldrich Chemie GmbH, Munich, Germany
Bradford 1x Dye Reagent	Bio-Rad, Hercules, USA
BSA ≥ 98 %	Carl Roth GmbH + Co. KG, Karlsruhe, Germany
Calcein	Invitrogen AG, Carlsbad, USA
Citric Acid	Merck KGaA, Darmstadt, Germany
CP 55,940	Tocris Bioscience, Bristol, United Kingdom
Cnr1 ViewRNA Cell Plus Probe Set	Affymetrix, United States
Dihydrorhodamine 123	Cayman Chemical, Ann Arbor, USA
DMEM	Thermo Fisher Scientific, Waltham, USA
DMSO	Carl Roth GmbH + Co. KG, Karlsruhe, Germany
EDTA	Sigma-Aldrich Chemie GmbH, Munich, Germany
ELISA buffer	Cayman Chemical, Ann Arbor, USA
Embedding Medium Tissue-Tek OCT	Sakura Finetek, Torrance, USA
Endothelial Cell Growth Medium	Promocell, Heidelberg, Germany
Eosin Y-solution	Sigma-Aldrich Chemie GmbH, Munich, Germany
Ethanol 99%	Klinikum der Universität München
Ethanol 99% (absolute)	VWR International, Radnor, USA
Evans blue	Sigma-Aldrich Chemie GmbH, Munich, Germany
Fetal Bovine Serum	Sigma-Aldrich Chemie GmbH
Forskolin	Sigma-Aldrich Chemie GmbH, Munich, Germany

Glucose	Merck KGaA, Darmstadt, Germany
GoTaq Probe qPCR Master Mix	Promega Biotechnology, United States
Haematoxylin solution	Sigma-Aldrich Chemie GmbH, Munich, Germany
HBSS	Gibco, Life Technologies.USA
HEPES solution 1 M	Sigma-Aldrich Chemie GmbH
Horse Serum	Vector Laboratories, Newark, United States
Human DiI-Low Density Lipoprotein	Kalen Biomedical, Germantown, USA
Hydrochloric acid	Merck KGaA, Darmstadt, Germany
Ibidi Mounting Medium With DAPI	ibidi GmbH, Germany
IBMX	Sigma-Aldrich Chemie GmbH, Munich, Germany
Immu Mount	Thermo Fisher Scientific, CA, USA
Isoflurane	CP Pharma, Germany
Isopropanol	KMF Laborchemie, Lohmar, Germany
JD-5037	Hycultec GmbH, Beutelsbach
Kaiser’s glycerol gelatine	Sigma-Aldrich Chemie GmbH, Munich, Germany
Ketamine	WDT eG, Garbsen, Germany
KT5720	Tocris Bioscience, Bristol, United Kingdom
Lipofectamine ™ RNAiMAX	Thermo Fisher Scientific, Waltham, USA
Mayer's hematoxylin solution	Sigma-Aldrich Chemie GmbH, Munich, Germany
Nile red	Sigma-Aldrich Chemie GmbH, Munich, Germany
Oil Red O	Sigma-Aldrich Chemie GmbH, Munich, Germany
Opti-MEM™ Serum Reduced Medium	Thermo Fisher Scientific, Waltham, USA
Paraformaldehyde	Merck KgaA, Darmstadt, Germany
PBS (for cell culture)	Gibco, Bleiswijk, Netherlands
PBS powder	Biochrom AG, Berlin, Germany
Penicillin streptomycin	Sigma-Aldrich Chemie GmbH, Munich, Germany
PeqGold Trifast	Peqlab Biotechnologie GmbH, Erlangen,
Phosphomolybdic acid hydrate	Sigma-Aldrich Chemie GmbH, Munich, Germany
Phosphotungstic acid hydrate	Sigma-Aldrich Chemie GmbH, Munich, Germany
Potassium chloride	Sigma-Aldrich Chemie GmbH, Munich, Germany
Propidium iodide	Invitrogen AG, Carlsbad, USA
QIAzol Lysis Reagent	Qiagen, Venlo, The Netherlands
Recombinant human TNF-α Protein	R&D Systems, Inc., Minneapolis, USA
RLT Plus Buffer	Qiagen, Venlo, The Netherlands
Rotenon	Sigma-Aldrich Chemie GmbH, Munich, Germany

Roti-Histofix 4 %	Carl Roth GmbH + Co. KG
SecureSeal™ Hybridization Chambers	Grace Bio-Labs, United States
siRNA buffer	Dharmacon Horizon Discovery, United Kingdom
Sodium chloride	Sigma-Aldrich Chemie GmbH, Munich, Germany
Sodium chloride 0.9%	B. Braun AG, Puchheim, Germany
Sodium citrate	Sigma-Aldrich Chemie GmbH, Munich, Germany
Tamoxifen	Sigma-Aldrich Chemie GmbH, Munich, Germany
TCL buffer 2x	Qiagen, Venlo, The Netherlands
Tissue-Tek O.C.T	Sakura Finetek Germany GmbH
Tritonx-100	Carl Roth GmbH + Co. KG, Karlsruhe, Germany
Trypsin-EDTA (0.05%)	Gibco, Life Technologies.USA
Trypsin-EDTA (0.25%)	Gibco, Life Technologies.USA
Tween 20	Sigma-Aldrich Chemie GmbH, Munich, Germany
Tween 80	Sigma-Aldrich Chemie GmbH, Munich, Germany
Weigert's iron hematoxylin solution	Sigma-Aldrich Chemie GmbH, Munich, Germany
Xylazine	WDT eG, Garbsen, Germany
Xylene	Sigma-Aldrich Chemie GmbH, Munich, Germany

DMEM = Dulbecco's modified Eagle's Medium; DMSO = Dimethyl sulfoxide; EDTA = Ehylenediaminetetraacetic acid; HBSS = Hanks' balanced salt solution; HEPES = 4-(2-hydroxyethyl)-1-piperazineethanesulfonic acid; PBS = Phosphate buffered saline; RBC = Red blood cell; TNFα=Tumor necrosis factor α; IBMX=3-Isobutyl-1-methylxanthine

4.1.2 Buffers and solutions

Table 2: Buffers, solutions and their composition

Buffers and solutions	Composition
ACK lysis buffer	150 mM NH_4Cl, 10 mM $KHCO_3$, 0.1 mM Na_2EDTA, pH 7.4
Anaesthesia	700 µL Ketamine (50 mg/ml), 500 µL Xylazine (20 mg/ml) with 4500 µL normal saline
Antigen retrieval buffer	630 mL ddH_2O, 12.6 mL solution A (2.101 g citric acid in 100 mL ddH_2O), 57.4 mL solution B (14.70 g sodium µcitrate in 500 mL ddH_2O), 320 µL Tween 20, pH 6.0.1.4 mM citric acid, 5.74 mM sodium citrate tribasic dihydrate, 0.035 % (v/v) tween 20
Aortic endothelial digestion cocktail	10 mg/mL collagenaseIV, 20 U/mL DNase I in PBS
Blocking solution	6 mL PBS, 600 µL 10% BSA (1%), 3 drops horse serum
DMEM medium	DMEM (10% FBS; 1% P/S)

Endothelial Cell Growth Medium	Low serum (2% V/V); EC growth factor; heparin, 1% P/S)
FACS buffer	0.5 % (w/v) albumin in PBS
Nile red solution	750 µL glycerol, 250 µL aqua dest., 5 µL Nile red stock solution
ORO stock solution	0.5 % (w/v) ORO in 99 % 2-propanol
PBS solution 1X	9.55 g PBS Dulbeccos in 1 L ddH_2O (pH 7.4)

ACK = Ammonium chloride potassium; BSA = Bovine serum albumin; DNase = Deoxyribonucle- ase; DMEM = Dulbecco's modified Eagle's Medium; FACS = Fluorescence-activated cell sorting; ORO = Oil Red O; ddH2O= Double distilled water.

4.1.3 Kits

Table 3: Kits

Kit	Company
Cholesterol CHOP-PAP kit + Calibrator	Roche, Basel, Switzerland
Cyclic AMP Select ELISA Kit	Cayman Chemical, Ann Arbor, USA
ddPCR Supermix for Probes (No dUTP)	Bio-Rad, Hercules, USA
One-Step RT-ddPCR Advanced Kit for Probes	Bio-rad, USA
peqGOLD Total RNA kit	Peqlab Biotechnologie GmbH, Erlangen,
PrimeScript RT Reagent Kit	Takara, Shiga, Japan
Probe qPCR master mix	Promega, Madison, USA
RNeasy Plus Mini Kit	Qiagen, Venlo, The Netherlands
Single Cell RNA Purification Kit	Norgen Biotek, Canada
Total Bile Acid Liquid	Sentinel Diagnostics, Sentinel CH. S.p.A. Italy
ViewRNA™ Cell Plus Assay-Kit	Invitrogen AG, Carlsbad, USA

4.1.4 Primers

Table 4: Murine primers for qPCR analysis

Murine gene	Assay ID or 5' to 3' primer sequence
Acadm	Mm01323360_g1
Cd36	Mm01135198_m1
Cnr1	Fw: 5'-ATGCGAAGGGGTTCCCTC-3'
	Rev: ATGGTACGGAAGGTGGTATCT
	Probe *FAM*-TGGCACCTCTTTCTCAGTCACGTTGAGC-*TAMRA*

Cnr1 (ddPCR)	Fw: 5'-ATGCGAAGGGGTTCCCTC-3'
	Rev ATGGTACGGAAGGTGGTATCT
	Probe 5'6-FAM-TGGCACCTC/ZEN/TTTCTCAGTCACGTTGAGC-3IABkFQ
Cpt1a	Mm01231183_m1
Cpt2	Mm00487205_m1
Fabp4	Mm00445878_m1
Gpihbp1	Mm01205849_g1
Hprt	Fw: 5'- GACCGGTCCCGTCATGC-3'
	Rev: 5'- TCATAACCTGGTTCATCATCGC-3'
	Probe: VIC-ACCCGCAGTCCCAGCGTCGTG-TAMRA
Hprt (ddPCR)	Fw: GACCGGTCCCGTCATGC
	Rev: TCATAACCTGGTTCATCATCGC
	Probe: 5HEX-ACCCGCAGT/ZEN/CCCAGCGTCGTG-3IABkFQ
Lipe	Mm00495359_m1
Lipg	Mm00495368_m1
Ppara	Mm00440939_m1
Pparg	Mm00440940_m1
Ppargc1a	Mm00447181_m1
Prdm16	Mm00712556_m1
Ucp1	Mm01244861_m1

Fwd = Forward; Rev= Reverse; MWG-Biotech AG provided the custom-designed primers and probes for qPCR, while Life Technologies supplied the TaqMan Gene Expression Arrays.

Table 5: Human primers for qPCR analysis

Human gene	Assay ID or 5' to 3' primer sequence
CAV1	Hs00971716_m1
CCL2	Hs00234140_m1
CNR1	Fw:5'- CTG GCA TCT ATC TGG TGA TTT-3'
	Rev: 5'- CTT AGA GCG TGA ACC GTA AG-3'
	Probe: 5'- CGA GAT ACC CAA GCA GCC TGA TGG -3' TAMRA
CXCL8	Hs00174103_m1
HPRT	Fw: 5'- TGG TCA GGC AGT ATA ATC CAA AGA-3'
	Rev: 5'- TCA AAT CCA ACA AAG TCT GGC TTA-3'
	Probe: 5'-AGC TTG CGA CCT TGAC-3' TAMRA
ICAM1	Hs00164932_m1
IL6	Hs00174131_m1
KLF2	Hs00360439_g1

NOS3	Hs01574665_m1
PFKFB3	Hs00998698_m1
SELE	Hs00174057_m1
VCAM1	Hs01003372_m1

Fwd = Forward; Rev= Reverse; MWG-Biotech AG provided the custom-designed primers and probes for qPCR, while Life Technologies supplied the TaqMan Gene Expression Arrays.

Table 6: siRNA SMARTpool Target Sequence

Human gene	siRNA SMARTpool Target Sequence
CAV1	CUAAACACCUCAACGAUGA
	GCAAAUACGUAGACUCGGA
	GCAGUUGUACCAUGCAUUA
	GCAUCAACUUGCAGAAAGA
CNR1	GCGAGAAACUGCAAUCUGU
	GACCAUAGCCAUUGUGAUC
	GGACAUAGAGUGUUUCAUG
	CAAGAGCACGGUCAAGAUU
Scrambled	UGGUUUACAUGUCGACUAA
	UGGUUUACAUGUUGUGUGA
	UGGUUUACAUGUUUUCUGA
	UGGUUUACAUGUUUUCCUA

ON-TARGETplus siRNA designed by Dharmacon Horizon Discovery, United Kingdom

4.1.5 Antibodies

Table 7: Murine antibodies for flow cytometry

Antigen	Conjugation	Dilution	Reference	Provider
CD11b	PerCP	1:500	101230	Biolegend
CD16/32	purified	1:1000	553142	BD
CD31	PE-Cy7	1:100	102417	Biolegend
CD36	APC	1:1000	Ab133625	Abcam
CD45	Alex eFluoro	1:400	47-0451-82	Invitrogen
CD45.2	FITC	1:500	553772	BD
CD54 (ICAM1)	APC	1:500	116119	Biolegend
CD106 (VCAM1)	PerCP	1:500	105715	Biolegend
CD107a	BV421	1:400	121617	Biolegend
CD115	APC	1:500	17-115-282	eBioscience
Live/dead	Zombie Green	1:800	77476	Biolegend

LOX1	AF647	1:100	FAB1564R	R&D system
Ly6C	PE- Cy7	1:500	560593	BD
Ly6G	APC-Cy7	1:500	127623	Biolegend
SRA1	FITC	1:500	ab151707	Abcam
SRB1	FITC	1:500	NB400-104F	NOVUS

Table 8: Antibodies used for immunohistochemistry

Antigen	Reference	Host	Dilution	Provider
CD31 (PECAM-1)	553370	Rat	1:50	BD
CD54 (ICAM1)	553250	Hamster	1:100	BD
CD68	MCA1957GA	Rat	1:400	Bio-Rad
CD106 (VCAM1)	553329	Rat	1:100	BD
CD144 (VE-Cadherin)	555289	Rat	1:100	BD
Caveolin-1	PA5-17447	Rabbit	1:100	Invitrogen
GPIHBP1	PA5-98598	Rabbit	1:100	Invitrogen
Hoechst 33342	H1399		1:1000	Invitrogen
vWF (Von Willebrand Factor)	Ab11713	Sheep	1:300	Abcam

Table 9: Antibodies used for TPLSM

Antigen	Reference	Host	Dilution	Provider
CD31/eFluor450 (PECAM-1)	48-0311-82	Rat	1:100	eBioscience™
CD106/A594 (VCAM1)	105724	Rat	1:100	BioLegend
Dil-LDL	770230-9	human	1:10	KalenBiomedic

Table 10: Isotype controls for immunohistochemistry

Immunoglobulin	Reference	Provider
Armenian hamser IgG	553969	BD
Normal Goat IgG	ab-108-c	R&D system
Normal rabbit IgG	315-005-003	JIR
Normal rat IgG	6-001-A	R&D system
Normal Sheep IgG	515-005-003	JIR

The working concentration of normal IgG for isotype control are applied same to the specific primary antibody.

Table 11: Secondary antibodies

Antigen	Source	Conjugation	Dilution	Reference	Provider
Anti-goat	Donkey	AlexaFluor594	1:100	705-585-003	JIR

Anti-hamster IgG	Goat	Cy3	1:300	127-165-160	JIR
Anti-rabbit IgG	Donkey	AlexaFluor647	1:600	711-605-152	JIR
Anti-rabbit IgG	Donkey	Cy3	1:300	711-165-152	JIR
Anti-rat	Donkey	AlexaFluor488	1:300	A21208	Invitrogen
Anti-rat	Donkey	Cy3	1:300	712-165-153	JIR
Anti-sheep	Donkey	DyLight® 488	1:300	ab96939	Abcam
Anti-sheep IgG	Donkey	Cy5	1:600	713-175-147	JIR
Anti-sheep IgG	Donkey	Cy3	1:600	713-165-003	JIR

Table 12: Enzymes for Aortic endothelial digestion

Enzyme	Final concentration	Company
Collagenase IV	10 mg/mL	Worthington Biochemical Corp, Lakewood, USA
DNAse I	20 U/mL	Roche, Basel, Switzerland

Table 13: Enzymes for BAT endothelial digestion

Enzyme	Final concentration	Company
Collagenase I	450 U/mL	Worthington Biochemical Corp, Lakewood, USA
Collagenase XI	125 U/mL	Worthington Biochemical Corp, Lakewood, USA
DNAse I	60 U/mL	Roche, Basel, Switzerland
Hyaluronuclease I	60 U/mL	Sigma-Aldrich Chemie GmbH, Munich, Germany

4.1.6 Cell lines

Table 14: Cell lines

Cell line	Description	Culture medium
F20 Flp-In T-Rex 293	Human embryonic kidney cells containing the FRT site, which allows targeted integration of a Flp-In expression vector (pcDNA5/FRT/TO) leading to stable expression levels of the gene of interest.	DMEM
THP-1 cells	THP-1 is a monocyte isolated from peripheral blood from an acute monocytic leukemia patient.	RPMI

HAoECs	Primary human aortic endothelial cell (C-12271,458Z035.1, Promocell) 61-year-old-female donors (C-12271, 434Z005.1, Promocell) 50-year-old-male donors	EC growth medium
HUVECs	Primary human umbilical vein endothelial cells (C-12203,Promocell) Pooled donors	EC growth medium

EC= Endothelial cell;

4.1.7 Consumables

Table 15: Material

Material	Company
0.4 mm µ-Slide I Luer flow chambers (For LSS)	ibidi GmbH, Germany
0.5 mL PD-Tips steril / RNAse free	Brand, Wertheim, Germany
0.8 mm µ-Slide I Luer flow chambers (For OSS)	ibidi GmbH, Germany
8 Well Chamber, removable microscopy glass slide	ibidi GmbH, Germany
8 Well high ibiTreat µ-Slide	ibidi GmbH, Germany
12 well cell culture plate	Corning, Taufkirchen, Germany
40 µm cell strainer blue	BD Falcon, Eysins, Switzerland
70 µm cell strainer white/grey	BD Falcon, Eysins, Switzerland
96 well white clear bottom microplate	PerkinElmer Inc., Waltham, USA
Cell culture flasks 25, 25 cm²	Sarstedt AG & Co. KG, Germany
Centrifuge tubes 15, 50 mL	Corning, Taufkirchen, Germany
Cover glass 10 mm	VWR, Ismaning, Munich, Germany
Cover slips 24x60 mm thickness 1.5 mm	Menzel-gläser, Braunschweig, Germany
Cryomold embedding dish 10 x 10 x 5 mm	Sakura Finetek, Torrance, USA
Cryotube, sterile, pointed, free-standing 1 mL, 2 mL	Corning, Taufkirchen, Germany
Disposable filtration system with 500 mL bottle	Corning, Taufkirchen, Germany
Disposable pipettes 5 to 25 mL	Corning, Taufkirchen, Germany
FACS tubes (5 mL Polystyrene round bottom)	BD Falcon, Eysins, Switzerland
FACS tubes + blue cell strainer	BD Falcon, Eysins, Switzerland
Filter pipette tips	Starlab, Hamburg, Germany
Microcentrifuge tube 0.5 to 5 mL	Starlab, Hamburg, Germany
Microlance needles 23G	BD Falcon, Eysins, Switzerland
Microscope slides 25 x 75 x 1 mm	Menzel-gläser, Braunschweig, Germany
Multiwell cell culture plates flat, sterile 6, 12, 24 well	Corning, Taufkirchen, Germany
Pasteur pipettes, glass, 225 mm	Brand, Wertheim, Germany
Pasteur pipettes, plastic, 2.5 mL, 150 mm	Brand, Wertheim, Germany

PCR tubes	Nippon Genetics, Düren, Germany
Perfusion Set (tubing sets for flow assays)	ibidi GmbH, Germany
Petri dishes 100 mm x 20 mm	Corning, Taufkirchen, Germany
qPCR 96 well plates	Nippon Genetics, Düren, Germany
qPCR clear seal	Nippon Genetics, Düren, Germany
Sealing tape	Corning, Taufkirchen, Germany
SecureSeal™ Hybridization Chambers	Grace Bio-Labs, USA
Syringe sterile 1 to 10 mL	BD Falcon, Eysins, Switzerland
Tissue-tek	Sakura Finetek, Staufen, Germany

4.1.8 Equipment

Table 16: Equipment

Equipment	Company
Centrifuge 5418 R	Eppendorf AG, Hamburg, Germany
Centrifuges Megafuge 1.0R	Heraeus, Hanau, Germany
CO_2 incubator CB 160	BINDER GmbH, Tuttlingen, Germany
Confocal microscope TCS-SP5	Leica Biosystems, Wetzlar, Germany
Cryotome CM3050S	Leica Biosystems, Wetzlar, Germany
ddPCR QX200 BioRad	Bio-Rad, Hercules, USA
Echocardiography Vevo® 3100	FUJIFILM VisualSonics, Toronto, Canada
Eppendorf Mastercycler	Eppendorf AG, Hamburg, Germany
FACS Canto II flow cytometer	BD Bioscience, San Jose, USA
FACSAria III Cell Sorter	BD Bioscience, San Jose, USA
Hood HERAsafe	Heraeus, Hanau, Germany
Ibidi pump system	ibidi GmbH, Germany
In situ Adapter	Eppendorf AG, Hamburg, Germany
Laboratory pH Meter 766	Knick GmbH, Berlin, Germany
Leica CM 3050S cryostat	Leica Biosystems, Wetzlar, Germany
Leica DM6000B microscopes	Leica Biosystems, Wetzlar, Germany
Leica DMi8 microscopes	Leica Biosystems, Wetzlar, Germany
Leica LMD7000 microscopes	Leica Biosystems, Wetzlar, Germany
Leica M205 FCA	Leica Biosystems, Wetzlar, Germany
Leica RM 2235 microtome	Leica Biosystems, Wetzlar, Germany
Nanodrop ND1000 Peqlab	VWR International, Radnor, USA
PCR Plate Spinners	VWR International, Radnor, USA

PCR Thermocycler Biometra Tpersonal	Biometra GmbH, Göttingen, Germany
QuantStudio 6 Real-Time PCR Systems	Thermo Fisher Scientific, Eugene, USA
Surgical tools complete set	F.S.T (Fine Science Tools)
TC20 Automated Cell Counter	Bio-Rad Laboratories GmbH, Feldkirchen, Germany
Tecan F200 PRO microplate reader	Tecan Group, Maennedorf, Switzerland
Thermomixer F1.5	Eppendorf AG, Hamburg, Germany
TissueLyser LT	Qiagen, Hilden, Germany
Two-photon excitation fluorescence microscope (LeicaSP5IIMP)	Leica Biosystems, Wetzlar, Germany
Vortex Mixer TX4	VELP Scientifica, Usmate, Italy
Water bath type 1004	Memmert WB14 (Memmert GmbH + Co. KG)
Water Purification System Milli-Q	Merck Millipore, Billerica, USA

4.1.9 Software

Table 17: Software

Software	Company
BD FACSDiva software	BD Bioscience, San Jose, USA
ddPCR software - Quantasoft	Bio-Rad Laboratories GmbH, Feldkirchen, Germany
FlowJo v10.3	Tree Star, Inc., OR, USA
GraphPad Prism 10.0.2	GraphPad Software Inc, USA
Image J software/FIJI	National Institutes of Health, USA
IMARIS x64 (7.6.5)	Bitplane, United Kingdom
LAS V4.3	Leica Biosystems, Wetzlar, Germany
LAS X Office	Leica Biosystems, Wetzlar, Germany
Leica LAS X 3.11 image processing software (3D analyses package)	Leica Biosystems, Wetzlar, Germany
QuantStudio 6 System Software	Thermo Fisher Scientific, CA, USA
VevoLAB Version 5.7.0	FUJIFILM VisualSonics, Toronto, Canada

4.2 Methods

4.2.1 Mouse model

4.2.1.1 Animal model of atherosclerosis

To investigate the impact of endothelial *Cnr1 in* atherosclerosis, *Cnr1*$^{flox/flox}$ mice[169] were first crossed with *Apoe*$^{-/-}$ mice to generate *Apoe*$^{-/-}$*Cnr1*$^{flox/flox}$ mice. *Apoe*$^{-/-}$*Cnr1*$^{flox/flox}$ mice were then crossed with *Bmx*^{CreERT} expressing mice[170] to achieve *Apoe*$^{-/-}$*Bmx*$^{Cre(+/-)}$*Cnr1*$^{flox/flox}$ mice. The deletion was induced by intraperitoneal injection (i.p.) of tamoxifen (1 mg per 20g body weight,

dissolved in corn oil) at 8 weeks of age, administered for 5 days to activate the inducible *Bmx*^{CreERT} transgene expression for selective Cre recombination in arterial ECs. Same administration was applied to *Apoe*$^{-/-}$*Bmx*$^{Cre(+/-)}$ and *Apoe*$^{-/-}$*Cnr1*$^{flox/flox}$ mice as control. Following tamoxifen induction, the mice rested for 10 days before being administered a Western diet (WD) for either 4 or 16 weeks. The diet consisted of 21% fat and 0.2% cholesterol (Ssniff, TD88137). Animals were housed in separate ventilated cages, with 4 to 6 mice in each cage. The environment was air-conditioned, with a 12-hour light-dark cycle and a temperature of 23°C and 60% relative humidity. All animal procedures were carried out ethically and approved by the local Ethics committee. (District Government of Upper Bavaria; License Number: 55.2-1-54-2532-111-13 and 55.2-2532.Vet_02-18-114) and adhered to institutional national guidelines, as well as the ARRIVE guidelines.

4.2.1.2 Mouse dissection

For each experiment, mice underwent anaesthesia with ketamine (80 mg/kg) and xylazine (12 mg/kg) adjusted to individual body weight via a 1 mL insulin syringe equipped with a 30 G needle for anaesthesia. Blood samples were collected by cardiac puncture using a 26 G needle microtube. Immune cell detection in blood was measured by flow cytometry using 50 µL blood per mouse. Plasma was collected after centrifugation at 3000 x g for 10 min to examine cholesterol and triglyceride levels. For the endocannabinoid measurement in plasma, the plasmas were snap frozen using liquid nitrogen and kept at -80 °C until analysis. Before the organ harvesting, any remaining blood was eliminated by 10 mL phosphate-buffered saline (PBS) perfusion. Following that, hearts, spleens, and femurs were collected, and aortas were prepared from the aortic arch down to the iliac bifurcation for quantifying lesions. Heart tissues were stored in Tissue-Tek and maintained at -20 °C for aortic root cryosections, while RNA extraction was conducted on rapidly frozen organs using liquid nitrogen. For flow cytometry analysis, organs were immersed in PBS and kept chilled on ice until they were prepared for subsequent procedures.

4.2.1.3 Pharmacological peripheral CB1 antagonist administration

To investigate the impact of the peripheral CB1 antagonist JD5037[171] on atherosclerosis, another atherosclerotic mouse model, *Ldlr*$^{-/-}$ mice[172], was employed. The mice were first fed eight weeks of WD to induce atherosclerotic plaque formation. Subsequently, the mice were randomly divided into two groups. One group received daily i.p. injection with JD5037 (3 mg/kg) for 8 weeks, while the other group (Vehicle group) was injected i.p. in the equal volume of vehicle buffer composed of 10% DMSO, 40% PEG300, 5% Tween 80, and 45% Saline. The mice in both groups were continuously fed with WD throughout the experiment. After 16 weeks of WD, the mice were harvested according to the described procedure. Aortic roots, aortic

arches and descending aortas were collected for atherosclerotic plaque lesion size measurement.

4.2.1.4 Permeability assay

Evans blue (EVB) solution at 0.5% was prepared in 0.9% saline and sterilized by filtering. Mice were intravenous (i.v.) injected through the tail with 200 µL of EVB solution per 25 mg mouse (40 mg/kg) and sacrificed 30 min post-injection. Upon euthanization, 5 mL of PBS was subsequently perfused through the mice to remove remaining blood. The entire aorta was collected, fixed with 4% paraformaldehyde (PFA) for 30 min, and positioned on slides for imaging (image settings for EVB excitation peaks: 470 nm and 540 nm, with an emission peak at 680 nm). Tilescan z-stacks of the whole aorta were taken with Leica DM6000B microscopes for EVB detection followed processed with Leica Application Suite LAS V4.3 software for EVB fluorescence intensity quantification.

4.2.2 Metabolic measurement

4.2.2.1 Plasma cholesterol and triglycerides measurement

The plasma cholesterol concentrations were detected utilizing a colorimetric assay known as CHOD-PAP (Roche). The plasma from WD-feeding mice was diluted at a 1:9 ratio with 0.9% saline solution prior to analysis, while the chow diet-feeding mice were diluted at a 1:3 ratio with 0.9% saline. Similarly, plasma triglyceride levels were detected by another colorimetric assay (CPO-PAP, Roche), which did not necessitate any dilution for the plasma samples. For calibration, the calibrators from the kit were dissolved in distilled water according to the kits´ instructions to a final cholesterol concentration of 160 mg/dl and a triglyceride concentration of 130 mg/dl. To establish the standard curve, the calibrators were diluted in 0.9% saline using serial dilution. A precise volume of 5 µL was transferred from each standard or from the diluted plasma samples into a 96-well microtiter plate with a flat bottom, and each sample was measured in duplicate. Subsequently, plates were filled with 200 µL per well of the CHOD-PAP CHOL reagent or the CPO-PAP TG for detection. After incubating at room temperature (RT) for 30 min, the plate was subjected to absorbance measurement at 450 nm using a Tecan Infinite F200 PRO microplate reader. The cholesterol and triglyceride concentrations of each sample were calculated in relation to the standard curve.

4.2.2.2 Plasma bile acid measurement

Colorimetric assay (TBA, Sentinel Diagnostics) was employed for the detection of plasma bile acid levels, without the need for dilution of the plasma samples. The enzyme 3-alpha-hydroxysteroid dehydrogenase (3-alpha-HSD) repeatedly catalyses the oxidation and reduction of serum bile acid molecules, leading to the accumulation of reduced co-enzyme

thio-NADH, which can be detected at a specific wavelength (404 nm). A volume of 2 µL was transferred from standard or plasma sample into a 96-well microtiter plate with a flat bottom. Each sample was measured in duplicate. Plates were loaded with 150 µL of reagent 1 (containing Thio-NAD^+) per well and incubated at RT for 300 seconds. Following this, 50 µL of reagent 2 (containing NADH and 3a-HSD) was added to each well, and the mixture was incubated at RT for 68 seconds for the initial reading. The second reading was taken after an additional 140 seconds of incubation. The absorbance at 404 nm was measured using a Tecan Infinite F200 PRO microplate reader for the plate. For calibration, the calibrators from the kit were dissolved in distilled water according to the kits' instructions to a final bile acid concentration of 50.2 µmol/L. Results were calculated following the formula.

Total bile acid (µmol/L)= $\mathrm{STD} \times \frac{\Delta Abs/\,min\,Sample}{\Delta Abs/\,min\,STANDARD}$

ΔAbs= Reading 2- Reading 1

4.2.2.3 Glucose tolerance tests

For the glucose tolerance test, mice underwent a 6-hour fasting period with access to water. Following the fasting period, an i.p. injection of glucose (2 g/kg) was administered to the mice. Blood samples were collected from the caudal vein, and glucose levels were measured at specific time intervals (0, 15, 30, 60, and 120 min) using a glucometer (Accu-Chek, Mannheim, Germany). The blood collection method remained consistent across all time points, ensuring uniformity in the experimental procedure.

4.2.3 Flow cytometry

4.2.3.1 General flow cytometry measurement procedure

An aliquot of 50 µL whole blood was directly transferred to ice-cold FACS tubes. Splenocytes were derived by gently mashing spleens through a 70 µm cell strainer into a 50 mL tube, followed by rinsing with 15 mL of FACS buffer. Femurs were first gathered in chilled PBS, with subsequent exposure of the distal metaphysis, and then transferred to a 1.5 mL Eppendorf tube with a pre-cut 1 mL tip. Following this, the tubes underwent centrifugation at 10,000 x g for 1 min to collect the bone marrow cells. Splenic, bone marrow and blood erythrocytes were then lysed with ammonium-chloride-potassium (ACK) buffer for 10 min at RT. After the ACK lysis step, splenocytes underwent additional filtration using a 40 µm cell strainer before proceeding to the staining process.

Cell suspensions were incubated with FACS staining antibody mix for 30 min at 4°C in the dark to label the leukocyte cell subsets. After incubation, the cell suspensions were washed with 1 mL of FACS buffer and then centrifuged at 400 x g for 5 min. The supernatant was removed, and the cell pellet was reconstituted with 300-500 µL of FACS buffer based on the cell count.

The cells were kept in the dark at 4°C until the analysis was conducted. The BD FACSCanto II flow cytometer (BD Biosciences) was applied to acquire flow cytometry data, which were later analysed using FlowJo v10.2 software (Tree Star, Inc). Cells from blood, spleen and bone marrow were first gated $CD45^{+}CD11b^{+}$ myeloid subsets and further gated as following: $CD115^{+}Ly6G^{-}$ (monocytes), $CD115^{-}Ly6G^{+}$ (neutrophils).

4.2.3.2 Endothelial cell sorting

For the transcriptomic profile of *Cnr1*-deficient EC during atherogenesis, aortic and brown adipose tissue EC from mice fed a 4-week WD were sorted and sent for bulk RNA sequencing. For isolating aortic EC, the murine vessels were first excised from the aortic arch to the iliac bifurcation. The excised vessels underwent digestion using 10 mg/mL collagenase IV (Worthington) and 20 U/mL DNase I (Table 12) at 37°C for 40 min. Subsequently, the digested aorta was filtered through a 30 µm cell strainer and rinsed with PBS to obtain aortic cells. Following centrifugation, the cells were suspended in a FACS staining antibody mix and incubated in the dark for 30 min at 4°C to label aortic EC subsets.

To isolate EC from BAT, the interscapular brown adipose tissue (BAT) was collected from the mice and transferred to a 12-well plate containing a 1 mL digestion cocktail (Table 13). The tissue was then cut into small pieces and left in the incubator to digest for 30 min at 37°C. Following digestion, the processed BAT was initially filtered through a 70 µm cell strainer, followed by a subsequent filtration through a 30 µm cell strainer to eliminate any remaining tissue fragments. The cells were then suspended in a FACS staining antibody mix and incubated in the dark for 30 min at 4°C to label BAT EC subsets.

After incubation, the cell suspensions were washed with 1 mL of FACS buffer and then centrifuged at 400 x g for 5 min. The supernatant was removed, and the cell pellet was reconstituted in 150 µL of FACS buffer for sorting. The BD FACSAria™ III Cell Sorter was employed for sorting EC from aorta and BAT by gating at Live $CD45^{low}CD31^{high}CD107a^{high}$ and Live $CD45^{-}CD31^{+}$ respectively (Table 7).

4.2.3.3 ROS production measured by flow cytometry

HAoECs were transfected with either 20 nM *CNR1* or scrambled siRNA (Table 6), following the transfection protocol in section 4.2.5.4. After 24 h of transfection, the cells were stimulated with 10 ng/mL TNFα for 30 min. Subsequently, the HAoECs were washed with PBS and incubated with 1 µM DHR-123 (Dihydrorhodamine) for 20 min at 37°C to label ROS production. The cells were then collected after trypsin-EDTA (0.25%) detachment, centrifuged at 300 x g for 5 min, and resuspended in 100 µL of FACS buffer for flow cytometry measurement. Data was obtained with BD FACSDiva software and then evaluated and analysed using FlowJo

v10.2 software; the geometric mean (MFI) for the ROS channel was plotted into the results graph.

4.2.4 Histology

4.2.4.1 Aorta en face preparation

Aortic arch and abdominal aortas were isolated from mice following euthanasia and heart perfusion with 10 mL of pre-cooled PBS. The isolated aortas were placed in 1.5 mL Eppendorf tubes with 1% PFA solution overnight and change to PBS stored at 4°C until further processing. After fixation, the thoracic aortas were transferred to a petri dish containing PBS. Sequentially, the aortas were carefully opened following the sequence (Figure 16) under a dissecting microscope (Leica), with the removal of fat and connective tissue. Subsequently, the opened aorta was fixed with minutiae pins (F.S.T) on the rubber slides. The abdominal aortas were cut along the yellow dotted lines, and the subsequent procedure followed the same.

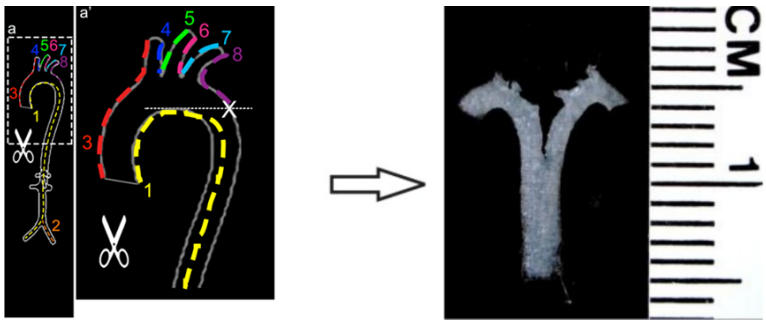

Figure 16. En face preparation of aorta.
Dotted lines along the vessel wall indicate sequence cuts to be made to open the vessels. Schematic adapted from Pei-Yu Chen *et al.*[173] The open vessel is shown on the right. Scale: 1 division = 1 mm. Images adapted from Kyung Ae Ko *et al.*[174]

4.2.4.1.1 En face lesion quantification

The en face aortic arch and abdominal aortas were prepared as described above. Subsequently, it underwent imaging using a Leica M205 FCA microscope equipped with a 2.5x objective. For quantifying lesions, the ImageJ software was employed to delineate lesion areas using the “polygon selection” tool (Figure 17). Subsequently, the selected areas underwent analysis within the Region of Interest (ROI) management function through measurement and recording. The relative plaque percentage was then determined by normalizing the plaque area to the aorta area.

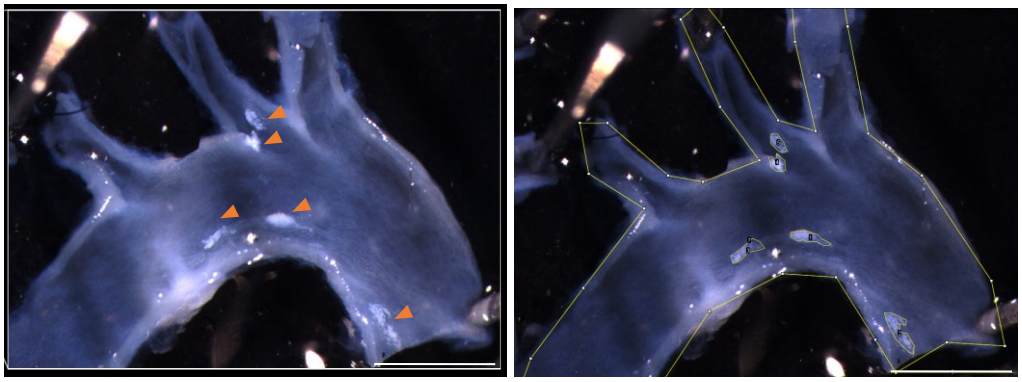

Figure 17. Lesion analysis of en face aorta.
Representative en face aortic arch from 4 weeks WD *Apoe*$^{-/-}$*Bmx*$^{Cre\ (+/-)}$ mice captured by Leica M205 FCA microscope, the errors on this image highlight the presence of plaques (Left). For lesion quantification image, the 'polygon selection' function from ImageJ software was employed to delineate lesion areas (Right). Scale bar: 1 mm

4.2.4.1.2 En face immunostaining of thoracic aortas

The en face thoracic aortas were isolated from mice to stain vascular endothelial (VE)-cadherin to check the impact of *Cnr1* in endothelial morphology. In contrast to the previous procedure, the heart of the mice was perfused with 20 mL of pre-cooled PBS containing 20% FBS, followed by an additional 10 mL of 4% PFA after euthanization.[174] The opened aortas were transferred to 12 well plate, each well containing 0.5 mL of 4% PFA for 10 min fixation. Subsequently, permeabilization was carried out using 0.1% Triton X-100 in PBS for a duration of 10 min. After a 30-min incubation in blocking buffer at RT, the aortas were exposed to primary antibodies, anti-CD144 and anti-CD54 (Table 8). The plate underwent an overnight incubation on a shaker at 4ºC. Afterwards, aortas were washed with PBS and incubated with secondary antibodies: anti-rat IgG or combination of AlexaFluor488 donkey and Cy3 goat anti-Armenian hamster.[174] The incubation occurred for 1 h on a shaker at 300 rpm at RT. After 3 times PBS washing, the tissues were then transferred to a slide glass smoothly while avoiding trapping bubbles. The slides were coated with Ibidi Mounting Medium containing DAPI and fixed by putting a 3.5 kg weight book on top for 5 min. This ensured the flattening of the tissues. Nail polish was applied at the 4 corners to seal the coverslips. The slides were imaged with confocal microscope TCS-SP5 (Figure 18). Fluorescence intensity of VE-Cadherin (CD144) and ICAM1 (CD54) were quantified by 5-10 images at the bifurcation of aortic arch (atheroprone sites) or descending thoracic aorta (atheroresistant sites) per animal with ImageJ software.

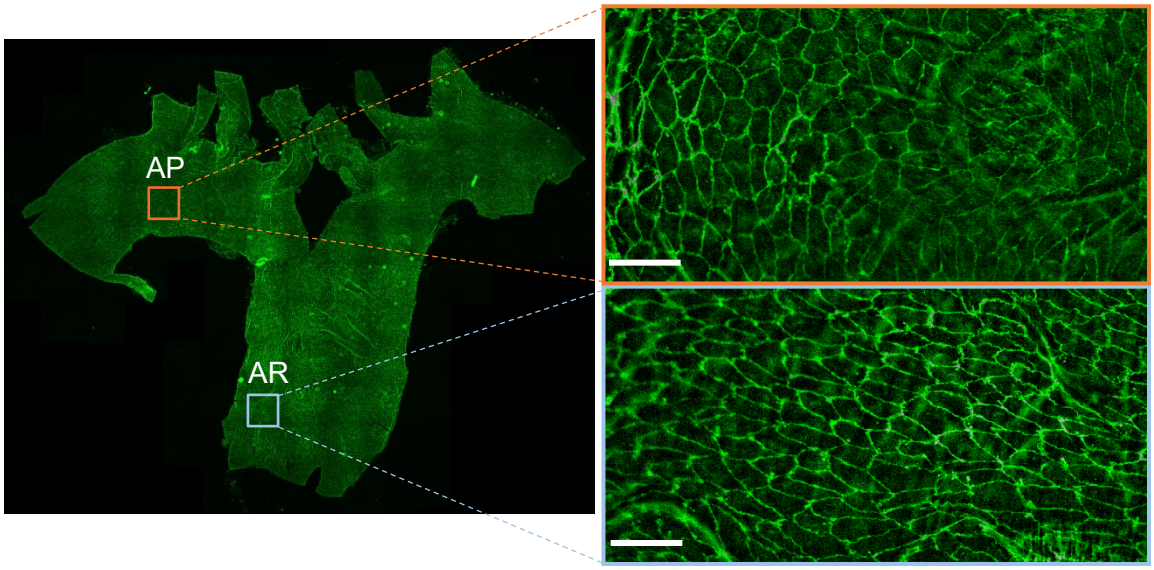

Figure 18. En face imaging of thoracic aorta.
On the left, representative en face thoracic aorta with zoomed-out view is presented, while on the right, specific regions are magnified: the aortic arch (atheroprone sites, AP, in orange) and the descending thoracic aorta (atheroresistant sites, AR, in blue) displaying distinct endothelial morphology. The images were captured using Leica DM6000B microscopes. Scale bar: 50 µm. VE-Cadherin in green.

4.2.4.2 Oil Red O staining for aortic roots

To perform transverse sections of the aortic root valves, first, the hearts were cut into half and placed flatly in the frozen blocks filled with OCT. To facilitate freezing, a pyrex beaker was filled with 2-methylbutane, which had been cooled with liquid nitrogen. These frozen blocks were sealed in airtight bags and stored at -20°C until further processing. For aortic root cryosections, 5 µm thick serial sections were sliced using Cryotome CM3050S machine. The sections were collected at the beginning of the three aortic valves' onset and continued until they were no longer visible. Typically, eight serial sections per slide for ten microscope slides, covering a total area of 400 µm were collected. Half of these sections were fixed in 4% Roti-Histofix for 10 min and stored at RT, while the unfixed sections were kept at -20°C for further immunofluorescence staining.

To evaluate the development of aortic root lesions, 5 µm thick cryosections of aortic root employed for Oil Red O (ORO) staining. After a 5 min rehydration in PBS, the slides were left to air-dry for an additional 5 min. The ORO working solution was prepared by diluting 120 mL of the ORO stock solution with 80 mL of ddH_2O. After an hour of stirring, the mixture was carefully filtered and utilized for lipid staining. The process took 15 min in the ORO working solution followed by dipping 10 times in 60% isopropanol. The slides received a brief rinse with running tap water, followed by nuclear counterstaining using hematoxylin. Upon completing the air-drying phase, Immu-Mount was used to mount the slides. Lesion quantification was carried out with LAS V4.3 software, and images were captured using the Leica DM6000B fluorescent microscope. Mean values were determined based on eight serial sections, each

stained with a 50 µm interval, for each mouse heart.

4.2.4.3 RNA fluorescence *in situ* hybridization (FISH) on murine tissues

To determine the endothelial *Cnr1* expression in the "atheroprone" and "atheroresistant" sites of aorta, RNA-FISH assay was performed employing viewRNA cell plus kit (Table 3) with the instructions kindly provided by Dr. Lucia Natarelli.[175] The en face thoracic aorta of *Apoe*$^{-/-}$ mice were placed in a 1.5 mL RNAase-free Eppendorf tube and incubated with a custom probe for murine *Cnr1* (1:60, VB6-17606, Table 1) for the target probe hybridization process at 40±1°C for 2h. Following this, the tissues underwent three washes with wash buffer at RT. Subsequently, the tissues were incubated with the pre-amplifier mixture at 40±1°C for 30 min, washed again with wash buffer, and then exposed to the amplifier mixture for an additional 1 h to enhance the signal. At the end of hybridization, tissues were incubated with blocker buffer for 1 h then incubated with a primary antibody anti-CD31 for detecting EC, followed by AlexaFluor488 anti-rat secondary antibody staining for 30 min at RT after washing with PBS (Table 11). The nuclei were stained with Hoechst 33342 at a concentration of 1:1000 in PBS with 0.1% Tween 20. The tissues were then transferred to a slide glass smoothly while avoiding trapping bubbles. The slides were coated with Immu-mount and fixed by putting a 3.5 kg weight book on top for 5 min. This ensured the flattening of the tissues. Nail polish was applied at the 4 corners to seal the coverslips.

For FISH in aortic root cryosections, the sections were collected from on RNAse-free slides (slides pre-treated with RNAse ZAP before collection). The cryosections were fixed in 4% PFA for 5 min, followed by treatment with pre-warmed 10 µg/mL proteinase K (diluted in PBS) for 5 min at RT. Subsequently, post-fixation was carried out with 100% ethanol for 1 min. The prepared slides were then mounted with SecureSeal™ Hybridization Chambers, enabling the sections to be incubated with the FISH solution. The slides were then placed on the in-situ adapter of the Eppendorf Mastercycler machine at 40±1°C following the same FISH procedure as described above. Afterwards, the chambers were removed, and the slides underwent three PBS washes. The slides were stained with CD31 and Hoechst 33342, following the same procedure. Images were taken using a confocal microscope TCS-SP5. An average of 5-10 images per condition per mouse were acquired and subsequently quantified using ImageJ software.

4.2.4.4 Hematoxylin-eosin staining of arch

Microtome was applied to cut the 5 µm thickness paraffin section of aortic arch and conducted lesion assessments using Haematoxylin-eosin (H&E) staining. The paraffin sections underwent a deparaffinization process, which included sequential treatments: 2 times xylene, followed by 100% ethanol, 95% ethanol, 70% ethanol, and 2 times H_2O washing, with each

treatment lasting 2 min. Nuclei were exposed to Mayer's haematoxylin solution at RT for 5 min, followed by a 5-min rinse in running tap water. Next, 3 min incubation with Eosin Y-solution. The slides underwent a dehydration process, comprising 95% ethanol, 100% ethanol, and xylene, with each step lasting 2 min. After allowing the slides to air dry, an antifade mounting medium (Entellan, Merk) was applied to mount the slides. Images were captured using the Leica DM6000B fluorescent microscope, and lesion size measurements were performed with LAS V4.3 software. Lesion size was assessed by calculating the cumulative inner vessel area ratio. For each mouse, 4 sections were selected range 200 µm with a 50 µm interval between each section. Average values were calculated from these measurements.

4.2.4.5 Masson trichrome staining

Masson Trichome staining was applied to examine the content of collagen and necrotic core within the plaque. The frozen aortic root cryosections were gently rinsed with distilled water and subsequently immersed in Bouin's solution at RT for overnight fixation. The next day, the sections were rinsed with tap water and incubated in Weigert's working haematoxylin for 10 min and Biebrich scarlet for 5 min, respectively. Then, the sections were incubated with a working solution containing phosphotungstic and phosphomolybdic acids for 15 min. An aniline blue solution was then carefully applied to the sections for the other 5 min at RT. Finally, sections were meticulously rinsed in a 1% acetic acid solution for 1 min and rinsed with distilled water before mounting. Between each step, the slides were washed with distilled water to remove any unbound material. Finally, the slides were dehydrated and mounted with non-water mounting media DPX. For image analysis, three valves of the aortic root were imaged by Leica Thunder DM6000B microscope at 20x magnification. Quantification was performed on 3-5 sections per animal for each condition. Both collagen and necrotic areas were normalized to the total plaque area using LAS V4.3 software (Leica) as a percentage. An unpaired T-test was applied for statistical analysis.

4.2.4.6 Nile red staining

Nile red staining was applied to examine the lipid content within the plaque. Five µm aortic root cryosections were first washed in distilled water for 5 min then stained for 5 min with 500 µL/mL Nile red solution diluted in glycerol and water. After washing, the slides were mounted with vectashield with DAPI. LAS V4.3 software was employed for lesion quantification, and the Leica DM6000B fluorescent microscope was utilized to capture images. Nile red signal was detected at (515/585 nm) and the fluorescence intensity of Nile red positive area was quantified by using LAS V4.3 software (Leica). Three to five sections were quantified as mean value for each animal. An unpaired T-test was applied for statistical analysis.

4.2.4.7 ICAM1, VCAM1 and CAV1 staining in aortic arch

Aortic arches were fixed in 1% PFA overnight and embedded in paraffin for longitudinal sectioning (5 µm). The tissue sections were first deparaffinized and underwent antigen retrieval using high-temperature microwave heating with antigen retrieval buffer (Table 2). The sections were cooled down at RT for at least 20 min and moved to PBS container to wash for 5 min. After 30 min of blocking, Tissue sections were then incubated overnight at 4ºC targeting CAV1, ICAM1, and vWF, or VCAM1 and vWF (Table 8). As negative controls, the appropriate IgG controls were applied (Table 11). Subsequently, the corresponding Alexa Fluor secondary antibodies were applied and left for 30 min at RT for staining. Finally, the slides were stained with Hoechst 33342 (Thermo Fisher) for nuclei and mounted with Immuno Mount™. Quantification was conducted on 4 sections per animal, with a 50 µm interval between each section imaged by a Leica Thunder DM6000B microscope at 20x magnification. To determine the percentage of ICAM1/VCAM1/CAV1-positive ECs, the number of ICAM1/VCAM1/CAV1-positive cells was calculated and normalized to vWF positive cells using LAS V4.3 software (Leica). An unpaired T-test was applied for statistical analysis.

4.2.4.8 GPIHBP1 immunofluorescence staining in brown adipose tissue

Brown adipose tissues (BAT) were fixed in 4% PFA overnight and embedded in paraffin for longitudinal sectioning (4 µm). The paraffin sections were first deparaffinized and antigen retrieval was performed as described above. Tissue sections were then incubated overnight at 4ºC with primary antibody against GPIHBP1 and vWF after blocking with blocker buffer for 30 min at RT, followed by corresponding secondary antibody staining for 30 min at RT (Table 8). Finally, the slides were stained with Hoechst 33342 for nuclei and mounted with Immuno Mount™. The stained sections were imaged using Leica Thunder DM6000B microscope (Leica). The double positive area of GPIHBP1 and vWF was quantified by using LAS V4.3 software (Leica).

4.2.4.9 *Ex-vivo* imaging of adhesion molecular and lipid uptake

VCAM*1* expression and DiI-LDL (3,3'-dioctadecylindocine-low density lipoprotein) uptake of endothelium was analysed in vital murine carotid arteries collected from *Apoe*$^{-/-}$*Bmx*$^{Cre\ (+/-)}$ (referred to *Cnr1*$^{EC\text{-}WT}$) and *Apoe*$^{-/-}$*Bmx*$^{Cre\ (+/-)}$ *Cnr1*$^{flox/flox}$ (referred to *Cnr1*$^{EC\text{-}KO}$) mice (n=5-7). Utilizing an *ex vivo* arterial perfusion assay as described in the previous publication (system was set up by Dr. Remco Megens),[176] freshly isolated carotid arteries were mounted in arterial perfusion chambers. These arteries were incubated with antibodies against VCAM1 (Table 9) under a static pressure of 80 mmHg for 10 min at 37°C. After a thorough PBS wash, DiL-LDL was loaded onto the arteries and incubated for 90 min at 80 mmHg and 37°C. Following the removal of unbound antibodies and DiL-LDL through artery flushing, visualization was carried

out using a Leica SP5 IIMP two-photon laser scanning microscope coupled to a Ti:sapphire laser (Spectra Physics MaiTai DeepSee) tuned at 800 nm. A 20× NA1.00 (Leica) water dipping objective was utilized, and spectral detection employed internal Hybrid Diode detectors (n=4) tuned for optimal contrast between various targets while maintaining sufficient fluorescence signal intensity from the arterial wall. Three-dimensional image processing and quantification of VCAM1 and DiL-LDL distribution per endothelial cell were performed using Leica LASX 3.11 software, utilizing 3D analyser and lightning plugins.

4.2.5 Cell culture and functional assays

Human Primary Aortic Endothelial Cells (HAoECs) from 61-year-old female donor (C-12271, PromoCell) were seeded on 0.2% Gelatin-coated plates or ibidi chamers in Endothelial Cell Growth Medium (ECGM; C-22010, PromoCell) supplemented with 1% Penicillin-Streptomycin at 37°C in a humidified atmosphere containing 5% CO2. Subculturing with trypsin-EDTA (0.25%) and medium refreshing were performed according to manufacturer´s protocol. Cells were used at passage 4 to 6 for experiments. F20 Flp-In T-Rex 293 cells were cultured with DMEM and passaged using Trypsin-EDTA (0.05%)

4.2.5.1 Shear stress assays

HAoECs were seeded in gelatin-coated ibidi chambers (Table 15) and exposed to either LSS 10 dyne/cm² or OSS 1±3 dyne/cm² using the ibidi pump system in Endothelial Cell Growth Medium (ECGM) for 24 h.[177, 178] Subsequently, cell lysis was performed, and RNA was extracted using the RNeasy Plus Mini Kit, following the manufacturer's instructions for detecting *Cnr1* and endocannabinoid synthesis and degradation enzyme mRNA expression. Every experiment was matched with a corresponding control derived from the same cell preparation, incubated for an identical duration but without the application of flow (Figure 19); they are referred to as static controls. These experiments were independently replicated 3 times.

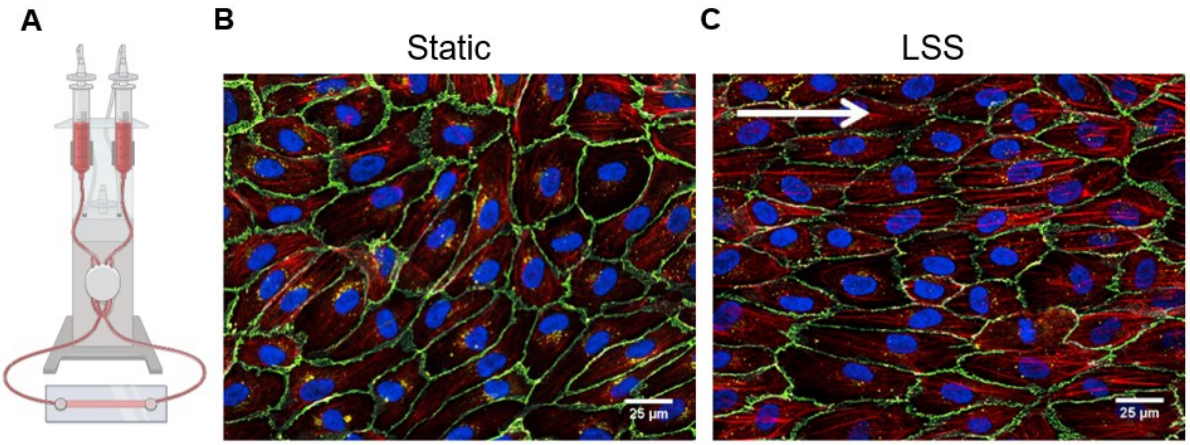

Figure 19. Application of shear stress *in vitro*.
(A) Schema of the perfusion chamber and the mechanism used to produce the shear stress. Representative immunofluorescence images of human umbilical vein endothelial cells (HUVEC) in **(B)** static and **(C)** LSS conditions. The error indicates the function of the flow. Cytoskeletal F-actin is stained with phalloidin (Red), the adherence junctions are labelled with VE-Cadherin (Green), Nuclei are stained with Hoechst 33342 (Blue). Images adapted from ibidi.com.[179]

4.2.5.2 Monocyte adhesion assay under flow

HAoECs were cultured as previously described. Cells were incubated with or without the CB1 agonist ACEA (1 µM) under LSS at 10 dyne/cm² in ibidi chambers for 24 h. Following the cessation of flow, the chambers were washed with PBS and then incubated with 5 ng/mL TNF-α (R&D) overnight. Subsequently, 1*10^5 monocytes/mL human leukaemia monocytic cells (THP-1), purchased from ATCC, were labelled with 0.5 µM calcein (Invitrogen) and added to the perfusion sets. THP-1 and HAoECs were co-cultured under LSS flow conditions at 37°C for 3 hours. After the system disconnected to the flow, the chambers were subjected to three rounds of pre-warmed PBS washing to remove unadhered monocytes, and the entire chambers were imaged using the Inverted Microscope Leica DMi8 S Platform with the Tilescan function at 20x magnification. For quantification, at least 5 different area views of images per condition were selected. Adhered THP-1 cells were identified by calcein labelling (494 nm/517 nm), and the number of adherent THP-1 monocytes to HAoECs was quantified per mm² using ImageJ software.

4.2.5.3 Dil-LDL uptake

HAoECs were cultured as described above, cells incubated with or without CB1 agonist ACEA (1 µM) under LSS for 24 h. Afterward, cells were washed with PBS and lysed for *ICAM1*, *VCAM1*, *NOS3*, *KLF2*, *PKKFB3* and *CAV1* mRNA detection. For Dil-LDL uptake assessment under ACEA treatment (Figure 20A), the chambers were disconnected after the flow and incubated with 1 µg/mL Dil-LDL in ECGM without supplements under static conditions for 1.5 h at 37°C. Following three washes with PBS, the cells were fixed with 2% PFA and

permeabilized with 0.1% Triton X-100. Afterwards, chambers were washed thrice with PBS and mounted with Ibidi Mounting Medium containing DAPI. The images were acquired by Inverted Microscope DMi8 S Platform (Leica) at 20x objective. Mean DiI-LDL (550nm/564nm) fluorescent intensity were quantified from 5-10 images per condition and calculated from 3-4 independent experiments using LAS V4.3 software (Leica)

For the AM281 combined with PKA inhibitor experiments (Figure 20B), the administration of AM281 occurred 20 min before exposing the HAoECs to OSS. To inhibit PKA activity, the PKA inhibitor KT5720 (1 μM) was added 1 h prior to AM281 treatment. After 24h OSS, the chambers were disconnected to the flow and incubated with 1 μg/mL DiI-LDL in ECGM without supplements under static conditions for 30 min at 37°C. The cells underwent fixation and permeabilization, followed by incubation with a primary antibody against CAV1 after 1h blocking. The next day, chambers were washed thrice with PBS, followed by 1h incubation with Alexa Fluor 647 anti-Rabbit secondary antibodies at RT. The chambers were mounted with Ibidi Mounting Medium containing DAPI and imaged using an Inverted Microscope DMi8 S Platform (Leica) at 63x objective. Mean DiI-LDL (550nm/564nm) and CAV1 fluorescent intensity were quantified from 5-10 images per condition and calculated from 3-4 independent experiments using LAS V4.3 software (Leica).

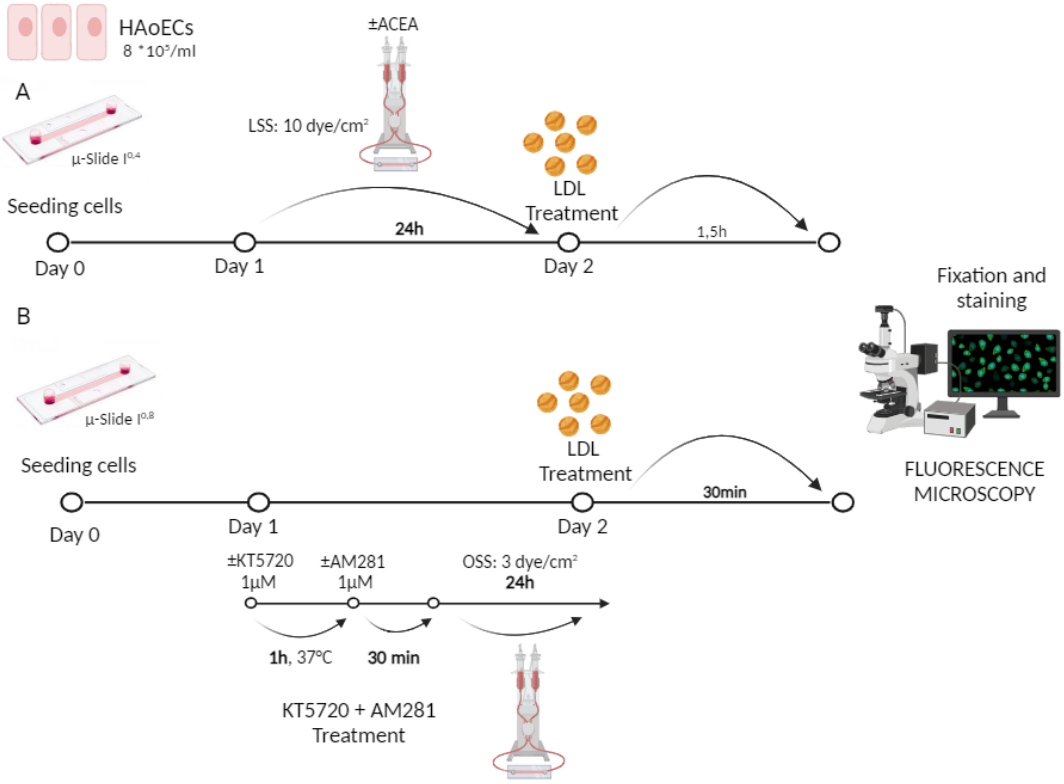

Figure 20. DiI-LDL uptake after shear stress exposure.
Schematic of the workflow for LDL uptake experiments in HAoECs. **(A)** Cells were treated with ACEA and exposed to 24 h of LSS before a 1.5-hour DiI-LDL incubation. **(B)** The cells were treated with a PKA inhibitor, followed by AM281, and subsequently exposed to 24 h of OSS before undergoing a 30 min period of DiI-LDL incubation. Images generated from Biorender.com (https://www.biorender.com/).

4.2.5.4 siRNA knockdown

SiRNA duplexes directed against human *CNR1* and *CAV1* (Dharmacon, Table 6). Scrambled siRNA (Dharmacon) was used as a control. The transfection medium was prepared according to manufacturer's protocol. In short, *siCNR1* and transfection medium were prepared separately. SiRNA against *CNR1/CAV1* was added to Opti-MEM (Gibco) without antibiotics in a 20 nM final concentration. Transfection medium was made adding RNAiMAX (ThermoFisher) to Opti-MEM. All solutions were incubated for 5 min at RT and subsequently carefully mixed incubated for another 20 min at RT. The final transfection solution was added to the cells with 800 µL ECGM and incubated overnight in at 37C°. Next day, medium was changed and 24 h after transfection, cells were lysed for RT-PCR experiment.

4.2.5.5 cAMP detection

4.2.5.5.1 GloSensor cAMP assay

To assess the signalling of G protein Gαi/o-coupled receptor CB1 in response to agonist ACEA or antagonist AM281 stimulation, the GloSensor cAMP assay was generated relies on a luciferase-based biosensor for real-time monitoring of intracellular cAMP changes. The GloSensor luciferase contains a cAMP binding site; upon binding to cAMP, this molecule undergoes a change in its shape or conformation, leading to luminescence activity directly correlating with the cAMP level. In this experiment, F20 Flp-In T-Rex 293 cells stably expressing CB1 after tetracycline stimulation, along with the GloSensor luciferase, were plated in a white 96-well microplate with a clear bottom. A culture medium supplemented with 4% Poly-D-lysine was used for cell seeding (100 µL per well). To stimulate receptor expression, 1 µg/mL tetracycline (achieving a final concentration of 0.5 µg/mL in the well) was introduced to 100 µL of the culture medium. Afterwards, the cells were placed at 37°C for a minimum of 48 h until reaching complete confluence. When the cells are 100% confluence, the cells were washed with HBSS buffer (Table 1). Then, 2.5% (v/v) Luciferin-EF (Promega) in 67.5 µL of HBSS buffer was first loaded in the plate for 1 hour's incubation in the dark at RT. After the incubation, a white adhesive bottom seal was applied to the clear bottom, and the basal luminescence was measured using a Tecan Infinite F200 PRO microplate reader at 23°C for 5-10 cycles until the values are stable. Subsequently, 7.5 µL of stimulus (10x) was added to each well to final 75 µL volume for 1:10 dilution, and the potential changes in intracellular cAMP levels were monitored for 5-10 cycles. This was followed by the addition treatment of forskolin (Final concentration 1µM), a direct activator of adenylyl cyclase, and the increasing cAMP levels were tracked for another 15 cycles. The relative light units were then normalized to the basal level (mean value of 5 cycles after reading stabilized).

4.2.5.5.2 Cyclic AMP (cAMP) measurement by ELISA

To measure intracellular cAMP concentrations, HAoECs glowed in 12 well plates were pretreated with 3-isobutyl-1-methylxanthine (0.5 mM, IBMX, Table 1) for 30 min and then stimulated with CB1 antagonist AM281 or CB1 agonists ACEA for 20 min. 3 µM Forskolin (Table 1) were used as positive control followed manufacturer's instructions. Cells were then lysed with 0.1 M HCl with 20 min incubation at RT and assayed for cAMP levels with a commercial kit (Cyclic AMP Select ELISA kit, table 3) according to manufacturer's instructions with slight alterations. Briefly, the plate was already with capture antibody coated, not necessary to rinse the plates prior to adding the reagents. The standards were diluted with 1mL ELISA buffer following a serial dilution in a 2-fold manner, covering a concentration range of 0.09 pmol/mL to 200 pmol/mL. Each plate contains a minimum of two blanks (Blk), two non-specific binding wells (NSB), two maximum binding wells (B_0), and an 8-point standard curve run in duplicate. The samples were diluted 1:2 in ELISA buffer and incubated 18 h at 4°C after loaded in the 96 well plate. Subsequently the plate was washed 5 times with wash buffer and added 200 µL of Ellman's reagents each well for development 90-120 min on an orbital shaker with a plastic film covered. Then, 5 µL tracer was added to the TA wells. After development, the plate cover was removed and read determined with a Tecan Infinite F200 PRO microplate reader at a wavelength between 405 and 420 nm. Interpolation was performed on sample values from a standard curve generated by fitting a fourth-order polynomial through nonlinear regression using GraphPad Prism 10.0.2.

Blk=Blank

TA=Total activity (5 µL Tracer)

NSB=Non-specific binding (100 µL ELISA buffer+50 µL Tracer)

B_0=Maximum Binding (50 µL ELISA buffer+50 µL Tracer+50 µL Antiserum)

Std/Sample (50 µL Std/Sample+50 µL Tracer+50 µL Antiserum)

4.2.6 Biomolecular methods

4.2.6.1 RNA isolation

Total RNA was extracted from murine organs with 500 µL of peqGOLD TriFast and Qiagen TissueLyser steel beads facilitated frozen tissue lysis at 50 Hz for 2 min. The cell suspension was transferred to a new 1.5 mL tube and chloroform (100 µL) was added for RNA extraction, followed by vortexing at maximum frequency for 30 s and by a 15 min centrifugation at 12000 x g, creating three distinct layers: the lower phase with proteins, the interphase with genomic DNA, and the upper RNA-containing phase. To prevent genomic DNA contamination, RNA was transferred to a new tube without touching the interphase. The RNA extraction was carried out using the peqGOLD Total RNA Kit from Peqlab Biotechnologie following the manufacturer's

instructions. For the cell lysis using RNeasy Plus Mini Kit (Table 3) followed the kit's instruction. The yield and purity of the RNA were determined using a Nanodrop 100.

4.2.6.2 Reverse transcription

A total of 1 µg of the isolated RNA was transformed into complementary DNA (cDNA) by using the PrimeScript RT reagent kit from TaKaRa, following the instruction provided in Table 18 for the reverse transcription (RT) reaction mix.

Table 18: RT reaction mix

Reagent	Amount for 1 µg RNA
5x PrimeScript Buffer	2 µL
PrimeScript RT Enzyme mix I	0.5 µL
Oligo dt Primer (50 µM)	0.5 µL
Random6mers (100 µM)	2 µL
RNA	1 µg
Add with RNase-free H_2O	10 µL

The reverse transcription (RT) was conducted in a PCR thermocycler, following the program outlined in Table 19. The transcribed cDNA was then diluted with RNase-free H2O to achieve a concentration of 5 ng/mL.

Table 19: RT program

Temperature	Time
37 °C	15 min
85 °C	5 s
4 °C	∞

4.2.6.3 Quantitative real time PCR (qPCR)

To assess gene expression differences across various groups, we employed quantitative real-time PCR with TaqMan technology, utilizing the KAPA PROBE FAST Universal qPCR kit from Peqlab Biotechnologie. The amplification of specific genes involved the use of primers and probes, either custom-designed from MWG or obtained from Life Technologies as pre-designed primer-probe mixes.

Table 20: Primer-probe mix

Self-designed 4x primer-probe mix		**Pre-designed 4x primer-probe mix**	
Primer fwd (100 µM)	4 µL	Primer-probe-Mix	0.5 µL
Primer rev (100 µM)	4 µL	Nuclease-free H_2O	ad 5 µL
Probe (100 µM)	1 µL		
Nuclease-free H_2O	ad 250 µL		

Table 21: qPCR reaction mix

Reagent	**Amount**
Master mix 2x	10 µL
Primer-probe mix 4x	5 µL
cDNA (5 ng/µL)	5 µL
Total	20 µL

Table 22: qPCR FAST program

Temperature	**Time**
95 °C	20 Sec
95 °C	1 Sec
60 °C	20 Sec

A 4x primer-probe mix was prepared following the instructions in Table 20. This mix was then combined in the qPCR reaction, as detailed in Table 21, and loaded into a semi-skirted 96-well qPCR plate. The qPCR was carried out using a 7900HT Sequence Detection System, following the program outlined in Table 22. The analysis was carried out using SDS2.4 Software. Hypoxanthine-Guanine-Phosphoribosyltransferase (*Hprt*) was used as the endogenous control. In the comparison of gene expression in brown adipose tissue, a second housekeeping gene, Ubiquitin C (*Ubc*), was utilized. Target gene expression was normalized to the endogenous control and presented as a fold change of the *Cnr1*$^{EC\text{-}WT}$ mice or static conditions, calculated using the following formulas:

$$dCt = Ct\ (gene\ of\ interest) - Ct\ (endogenous\ control)$$

$$ddCt = dCt\ (treated) - average\ dCt\ (untreated)$$

$$fold\ change = 2^{-ddCt}$$

4.2.6.4 Droplet digital PCR

The Bio-Rad ddPCR system, QX200, was used for ddPCR detection. The reaction mixture comprised 2× ddPCR Supermix from Integrated DNA Technologies and 20× primers and probes (at concentrations of 900 nM and 250 nM, respectively). The total volume of the cDNA in the reaction was 20 µL (Table 23). Droplet generation was executed using the QX200 droplet generator (Bio-Rad) by combining 20 µL of the reaction mix with 70 µL of droplet generation oil for probes (Bio-Rad) on DG-8 cartridges covered with gaskets (BioRad). Subsequently, 42 µL of the resulting droplet solution, containing up to 20,000 droplets, was transferred to the appropriate PCR plate (BioRad) and sealed with a piercing foil using the PCR plate sealer (Bio-Rad). The cycling process was carried out in the ddPCR cycler, featuring the following conditions outlined in Table 24: 60 min at 50 °C (reverse transcription), 10 min at 95°C (enzyme activation), 30 seconds at 94°C (denaturation), and 1 min at 60°C (annealing/extension) for 40 cycles, concluding with 10 min at 98°C (enzyme deactivation). The PCR plate was inserted into the droplet reader (Bio-Rad) and analysed using QuantaSoft software (Bio-Rad).

Table 23: Preparation of the reaction mix.

Component	Volume per Reaction,µL	Final Concentration
Supermix	5	1x
Reverse transcriptase	2	20 U/µL
300 mM DTT	1	15 mM
Target primers/probe	Variable	900 nM/250 nM
RNase-/DNase-free water	Variable	-
Total RNA	Variable	100 fg-100 ng per reaction
Total volume	20	-

Table 24: Thermal cycling conditions

Cycling Step		Temperature (°C)	Time	Number of Cycles
Hold (QX ONE ddPCR sysem only)		25	3 min	1
Reverse transcription		42-50	60 min	1
Enzyme activation		95	10 min	1
Denaturation		95	30 Sec	40
Annealing/extension		55-65	1 min	40
Enzyme deactivation		98	10 min	1
Hold	QX200 ddPCR System	4	Infinite	1
	QX ONE ddPCR System	25	1 min	1

4.2.6.5 RNA sequencing

As detailed above, EC were isolated and sorted from the aorta and BAT of 4 weeks WD Cn*r1*$^{EC\text{-}WT}$ or *Cnr1*$^{EC\text{-}KO}$ mice (n=6). The sorted EC were lysed with RLT Plus Buffer (Qiagen) and kept at -80°C until RNA extraction. The RNA extraction and library operations were conducted in collaboration with Prof. Enard (LMU), and libraries were sequenced at the LMU GeneCenter. The bioinformatic analysis was performed by a colleague, Guo Li.

To perform differential gene expression analysis, DESeq2 (Version 1.37.4), a Bioconductor package implemented in R version 4.2.0 (2022-04-22), was utilized. The analysis was executed on an Ubuntu 20.04.3 LTS system, employing the negative binomial distribution for the necessary computations. Initially, size factors and sample dispersion were estimated, followed by utilizing Negative Binomial GLM fitting and computing Wald statistics using DESeq2. DESeq2 was applied to identify differentially expression genes (DEGs) based on the criterion of an adjusted P value below 0.10.[180, 181] Gene ontology (GO) enrichment analysis was conducted using the enrichplot (Version 1.17.2) Bioconductor package,[182] employing DEGs filtered by an adjusted P value < 0.10. The CHEA3 web server was employed to predict the top 15 transcription factors (TFs) regulating DEGs.[183] The volcano plot was created using the ggplot2 package (Version 3.4.0). Gene Set Enrichment Analysis (GSEA) was performed using GSEA software (version 4.3.2), which was tailored for the Windows operating system. The analysis utilized curated gene sets (M2), ontology gene sets (M5) and Hallmark gene sets sourced from mouse collections.[184] Pathways were considered significant according to predefined criteria, encompassing a normalized enrichment score below -1 or above 1, a false discovery rate below 0.25, and a nominal P value less than 0.05.[185]

4.2.7 Statistic

Statistical analysis was conducted using GraphPad Prism version 10.0.2 (GraphPad Software, Inc.). The data is presented as the mean ± standard error of the mean (SEM). Normality was assessed using either the D'Agostino Pearson omnibus or Shapiro-Wilk normality test within the software. The Mann-Whitney U test was utilized when the data did not adhere to a normal distribution. For comparisons between two groups, the student's unpaired t-test was applied if the data exhibited a Gaussian distribution (a normal distribution with equal variances) after confirming variances through an F-test. In cases where variances significantly differed, Welch's t-test was employed. In the context of multiple groups with consideration for a single variable in comparisons, either one-way analysis of variance (ANOVA) with Tukey post hoc test or repeated-measures (RM) one-way ANOVA with Tukey post hoc test, depending on the experimental design. When two independent factors were involved, a two-way ANOVA with a Bonferroni post hoc test was applied for statistical testing. Outliers were identified using Tukey's method. P-values less than 0.05 were considered statistically significant.

5. RESULTS

5.1 Endothelial CB1 expression is induced by atheroprone shear stress

5.1.1 Endothelial *Cnr1* mRNA expression in atheroresistant and atheroprone region of *Apoe*$^{-/-}$ aorta

Previous studies have illustrated that ECs exhibit distinct phenotypes instructed by their specific location within the artery. In the descending thoracic aorta, which is defined as an atheroresistant region, ECs experience uniform and laminar blood flow. However, at branch points such as the inner curvature of the aortic arch, the blood flow is disturbed, making the arterial wall susceptible to atherosclerosis (= atheroprone area).[186] This prompted us to study whether the expression of the CB1 receptor on ECs is influenced by shear stress. To explore this, an en face *in situ* hybridization was conducted to detect the mRNA expression of endothelial *Cnr1* in the atheroresistant and atheroprone regions of the aorta in 8-week-old *Apoe*$^{-/-}$ mice. Interestingly, a more intense endothelial *Cnr1* expression signal was detected in atheroprone regions of the aortic arch, compared to the atheroresistant region of the descending thoracic aorta (Figure 21A-D). This observation suggests that the expression of endothelial *Cnr1* is differently regulated in response to shear stress.

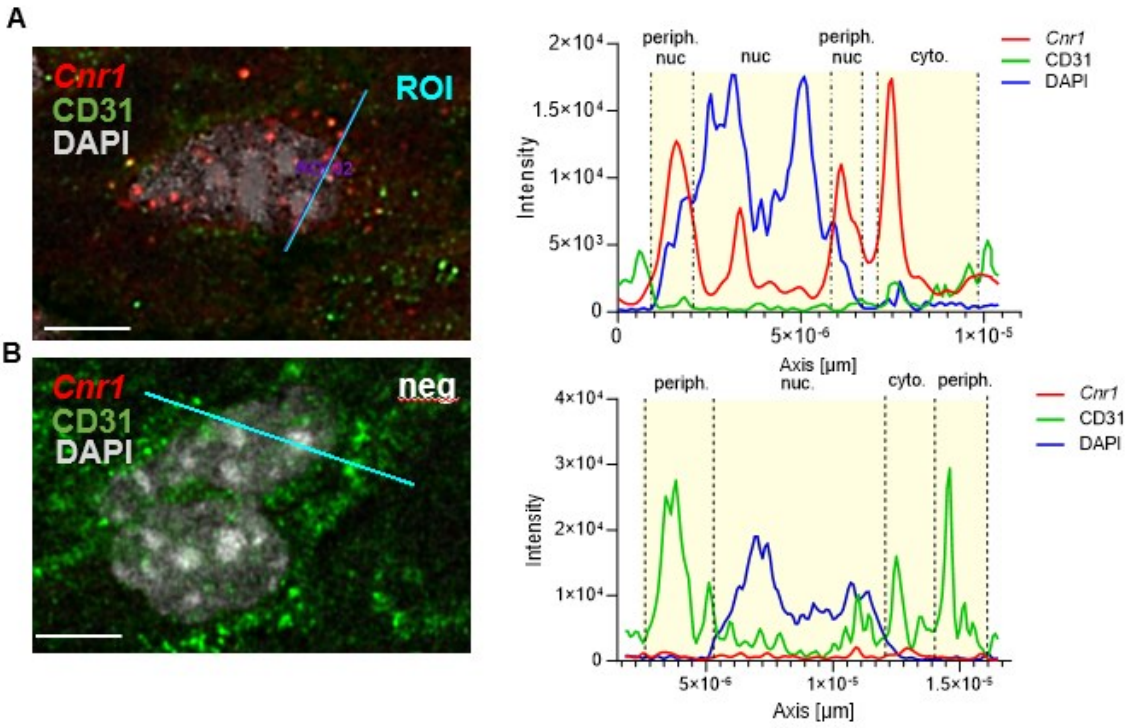

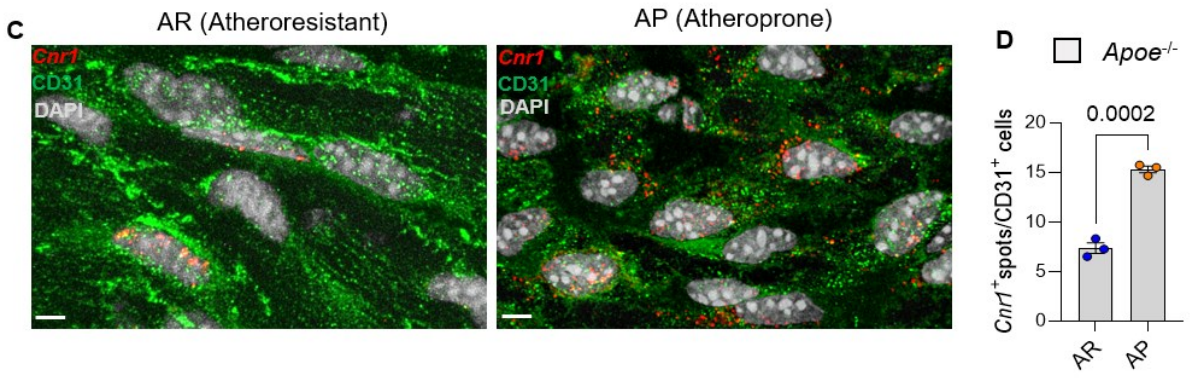

Figure 21. *In situ* endothelial *Cnr1* expression in *Apoe*$^{-/-}$ thoracic aorta.
(A-B) En face *in situ* hybridization was performed for *Cnr1* and corresponding negative control in thoracic aortas of 8-week-old *Apoe*$^{-/-}$ mice The intensity of *Cnr1* (Red), CD31 (Green) and DAPI (Grey) within endothelial cells in the region of interest (ROI) was quantified using IMARS, as presented on the **right** Scale bar: 5 µm. **(C)** *Cnr1* fluorescence *in situ* hybridization within the descending thoracic aorta (atheroresistant, AR) and aortic arch (atheroprone, AP) of the same *Apoe*$^{-/-}$ mouse. **(D)** A total of 3 *Apoe*$^{-/-}$ mice were included in the analysis; 10-15 images per mouse were acquired for quantification. The data were presented as the mean ± standard error of the mean (S.E.M.), with each data point on the graph representing an individual mouse. The P values were calculated through an unpaired Student's t-test.

5.1.2 Human endothelial *CNR1* mRNA expression is induced by oscillatory shear stress

To futher explore this regulation *in vitro*, a flow culture model was established with the ibidi pump system to modulate shear stress responses in HAoECs (Figure 19).[177, 178] As expected, after exposure to LSS for 24 h, HAoECs had a more elongated shape and were aligned in flow direction as opposed to cells cultured in static conditions. Instead, a cobblestone-like morphology was observed in HAoECs after exposure to OSS for 24 h (Figure 22A). In line with the *in vivo* data in *Apoe*$^{-/-}$ thoracic aortas, 2-fold higher *CNR1* mRNA levels were observed in HAoECs cultured under OSS conditions compared to static conditions (Figure 22B). This was accompanied by a relative increase in mRNA expression of the endocannabinoid synthesis enzyme *DAGL* and a relative decrease in the expression of the endocannabinoid degradation enzyme *MAGL*, although these changes did not reach significance (Figure 22B). Collectively, these data indicate that endothelial CB1 expression is regulated in response to the blood flow with enhanced endocannabinoid-CB1 signalling under OSS conditions in the atheroprone region of the aorta.

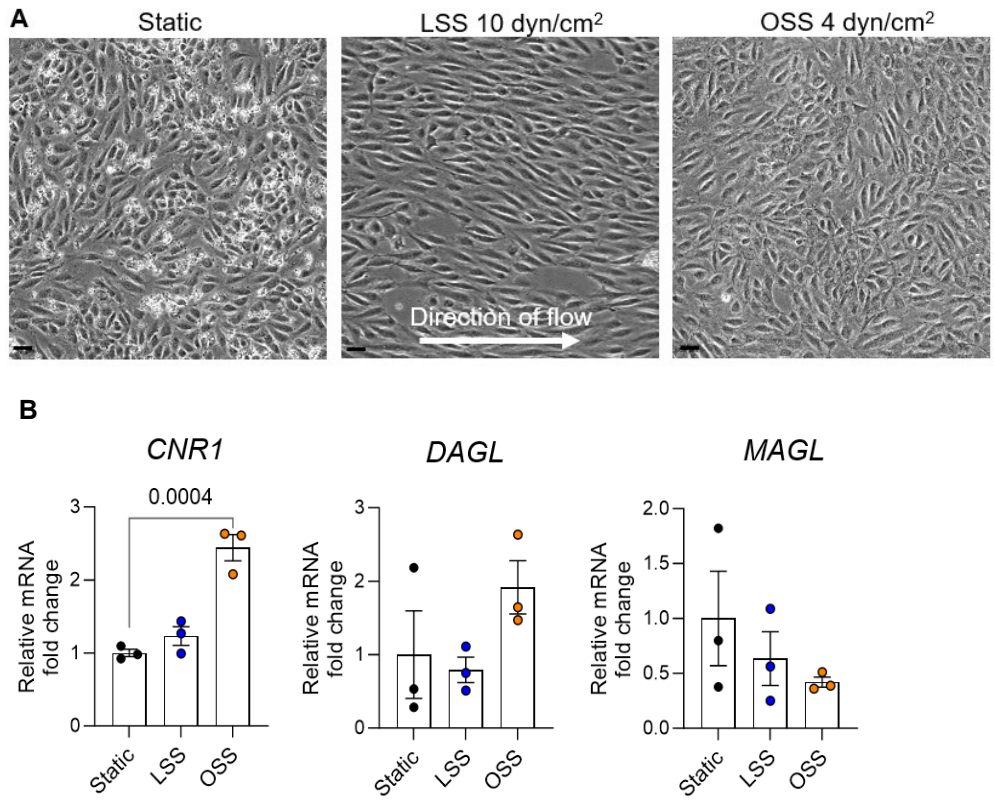

Figure 22. HAoECs cell culture under flow generates minimal mechanical shear stress.
(A) Representative images of HAoECs after 24 h exposure to LSS (10 dyn/cm^2) or OSS (3 dyn/cm^2) compared to static conditions. Scale bar: 50 µm. **(B)** *CNR1* and endocannabinoid synthesis and degradation enzyme *DAGL* and *MAGL* mRNA levels determined by RT-qPCR. The data are displayed as mean ± s.e.m., and each dot on the graph represents an independent experiment (n=3). The P values were calculated through a one-way ANOVA followed by a post-hoc Tukey multi-comparison test. Exact p-values are shown in the graph.

5.2 Endothelial *Cnr1* deficiency affects aortic endothelial morphology and integrity

5.2.1 *Cnr1* expression in murine endothelial cells and mouse model establishment

To study the specific role of endothelial CB1 in atherosclerosis, *Cnr1*$^{flox/flox}$ mice were bred with *Bmx*$^{CreERT+/-}$ mice on an *Apoe*$^{-/-}$ background to generate endothelial cell-specific *Cnr1* deficient mice (*Apoe*$^{-/-}$*Bmx*$^{Cre(+/-)}$*Cnr1*$^{flox/flox}$), here after referred as *Cnr1*$^{EC\text{-}KO}$ mice. The deletion was induced by intraperitoneal injection of tamoxifen at 8 weeks of age, administered continuously for 5 days to activate the inducible *Bmx*^{CreERT} transgene expression for selective Cre recombination in arterial endothelial cells (Figure 23A).[187] Similarly, tamoxifen was administered to *Apoe*$^{-/-}$*Bmx*$^{Cre(+/-)}$ mice, referred to as *Cnr1*$^{EC\text{-}WT}$ mice. In aortic root sections from *Cnr1*$^{EC\text{-}WT}$ mice, *in situ* hybridization revealed the expression of *Cnr1* in ECs of atherosclerotic plaque. These ECs were identified through CD31$^+$ immunofluorescence staining. However, the *Cnr1* signal was absent in the ECs from *Cnr1*$^{EC\text{-}KO}$ mice (Figure 23B),

This result confirms the successful knockdown of endothelial *Cnr1* in our mouse model.

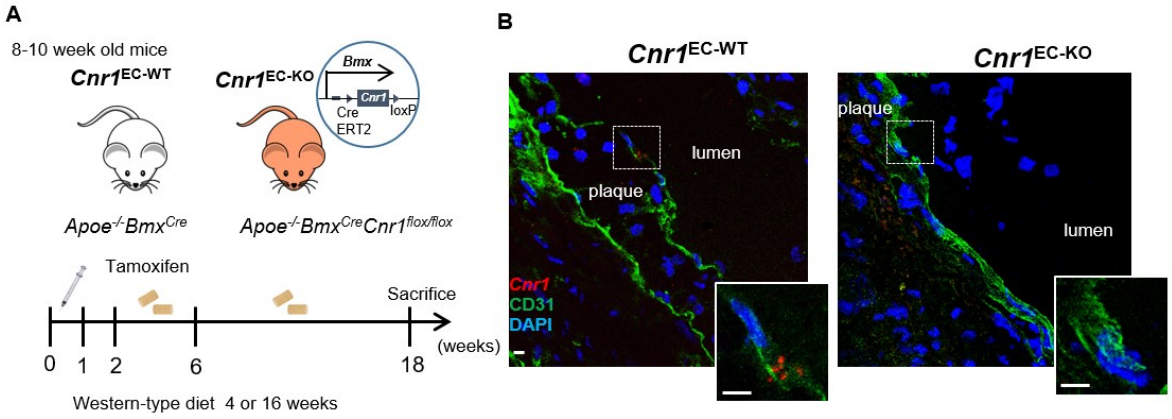

Figure 23. Validation of mouse model with selective endothelial *Cnr1* depletion.
(A) Experimental scheme: age-matched *Cnr1*$^{EC-WT}$ and *Cnr1*$^{EC-KO}$ received daily intraperitoneal injections of tamoxifen for 5 days and were subsequently fed with 4 or 16-week Western diet (WD). (**B**) Representative images of *in situ* hybridization for *Cnr1* (red) combined with CD31 (green) immunostaining to detect ECs, and Hoechst 33342 staining (blue) of nuclei in aortic root sections of *Cnr1*$^{EC-WT}$ and *Cnr1*$^{EC-KO}$ mice. Scale bar: 20 µm (overview) and 5 µm (insert).

5.2.2 Depletion of *Cnr1* in endothelial cells alters the morphology of the aortic endothelium

Oscillatory flow disrupts ECs alignment and promotes vascular inflammation, leading to the upregulation of ICAM1 expression.[188,189,190] Given that endothelial CB1 expression is induced by OSS, it is intriguing to speculate that depletion of *Cnr1* may contribute to endothelial cell alignment and anti-inflammatory responses. Therefore, en face staining for the EC junctional protein vascular endothelial (VE)-cadherin and adhesion molecule ICAM1 was carried out with thoracic aortas isolated from *Cnr1*$^{EC-KO}$ and *Cnr1*$^{EC-WT}$ mice (Figure 24A). No significant differences in VE-cadherin expression were observed between *Cnr1*$^{EC-KO}$ and *Cnr1*$^{EC-WT}$ mice, possibly due to the high variability between the individual data points (Figure 24B). ECs in *Cnr1*$^{EC-KO}$ aortas appeared more elongated than those in *Cnr1*$^{EC-WT}$, although the measurement of the elongation factor did not reveal a statistically significant difference (Figure 24C). Consistent with earlier discoveries,[191, 192] elevated ICAM1 expression was observed in the EC of the aortic arch (atheroprone region) compared to those in the descending thoracic aorta (atheroresistant region) in this study. Notably, downregulation of ICAM1 expression was found in ECs from both regions of *Cnr1*$^{EC-KO}$ mice compared to those in *Cnr1*$^{EC-WT}$ mice, indicating an anti-inflammatory response resulting from endothelial *Cnr1* depletion (Figure 24D).

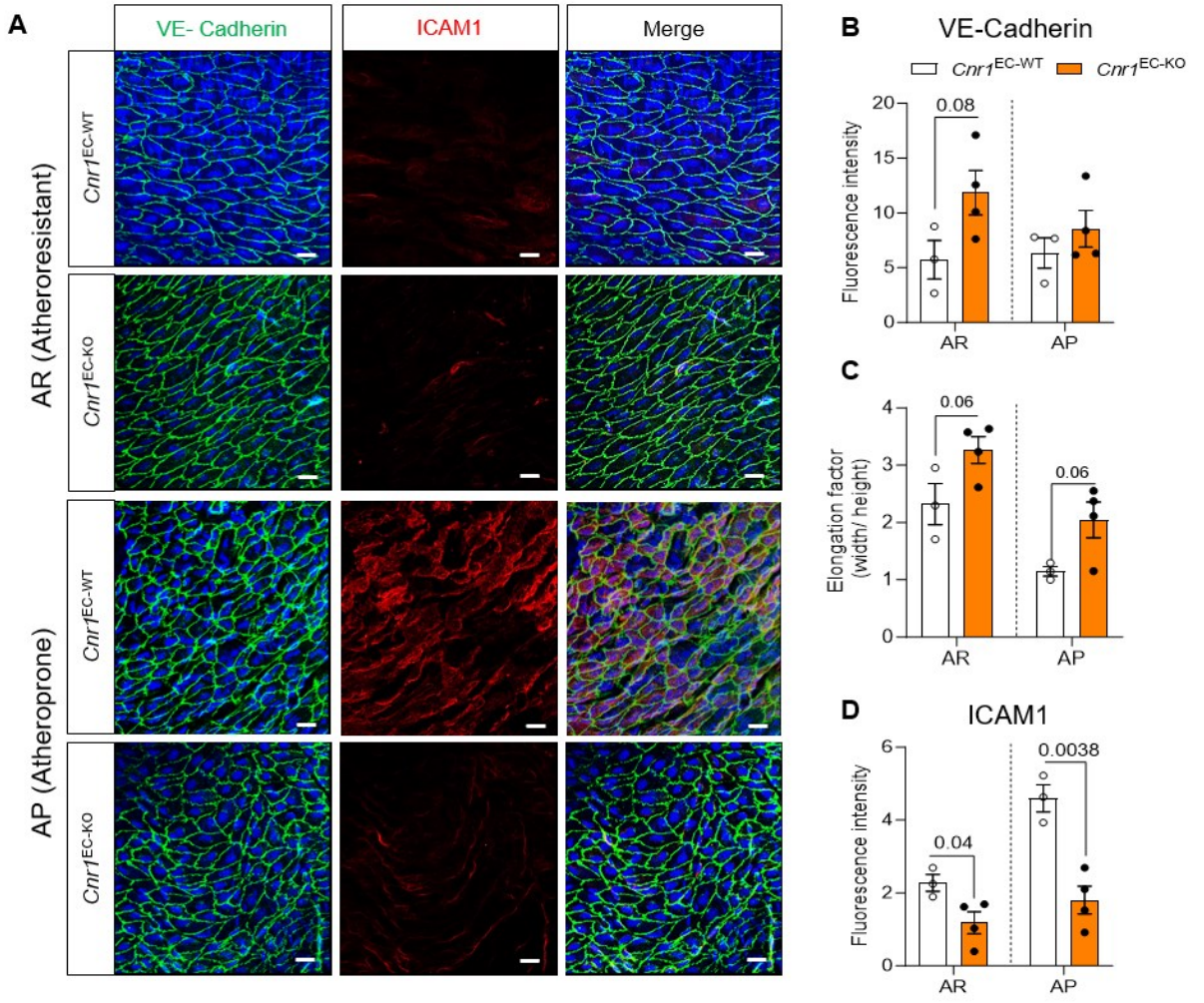

Figure 24. En face VE-cadherin and ICAM1 staining in *Cnr1*$^{EC-KO}$ and *Cnr1*$^{EC-WT}$ aorta.
(A) The aortic arch (atheroprone, AR) and descending thoracic aorta (atheroresistant, AR) were isolated and prepared for en face staining from *Cnr1*$^{EC-WT}$ mice (n = 3) and *Cnr1*$^{EC-KO}$ mice (n = 4). Staining for VE-cadherin (green), ICAM1 (red), and DAPI (blue) to visualize the intercellular junctions, adhesion molecules and nuclei. The images were captured by confocal microscopy. Scale bar: 20 µm. **(B-C)** VE-Cadherin, ICAM1 fluorescence intensity (in 10-15 images per mouse) and **(D)** EC elongation factor (of 20 randomly selected cells per image) were quantified with ImageJ. Data are shown as mean ± s.e.m. P values were obtained using an unpaired Student's t-test for AR and AP separately.

5.2.3 Impact of endothelial *Cnr1* deficiency on endothelial integrity

Enhanced arterial inflammation leads to increased endothelial permeability, thereby fostering the formation of intimal lesions through the facilitation of inflammatory leukocyte extravasation.[193] Next, the impact of endothelial CB1 on vascular permeability was assessed by monitoring the leakiness of aortic arches and descending aortas through the intravenous injection of Evans blue into mice fed with atherogenic diet for four weeks to induce arterial inflammation (Figure 25A). Remarkably reduced Evans blue leakage was observed in the aorta of *Cnr1*$^{EC-KO}$ mice, particularly in atheroprone sites such as the inner curvature of the aortic arch, indicating preserved endothelial integrity in *Cnr1*$^{EC-KO}$ mice (Figure 25B).

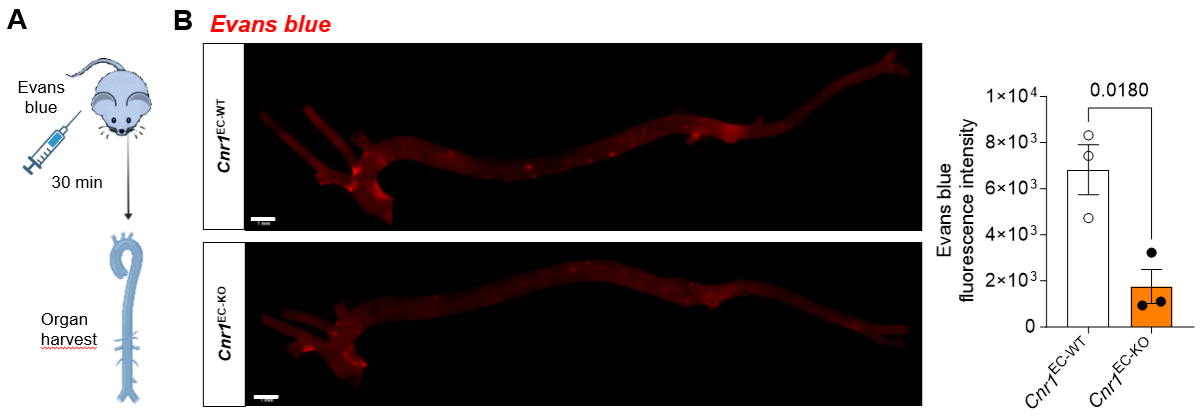

Figure 25. Evans blue intravenous injection in *Cnr1*$^{EC\text{-}KO}$ and *Cnr1*$^{EC\text{-}WT}$ mice.
(A) Schematic representation of endothelial permeability assay, based on Evan´s blue extravasation into aortas 30 min after i.v. Injection. **(B)** Representative images and quantification of Evan´s blue fluorescence intensity in aortas of *Cnr1*$^{EC\text{-}KO}$ and *Cnr1*$^{EC\text{-}WT}$ mice (n =3). Images were taken with a Leica DM6000B microscope and quantified by LAS V4.3 software. Scale bar: 1 mm. Data are shown as mean ± s.e.m. P values were calculated through an unpaired Student's t-test by GraphPad Prism.

5.3 The impact of endothelial CB1 deficiency on atherosclerosis progression

5.3.1 Effects of endothelial *Cnr1* on plaque development

To further investigate the functional role of endothelial CB1 in atherosclerosis, *Cnr1*$^{EC\text{-}KO}$ and *Cnr1*$^{EC\text{-}WT}$ mice were fed with WD for 4 weeks or 16 weeks, respectively, to assess early and advanced atherosclerosis. At the 4-week time point, both male and female *Cnr1*$^{EC\text{-}KO}$ mice exhibited comparable plaque sizes to those of *Cnr1*$^{EC\text{-}WT}$ mice in aortic roots (Figure 26A and 26B), while female *Cnr1*$^{EC\text{-}KO}$ mice developed less plaques in the aortic arch compared to *Cnr1*$^{EC\text{-}WT}$ mice (Figure 26C). No significant differences in circulating leukocyte counts were observed between *Cnr1*$^{EC\text{-}KO}$ and *Cnr1*$^{EC\text{-}WT}$ groups, both in male and female mice (Figure 26D).

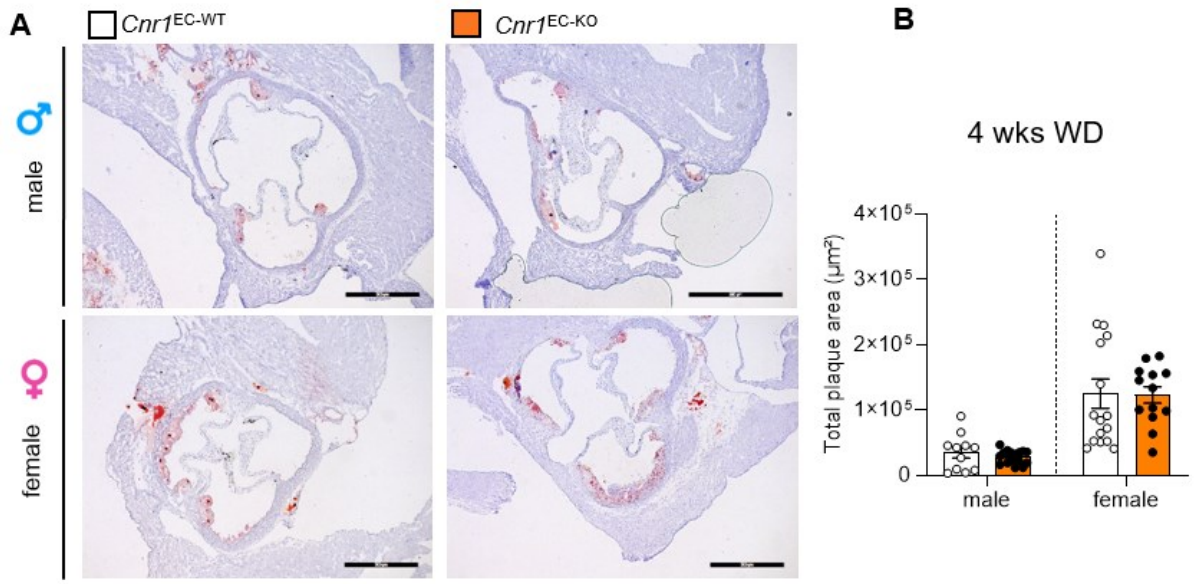

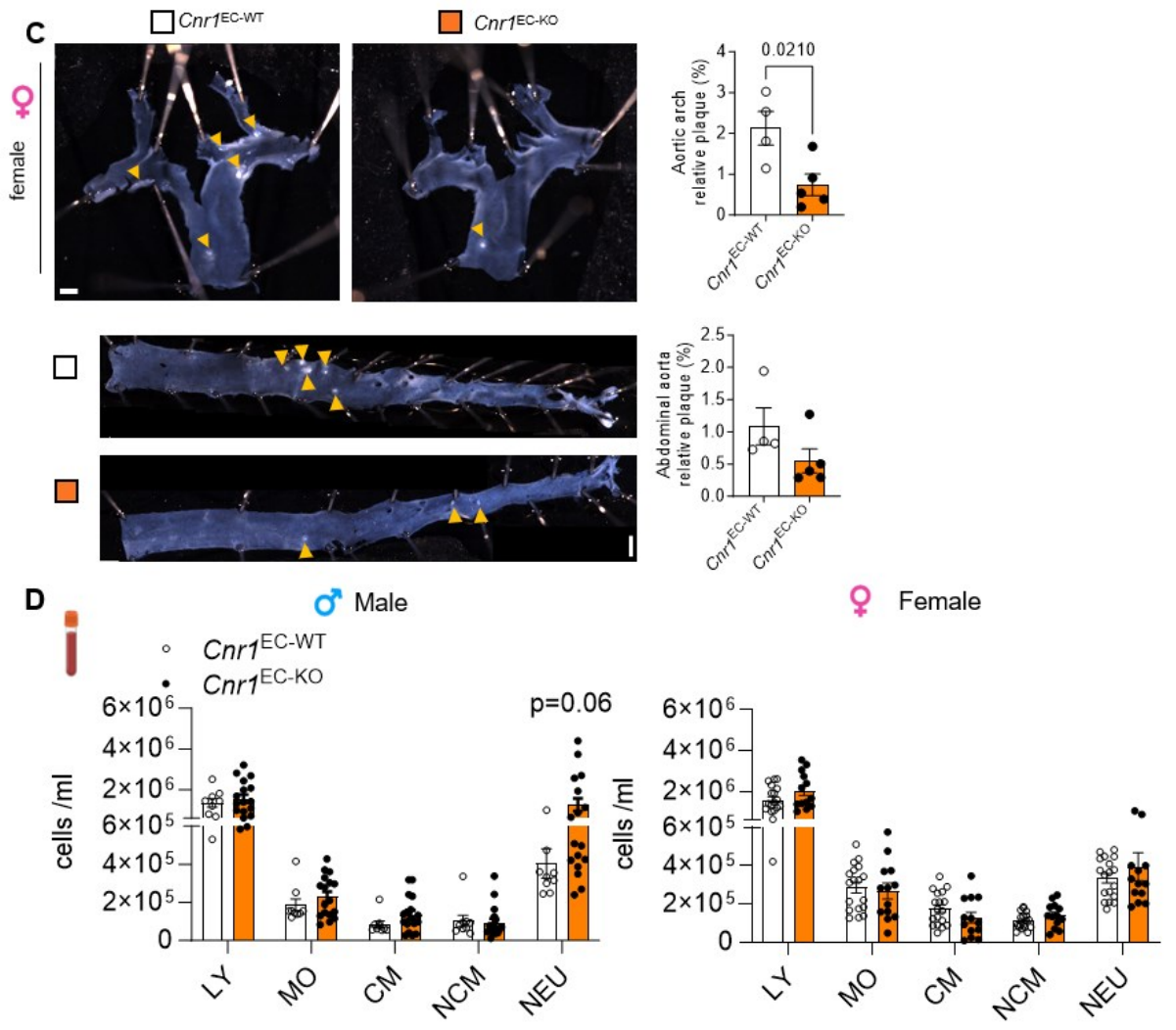

Figure 26. Effect of endothelial *Cnr1* deficiency on early stages of atherogenesis.
(A) Representative Oil-Red-O (ORO) stainings of aortic roots of male (n=11-16) and female (n=13-16) *Cnr1*$^{EC-WT}$ **and** *Cnr1*$^{EC-KO}$ mice after 4 weeks of WD; Scale bar: 500 µm. **(B)** Quantification of absolute lesion area. **(C)** Representative images and analysis of arch and descending aorta showing accumulation of lesion area from female *Cnr1*$^{EC-WT}$ and *Cnr1*$^{EC-KO}$ mice (n = 4-5) after 4 weeks of WD. Scale bar: 1 mm. **(D)** Flow cytometry analysis of lymphocytes, monocytes, classical, non-classical monocytes, and neutrophils from peripheral blood of *Cnr1*$^{EC-WT}$ and *Cnr1*$^{EC-KO}$ mice fed a WD for 4 weeks. P values were calculated through an unpaired Student's t-test by GraphPad Prism.

After 16 weeks of atherogenic diet feeding, female *Cnr1*$^{EC-KO}$ mice exhibited smaller atherosclerotic plaques in the aortic roots compared to corresponding *Cnr1*$^{EC-WT}$ controls (Figure 27A-27C), suggesting that loss of endothelial *Cnr1* protects against atherosclerosis. *Apoe*$^{-/-}$*Cnr1*$^{flox/flox}$ mice were used as a separate control group to exclude any effects of either *Cnr1*$^{flox/flox}$ or *Bmx*^{Cre} transgene insertion on the atherosclerosis phenotype. Interestingly, the effect of endothelial *Cnr1* deficiency on lesion development was not observed in male mice, suggesting that endothelial *Cnr1* might play a sex-specific role in the context of atherosclerosis.

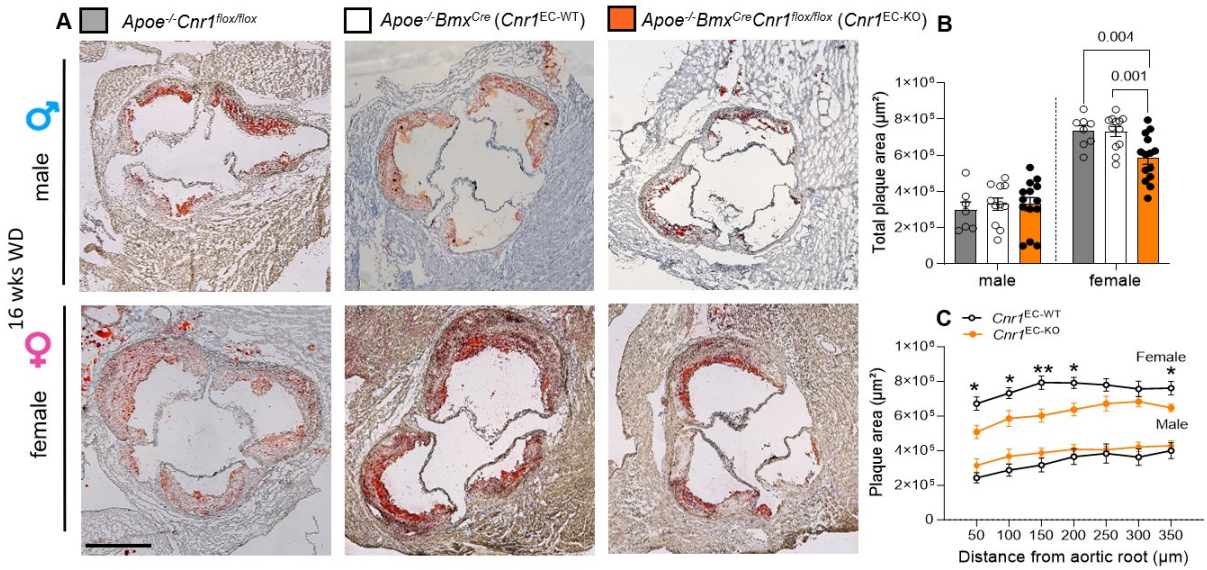

Figure 27. Effect of endothelial *Cnr1* deficiency on advanced stages of atherogenesis.
(A) Representative ORO staining of aortic roots of male (n=7-14) and female (n=8-14) *Cnr1*$^{EC\text{-}WT}$ and *Cnr1*$^{EC\text{-}KO}$ mice after 16 weeks of WD; Scale bar: 500 µm. **(B)** Quantification of absolute lesion area. **(C)** Plaque area per aortic root section. Data are mean ± s.e.m. Exact p-values are indicated or shown as **p<0.01 and *p<0.05 by One-way ANOVA followed by a post-hoc Tukey multi-comparison test.

5.3.2 Effects of endothelial *Cnr1* on cholesterol levels and plaque lipid deposition

Unexpectedly, *Cnr1*$^{EC\text{-}KO}$ mice exhibited elevated circulating plasma cholesterol levels (Figure 28A) and altered lipoprotein profiles compared to the *Cnr1*$^{EC\text{-}WT}$ group (Figure 28B). The increase in circulating plasma cholesterol could be a consequence of reduced lipid uptake into tissues.

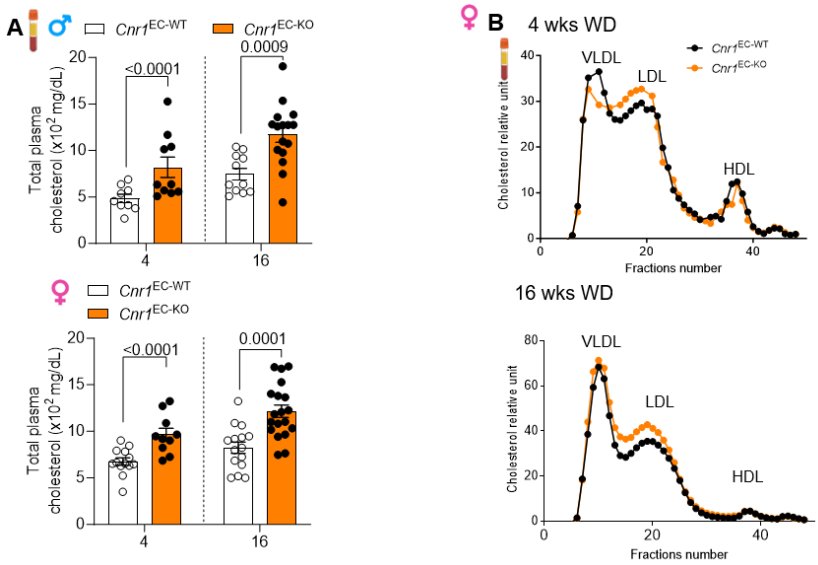

Figure 28. Effect of *Cnr1* deficiency on plasma cholesterol levels.
(A) Plasma total cholesterol from *Cnr1*$^{EC\text{-}WT}$ and *Cnr1*$^{EC\text{-}KO}$ mice and **(B)** HPLC analysis of lipoprotein profiles from female *Cnr1*$^{EC\text{-}WT}$ and *Cnr1*$^{EC\text{-}KO}$ mice fed a WD for 4 or 16 weeks. P values were obtained using an unpaired Student's t-test.

Subsequently, the advanced aortic root lesions were further characterized for neutral lipid deposition, necrotic core, and macrophage composition (Figure 29). Within the plaque of female *Cnr1*$^{EC-KO}$ mice, a significant reduction in lipid accumulation and a noteworthy increase in collagen content were observed. These findings suggest a shift towards a more stable plaque phenotype in female *Cnr1*$^{EC-KO}$ mice.

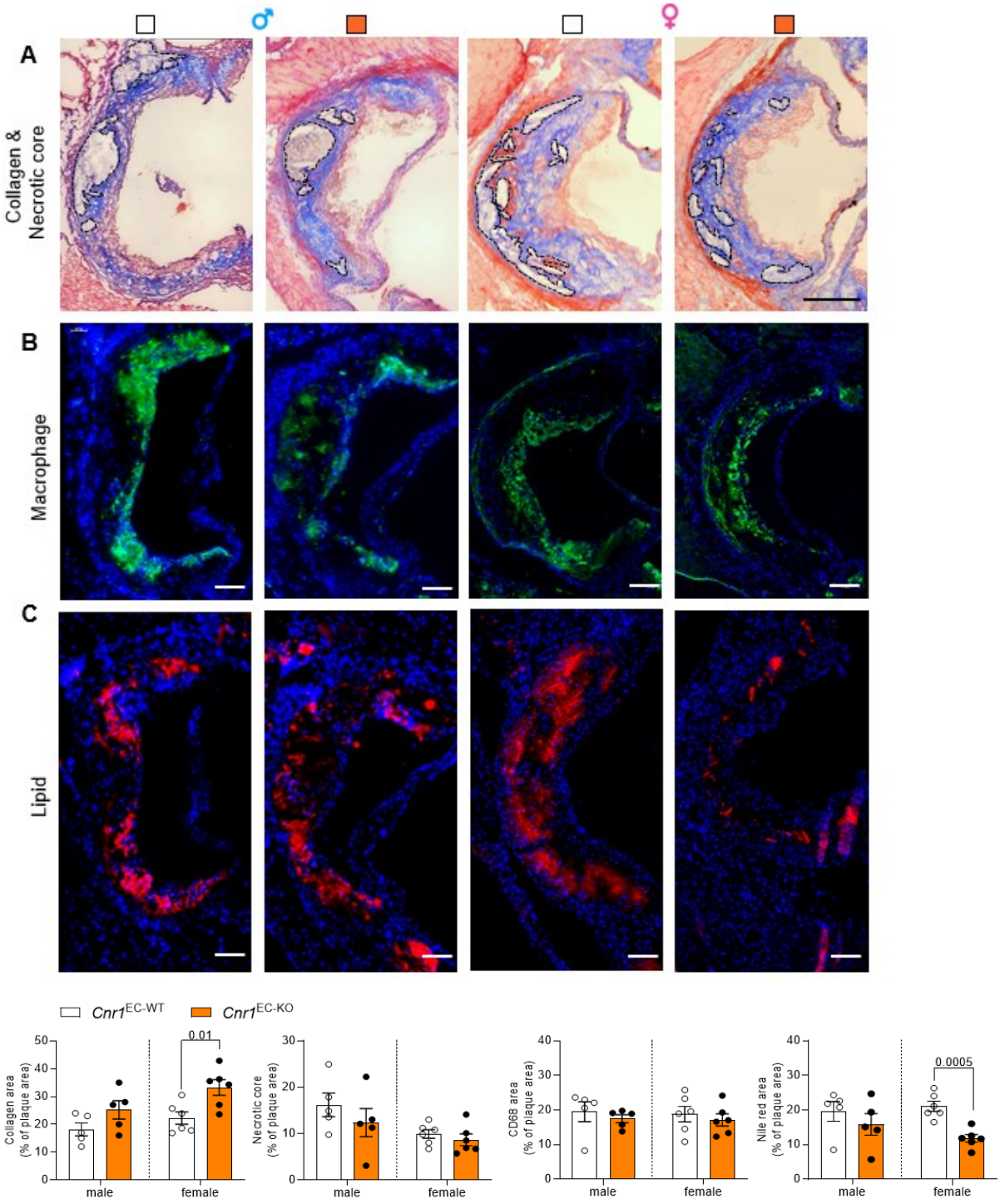

Figure 29. Effect of *Cnr1* deficiency on plaque composition.
Representative aortic root plaque images from *Cnr1*$^{EC-WT}$ and *Cnr1*$^{EC-KO}$ mice after 16 weeks WD (n=5-6) stained with **(A)** Masson's trichrome stain for collagen and necrotic core area (encircled by dotted lines) quantification. Scale bar: 200 µm. **(B)** CD68 and **(C)** Nile red staining for macrophage or lipid area content quantification, respectively. Scale bar: 100 µm. An unpaired Student's t-test were conducted separately for males and females, and exact P values are indicated.

5.4 CB1 profoundly regulates the transcriptomic landscape linked to inflammatory and metabolic signalling in endothelial cells

5.4.1 Transcriptomic profile of *Cnr1* deficient aortic endothelial cells during atherogenesis

Next, to investigate the transcriptomic genes and pathways governed by endothelial *Cnr1* signalling, aortic endothelial cells were sorted from both the *Cnr1*$^{EC\text{-}WT}$ and *Cnr1*$^{EC\text{-}KO}$ mice after 4 weeks of WD and sent for RNA sequencing. Principal component analysis (PCA) revealed clearly distinct transcriptomic profiles between the *Cnr1*$^{EC\text{-}KO}$ and *Cnr1*$^{EC\text{-}WT}$ samples (Figure 30A). A total of 303 differentially expressed genes (DEGs) were identified, including 129 down- and 174 upregulated genes. Notably, the expression of several pro-inflammatory cytokines and chemokines, such as *Il6*, *Ackr3*, *Cxcl12*, and *Ccl2*, were markedly reduced in *Cnr1*$^{EC\text{-}KO}$ ECs, indicating a potential shift toward a less inflammatory state (Figure 30B). Conversely, genes associated with cellular matrix, including *Itga8*, *Itga3*, as well as the transcription factor *Prdm16*, which plays a critical role in maintaining endothelial function and supporting arterial flow recovery,[194] were upregulated in *Cnr1*$^{EC\text{-}KO}$ ECs when compared to the *Cnr1*$^{EC\text{-}WT}$ group. These findings collectively suggest a complex interplay of gene expression alterations that may underlie the CB1-dependent regulation of EC function and physiology.

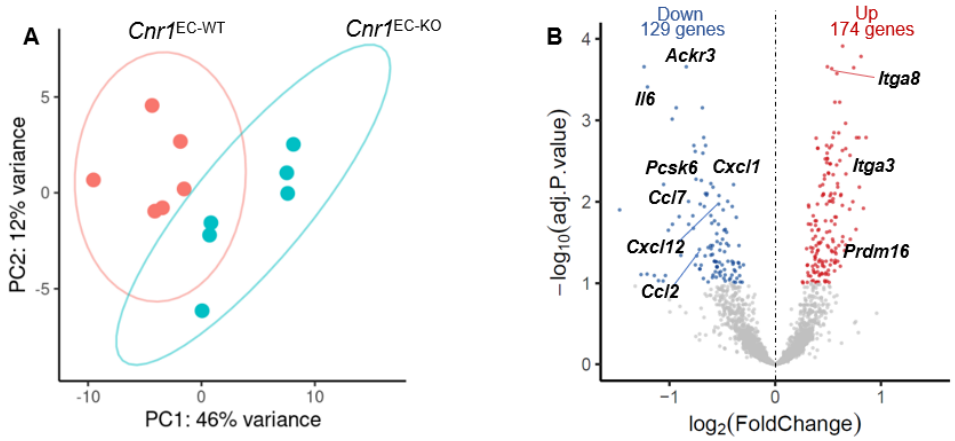

Figure 30. Transcriptomic profile of aortic endothelial *Cnr1* signalling.
Aortic endothelial cells (sorted as CD45^{-}CD107a^{low}CD31^{high}) [195] were isolated from female *Cnr1*$^{EC\text{-}KO}$ and *Cnr1*$^{EC\text{-}WT}$ mouse aortas (n=6) after 4 weeks of WD for RNA-seq. **(A)** Principal component analysis (PCA) to visualize the heterogeneity of transcriptomic profiles between the two groups. (**B**) Volcano plot showing differentially expressed genes (DEGs) with 174 significantly up- and 129 down-regulated genes in female *Cnr1*$^{EC\text{-}KO}$ versus *Cnr1*$^{EC\text{-}WT}$ mice.

Interestingly, GO analysis uncovered that the transcriptomic signature regulated by *Cnr1* deficiency affects cellular components including membrane raft (GO:0045121; padj = 2.05e^{-05}) and caveola (GO:0005901; padj = 0.0003), indicating that CB1 might affect endothelial lipid raft dependent signal transduction (Figures 31A). To identify putative upstream transcription factors (TFs) of the DEG signature in *Cnr1*-deficient ECs, ChIP-X Enrichment Analysis 3 (CHEA3) was performed (Figures 31B). *Fos and Jun* emerged as the primary transcription factors (TFs) regulating the DEG network. These TFs are well-known as activator protein 1 (AP-1) regulators, mediating various cellular processes such as the regulation of cytokines and chemokines, as well as cell migration and differentiation.[196] Additionally, gene set enrichment analysis (GSEA) revealed a strong correlation with the JNK_c-Jun and Il6_Stat3 signalling pathway (Figures 31C and 31D). Collectively, these data indicate that CB1 promotes a pro-inflammatory, activated phenotype in ECs, likely involving a JNK-JUN-dependent intracellular pathway.

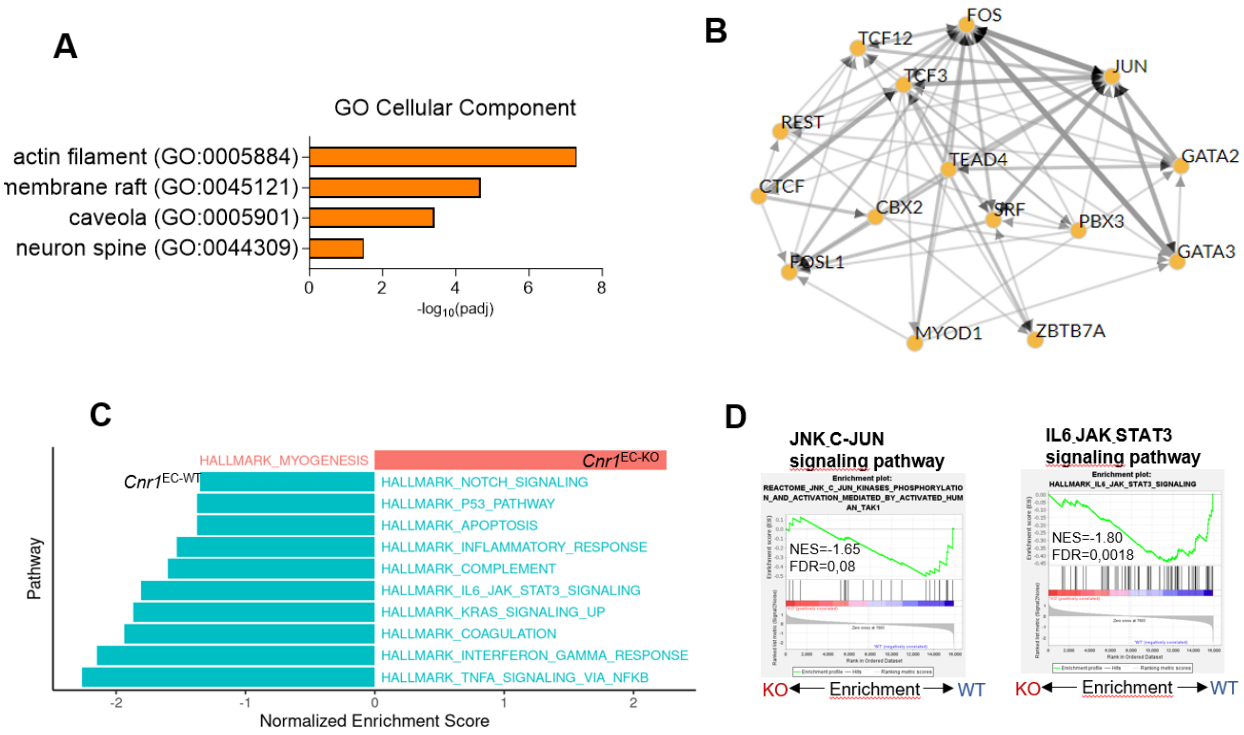

Figure 31. Pathways and transcription factors regulated by aortic endothelial *Cnr1* signaling. **(A)** Significantly regulated pathways in *Cnr1* deficient ECs, based on GO analysis. **(B)** CHEA3 was used to predict the top 15 transcription factor (TF) -Co-Regulatory Networks modulated by endothelial *Cnr1* deficiency. **(C)** GSEA identified significantly enriched signalling pathways and **(D)** representative pathways with normalized enrichment score (NES) and false discovery rate (FDR) q-value are shown. NES below -1 or above 1 and an FDR q-value below 0.25 is considered significant.

5.4.2 Validation of the key regulated genes in HAoECs

To strengthen the RNA sequencing findings, some representative pro-inflammatory markers among the identified DEGs were further studied in HAoECs following transfection with *CNR1* or scrambled siRNA. A knockdown efficiency of approximately 80% was achieved with the *CNR1* siRNA. The expression of pro-inflammatory genes *CXCL8*, *CCL2*, and *ICAM1* was significantly attenuated in *CNR1*-silenced HAoECs (Figure 32A), confirming a reduced pro-inflammatory phenotype in the absence of endothelial CB1 signalling. Given that enhanced vascular inflammation disrupts vascular homeostasis and induces endothelial oxidative stress,[19] it raises the question of whether CB1 signalling affects ROS production. Flow cytometry analysis revealed a reduction in TNF-α-stimulated ROS production in HAoECs upon *CNR1* silencing (Figure 32B), indicating the potential restoration of endothelial function in absence of CB1.

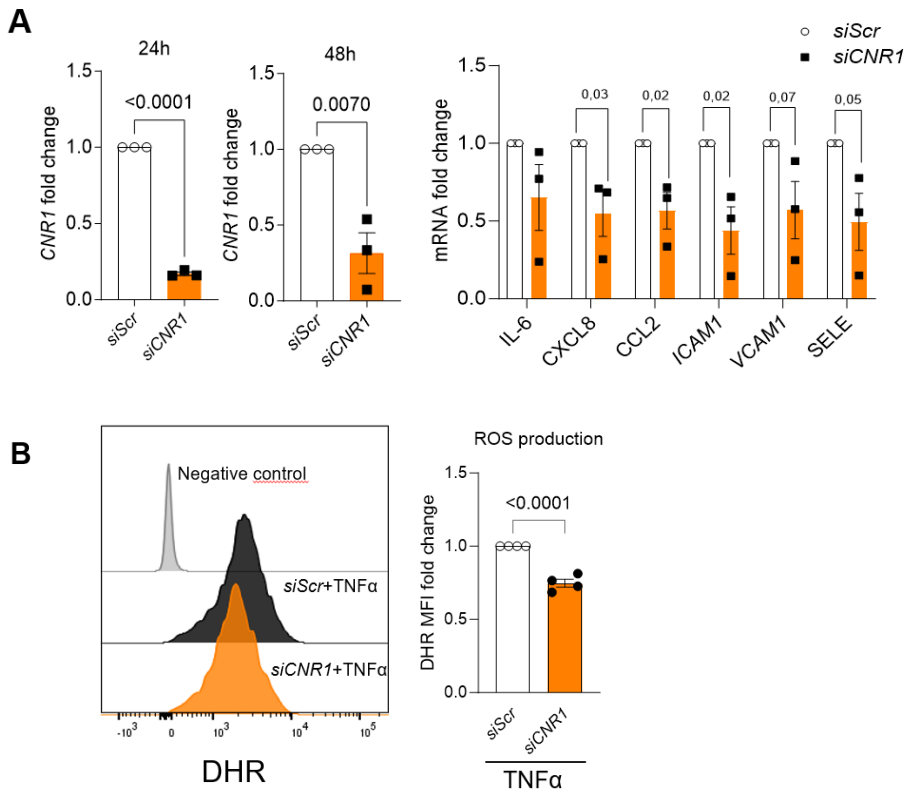

Figure 32. Endothelial *CNR1* silencing reduces vascular inflammation.
(A) Pro-inflammatory gene expression after transfection with 20 nM *CNR1* (*siCNR1*) or scrambled siRNA (*siScr*) in HAoECs (n = 3 independent experiments). **(B)** Flow cytometric analysis of ROS determined by DHR123 in HAoECs (n=4 independent experiments). Data are shown as mean ± s.e.m. P values were obtained using a two-tailed unpaired Student's t-test.

5.4.3 Endothelial CB1 signalling under shear stress influences monocyte adhesion

Subsequently, the question was raised whether endothelial stimulation with a synthetic CB1 agonist would promote inflammation. To this end, HAoECs were treated with the CB1 agonist

ACEA under static and LSS conditions, respectively. The ACEA treatment was observed to inhibit atheroprotective flow (LSS)-mediated reduction of *ICAM1,* vascular cell adhesion molecule-1 (*VCAM1*), and the glycolytic enzyme *PFKFB3* expression. Additionally, ACEA treatment hindered the enhancement of flow-responsive expression of *KLF2* and *NOS3* (eNOS-encoded gene) mediated by LSS (Figure 33A). Nevertheless, no difference was detected between vehicle and ACEA treatment under static conditions, suggesting that CB1 activation requires mechanical shear force to promote a pro-inflammatory phenotype. ICAM1 acts as a pivotal player for monocytes to adhere to ECs.[197] Therefore, a monocyte adhesion assay was conducted. Labelled THP1 monocytes were co-cultured with HAoECs in the presence or absence of the CB1 agonist ACEA treatment under LSS. A significantly increased number of adhered monocytes was observed when stimulating HAoECs with ACEA compared to the vehicle control (Figure 33B), indicating that the activation of CB1 induces a pro-inflammatory signature in endothelial cells, which in turn promotes increased monocyte adhesion.

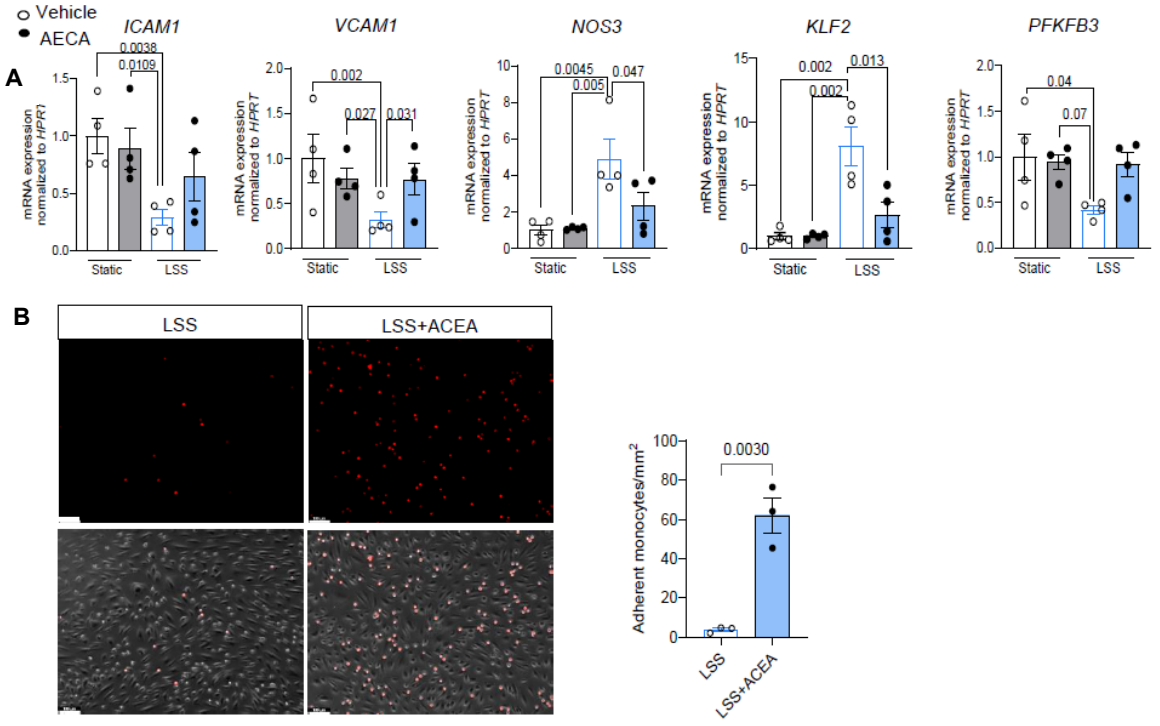

Figure 33. Endothelial cannabinoid receptor 1 mediates monocyte adhesion.
(A) HAoECs were treated with or without 1 µM ACEA under static and LSS (10 dye/cm^2) conditions for 24 h, respectively. RT-qPCR assessed the relative mRNA levels of inflammatory molecules *ICAM1* and *VCAM1*, regulators of glycolysis *PFKFB3*, and anti-inflammatory molecules *KLF2* and *NOS3*. Data were analysed by two-way ANOVA with Tukey correction for multiple comparisons. n=4 independent experiments. **(B)** HAoECs were initially incubated with or without 1 µM ACEA under LSS for 24 h. Following this, a monocyte adhesion assay was conducted by incubating ECs with calcein-labelled THP-1 cells under LSS (3 h) after 5 ng/mL TNF-α overnight activation. The number of adherent THP-1 cells was determined in 10-15 random fields per experiment. (n=3 independent experiments) Data are shown as mean ± s.e.m. P values were calculated using an unpaired Student's t-test. Scale bar: 100 µm.

5.5 Endothelial *Cnr1* deficiency improves metabolic parameters in eWAT, BAT and liver

5.5.1 Impact of endothelial *Cnr1* deficiency on lipid metabolism

Emerging evidence indicates that the endocannabinoid-CB1 signalling axis enhances energy storage within the adipose tissue while reducing energy expenditure, affecting both lipid and glucose metabolism.[198] Surprisingly, the depletion of *Cnr1* in EC was sufficient to attenuate the body weight gain over 16 weeks WD (Figure 34A). The decrease in weight gain was associated with reduced accumulation of visceral white and brown fat (Figure 34B). Clear reductions in adipocyte size in epididymal white adipose tissue (eWAT) were observed through histological staining despite no significant changes of lipid droplet deposition found in BAT at the 4-week WD time point (Figure 34C and 34D). Besides, higher mRNA expression of *Gpihbp1*, an endothelial cell transporter for lipoprotein lipase, as well as lipolysis-related genes, were detected in the BAT of *Cnr1*$^{EC\text{-}KO}$ mice (Figure 34E). The upregulation of GPIHBP1 was confirmed at the protein level and colocalized by immunostaining with capillary endothelial cells in BAT of *Cnr1*$^{EC\text{-}KO}$ mice (Figure 34F). The endothelial cell transcription factor *Prdm16*, which accelerates browning and thermogenesis, also exhibited higher expression in the BAT of *Cnr1*$^{EC\text{-}KO}$ mice. This prompted further investigation of the underlying cellular mechanisms. Endothelial cells were sorted from the BAT of *Cnr1*$^{EC\text{-}KO}$ and *Cnr1*$^{EC\text{-}WT}$ mice for RNA sequencing. GO analysis revealed that the pathways regulated by BAT endothelial CB1 were linked to mitochondrial respiration and ATP biosynthesis, suggesting increased mitochondrial activity in the BAT of *Cnr1*$^{EC\text{-}KO}$ mice (Figures 34G). Similar effects on BAT metabolic changes, as detailed in female mice, were observed in male *Cnr1*$^{EC\text{-}KO}$ mice (Figures 34H).

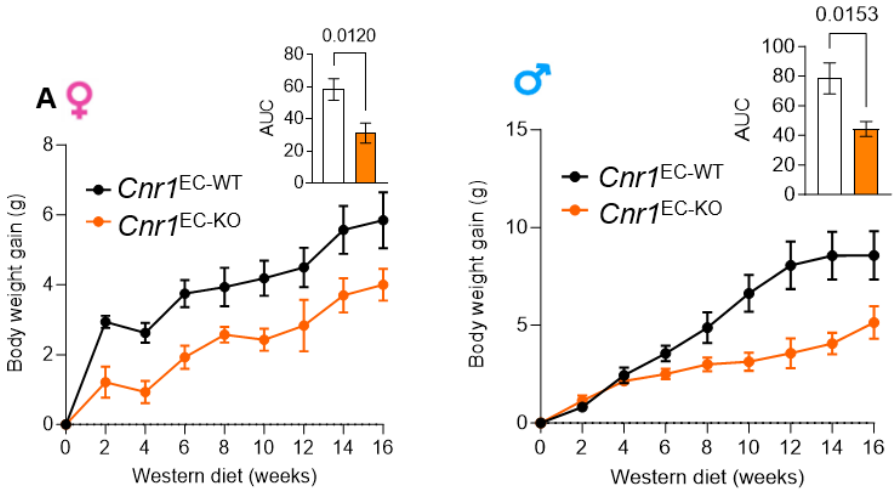

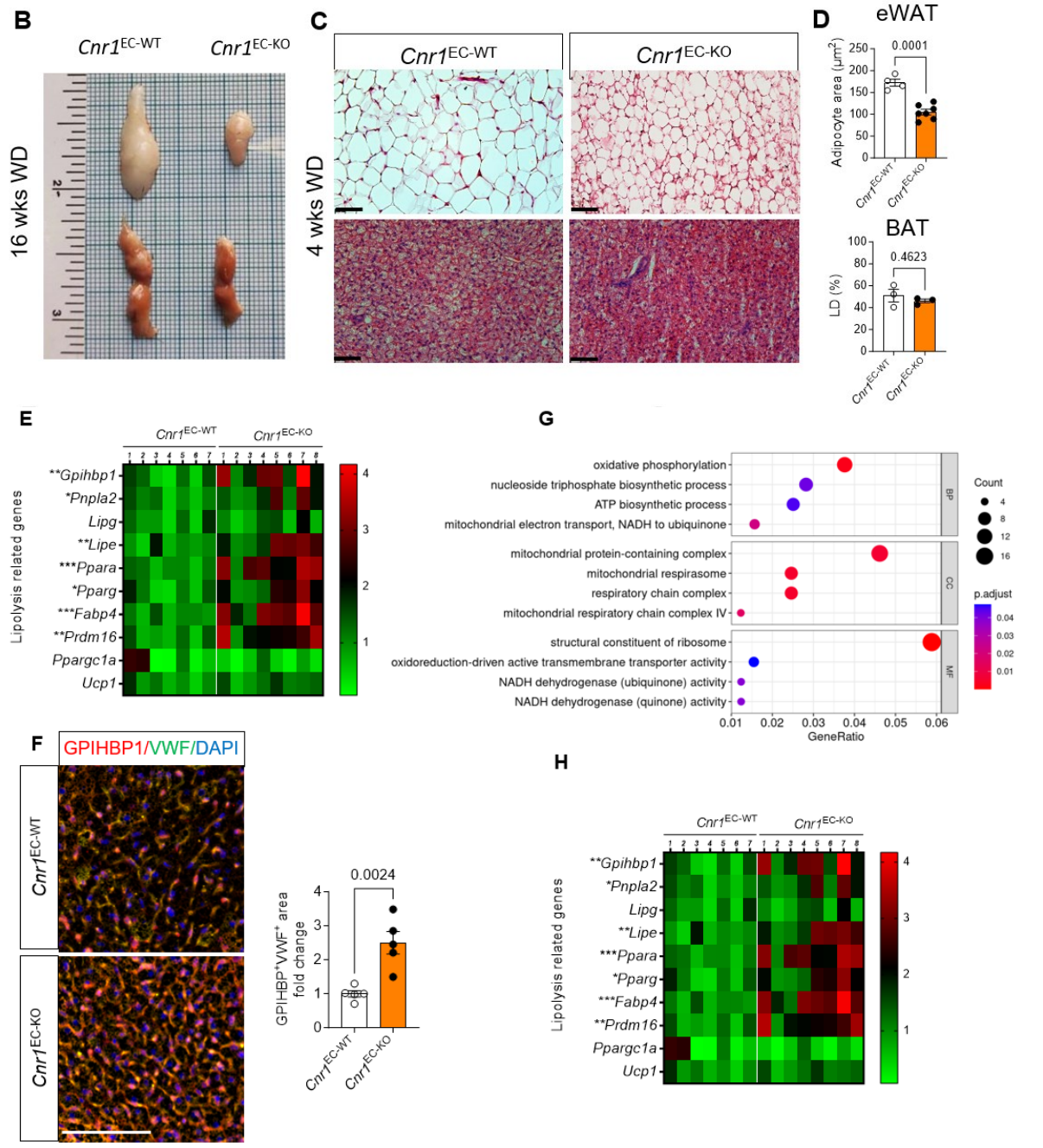

Figure 34. Impact of endothelial *Cnr1* deficiency on lipid metabolism.
(A) Body weight gain and area under the curve (AUC) over 16 weeks WD in female and male age-matched *Cnr1*$^{EC\text{-}WT}$ and *Cnr1*$^{EC\text{-}KO}$ mice (n=7-8). **(B)** Representative images of eWAT and BAT from female mice after 16 weeks of WD. **(C)** H&E staining of eWAT and BAT from female *Cnr1*$^{EC\text{-}WT}$ and *Cnr1*$^{EC\text{-}KO}$ after 4 weeks of WD. Scale bar, 200 µm **(D)** Quantification of adipocyte size in eWAT and relative lipid droplet (LD) content in BAT. **(E)** Gene expression analysis (qPCR) in BAT of female *Cnr1*$^{EC\text{-}WT}$ and *Cnr1*$^{EC\text{-}KO}$ mice after 4 weeks of WD (n = 7-8). **(F)** Costaining of GPIHBP1 (red) and von Willebrand factor (vWF, green) for capillary vessels in BAT of *Cnr1*$^{EC\text{-}WT}$ and *Cnr1*$^{EC\text{-}KO}$ mice after 4 weeks of WD. Scale bar, 100 µm. Quantification of GPIHBP1^{+} VWF^{+} fluorescence intensity on the **right**. (**G**) RNA sequencing and GO enrichment analysis revealed top pathways regulated in sorted BAT endothelial cells from *Cnr1*$^{EC\text{-}KO}$ mice, analyzed after 4 weeks WD. **(H)** Gene expression analysis (qPCR) in BAT of male *Cnr1*$^{EC\text{-}WT}$ and *Cnr1*$^{EC\text{-}KO}$ mice after 4 weeks of WD (n = 9). Data are shown as mean ± s.e.m. P values were calculated using an unpaired Student's t-test in GraphPad Prism. Scale bar: 100 µm.

5.5.2 Impact of endothelial *Cnr1* deficiency on liver metabolism

Moreover, *Cnr1*$^{EC-KO}$ mice had reduced lipid droplet accumulation, as observed by Oil Red O staining of liver sections (Figures 35A) along with decreased total liver cholesterol levels (Figures 35B). The hepatic qPCR gene expression analysis at the same time point demonstrated a notable increase in transcription of various metabolic markers, indicating enhanced hepatic β-oxidation in *Cnr1*$^{EC-KO}$ mice (Figures 35C). Nevertheless, the plasma bile acid levels were not affected (Figure 35D). Enhanced fatty acid beta-oxidation in the liver could potentially lead to reduced cytoplasmic lipid accumulation and improved insulin sensitivity.[199] Therefore, an intraperitoneal glucose tolerance test (ipGTT) was conducted. Both male and female *Cnr1*$^{EC-KO}$ mice exhibited improved glucose disposal rates compared to the age-matched *Cnr1*$^{EC-WT}$ mice (Figure 35E).

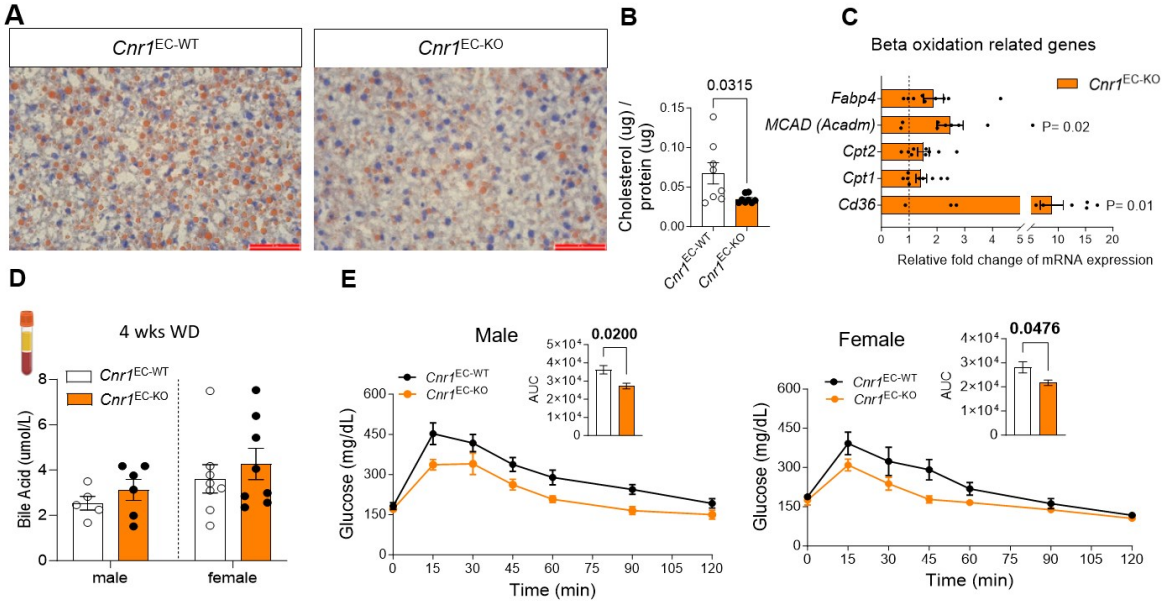

Figure 35. Endothelial *Cnr1* deficiency affect liver metabolism.
(A) Representative hepatic ORO staining and **(B)** liver cholesterol levels in female *Cnr1*$^{EC-WT}$ and *Cnr1*$^{EC-KO}$ mice after 4 weeks of WD (n=8). **(C)** Gene expression analysis (qPCR) in liver tissue in female *Cnr1*$^{EC-KO}$ and age-matched *Cnr1*$^{EC-WT}$ mice after 4 weeks of WD (n = 8-9). **(D)** Plasma bile acid levels in male (n=5-6) and female (n=8) *Cnr1*$^{EC-WT}$ and *Cnr1*$^{EC-WT}$ mice after 4 weeks of WD. **(E)** Levels of plasma glucose during intraperitoneal glucose tolerance test and AUC in *Cnr1*$^{EC-WT}$ and *Cnr1*$^{EC-KO}$ after 4 weeks of WD (n = 4). Data presented as mean ± s.e.m. P values were calculated through an unpaired Student's t-test.

5.5.3 Plasma endocannabinoid levels in male and female mice

The plasma from female and male *Apoe*$^{-/-}$ mice was collected to measure circulating endocannabinoid concentrations (performed in collaboration with Prof. Mario van der Stelt, University of Leiden, The Netherlands). Male and female *Apoe*$^{-/-}$ mice showed comparable levels of circulating endocannabinoids, including 2-arachidonoylglycerol (2-AG), anandamide (AEA), oleoylethanolamide (OEA), and palmitoylethanolamide (PEA) in their plasma (Figure 36). However, higher *Cnr1* mRNA levels were detected in sorted aortic endothelial cells from

female versus male mice. Hence, it may be speculated that the more pronounced phenotype observed in female *Cnr1*$^{EC\text{-}KO}$ mice compared to males could be attributed to differences in endothelial CB1 expression *per se*. Overall, these findings uncovered that endothelial *Cnr1* deficiency leads to metabolic alterations in epididymal WAT, BAT and liver and improved insulin sensitivity.

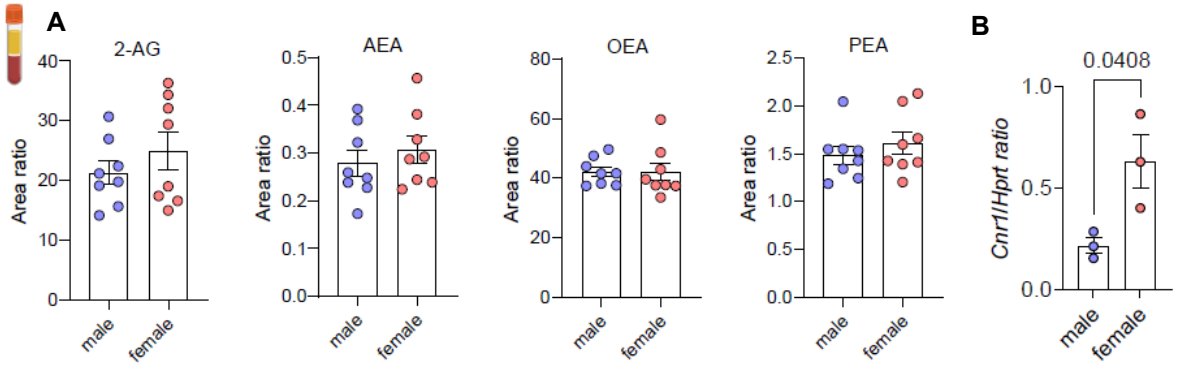

Figure 36. Circulating endocannabinoid levels in *Apoe*$^{-/-}$ male and female mice.
(A) Plasma endocannabinoid levels between male and female in *Apoe*$^{-/-}$ mice. **(B)** Expression of *Cnr1* measured by droplet digital PCR (ddPCR) in sorted aortic endothelial cells from *Cnr1*$^{EC\text{-}WT}$ male and female mice (n = 3) normalized to *Hprt*. Data presented as mean ± s.e.m. P values were calculated through an unpaired Student's t-test.

5.6 Endothelial *Cnr1* deficiency affects LDL uptake

5.6.1 Impact of endothelial *Cnr1* deficiency on LDL uptake

Having observed reduced lipid accumulation in the liver and aorta of the *Cnr1*$^{EC\text{-}KO}$ mice, it was hypothesized that CB1 might affect the lipid uptake by endothelial cells. To this end, fresh carotid arteries were extracted from *Cnr1*$^{EC\text{-}KO}$ and *Cnr1*$^{EC\text{-}WT}$ mice after 4 weeks WD. Subsequently, an *ex vivo* arterial perfusion assay was employed to perfuse the arteries with fluorescently labelled native LDL (DiI-LDL).[176] Two-photon laser scanning microscopy (TPLSM) imaging (Figure 37A and 37B) revealed that deficiency of *Cnr1* in endothelial cells resulted in markedly reduced retention of LDL particles across the endothelial layer, suggesting a role for CB1 in the regulation of endothelial LDL uptake. The same method was applied to assess VCAM1 expression in *Cnr1*$^{EC\text{-}KO}$ and *Cnr1*$^{EC\text{-}WT}$ vessels, confirming again a reduced vascular cell VCAM1 expression in *Cnr1*$^{EC\text{-}KO}$ mice (Figure 37C and 37D).

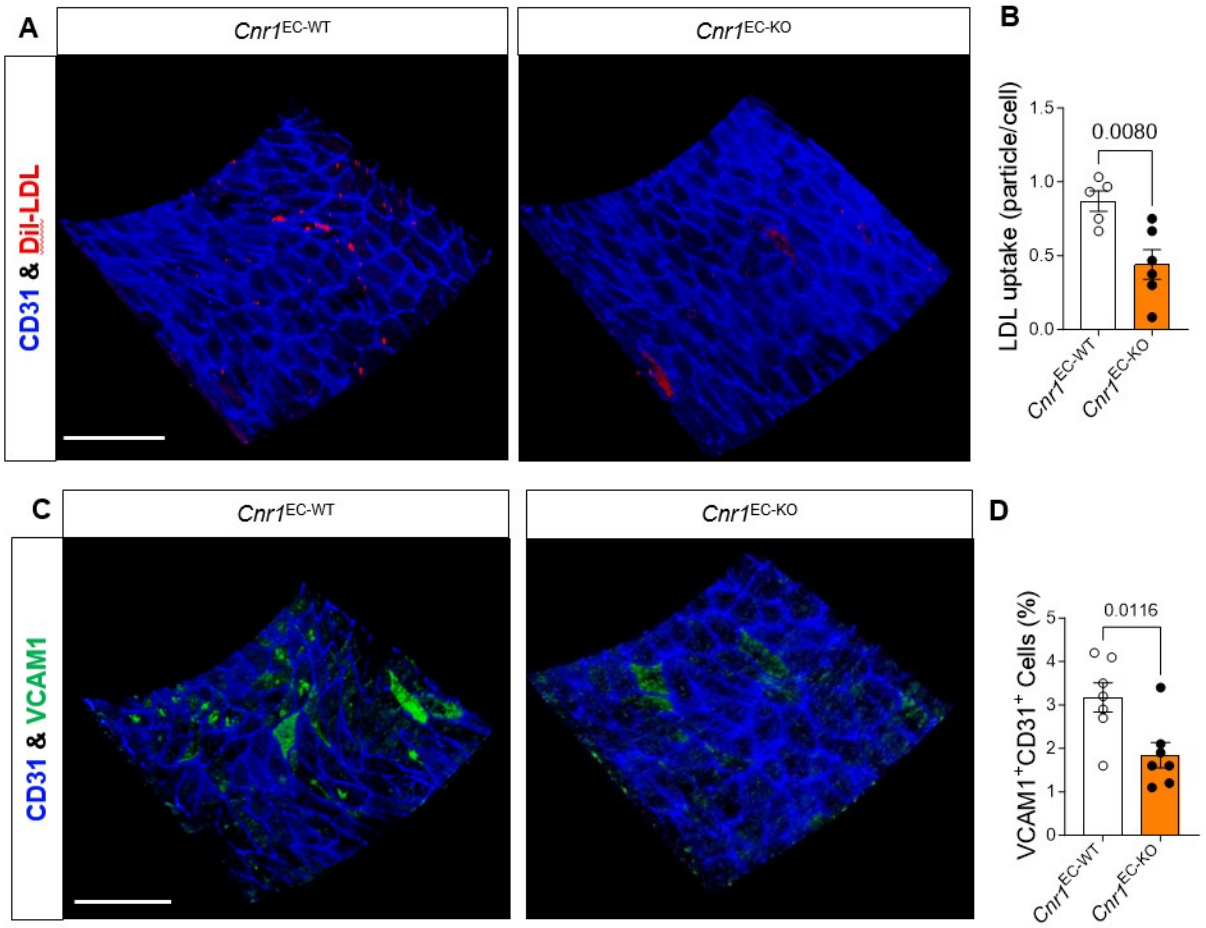

Figure 37. Endothelial *Cnr1* mediate vascular inflammation and lipid uptake.
(A) Representative TPLSM 3D images of uptaken Dil-LDL particles in *ex vivo* perfused carotid arteries from female *Cnr1*$^{EC\text{-}WT}$ and *Cnr1*$^{EC\text{-}KO}$ mice after 4 weeks WD; CD31 was used to stain ECs. Scale bar, 100 µm. Quantification is shown on the **right (B)** normalized to endothelial cell number (n=5-6 mice per group). **(C)** Representative TPLSM 3D images of VCAM1 and **(D)** percentage of VCAM1^{+}CD31^{+} cells in *ex vivo* perfused carotid arteries from *Cnr1*$^{EC\text{-}WT}$ and *Cnr1*$^{EC\text{-}KO}$ mice after 4 weeks of WD (n = 7). Scale bar, 100 µm. P values were calculated through an unpaired Student's t-test by GraphPad Prism.

5.6.2 Impact of endothelial *Cnr1* deficiency on lipid receptors

To further address how *Cnr1* deficiency affected endothelial LDL uptake, flow cytometry was employed to evaluate the surface expression levels of various endothelial lipid uptake receptors on aortic endothelial cells. No significant alterations were detected in the surface levels of LOX-1, SRB1, SRA1, and CD36 between the *Cnr1*$^{EC\text{-}KO}$ and *Cnr1*$^{EC\text{-}WT}$ aortic endothelial cells (Figure 38A). However, the above-described RNA sequencing data of sorted *Cnr1*$^{EC\text{-}KO}$ aortic endothelial cells showed significant downregulation of *Acvrl1* expression, also referred to as ALK1 encoding gene, which serves as a low-affinity, high-capacity receptor for LDL in endothelial cells (Figure 38B).

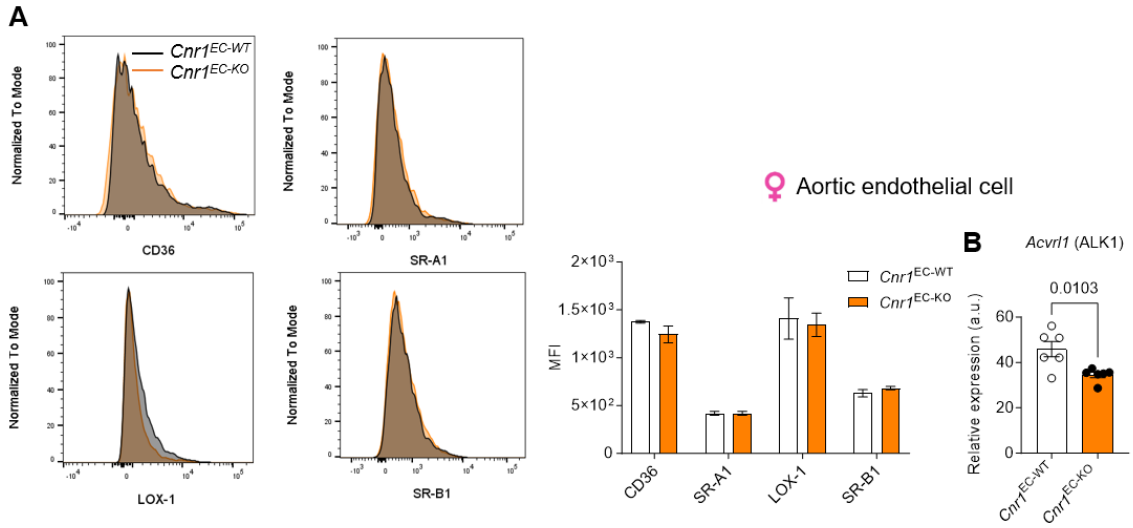

Figure 38. Impact of endothelial *Cnr1* on endothelial lipid receptors.
(A) Flow cytometry analysis of lipid receptors SR-B1, LOX-1, SR-A1 and CD36 on sorted aortic endothelial cells from female *Cnr1*$^{EC\text{-}WT}$ and *Cnr1*$^{EC\text{-}KO}$ mice, gated as Live CD45^{-}CD31^{+}CD107a^{+} and **(B)** RNA-Seq expression quantification of *ALK1* from sorted aortic endothelial cells from *Cnr1*$^{EC\text{-}KO}$ and *Cnr1*$^{EC\text{-}WT}$ mice (n=6). by GraphPad Prism.

5.6.3 Impact of endothelial *Cnr1* deficiency on Cav1

Previous studies have described that LDL entry into the endothelium can occur independently of the LDL receptor (LDLR), including mechanisms involving the ALK1 receptor or caveolae-dependent transcytosis.[113, 115, 117, 121] Furthermore, the sequencing data and GO pathway analysis indicated the regulation of membrane rafts and caveola in *Cnr1* deficient endothelial cells. Caveolae are flask-shaped, shear stress-sensitive signalling domains in the plasma membrane of endothelial cells.[108] CAV1, a major component of caveolae, has been demonstrated to co-localize with ALK1 within caveolae-enriched domains of ECs.[200] The absence of CAV1 has shown to contribute to reduced DiI-LDL uptake in isolated aortas and less atherosclerosis despite elevated total cholesterol levels.[115] Thus, co-immunostaining of endothelial cells (CD31) and CAV1 in aortic root sections of *Cnr1*$^{EC\text{-}KO}$ and *Cnr1*$^{EC\text{-}WT}$mice at the 4 weeks WD time point was employed to confirm that endothelial *Cnr1* affects caveolar membrane domains. The analysis revealed a significant reduction of CAV1 expression in *Cnr1*$^{EC\text{-}KO}$ endothelial cells (Figure 39A and 39B), providing a possible explanation for the reduced LDL uptake in *Cnr1*$^{EC\text{-}KO}$ mice. To explore this possibility in more detail, HAoECs were treated with the CB1 antagonist AM281 under OSS in the presence of DiI-LDL, revealing a strongly reduced CAV1 level when blocking CB1 signalling (Figure 39C and 39D). *Vice versa*, when HAoECs were subjected to LSS, activation of CB1 with the agonist ACEA led to an upregulation of DiI-LDL uptake, accompanied by an increase in CAV1 expression (Figure 39E and 39F). In summary, these results support the direct regulation of endothelial lipid transport by CB1, possibly affecting the endothelial caveolae structure through modulation of CAV1 expression.

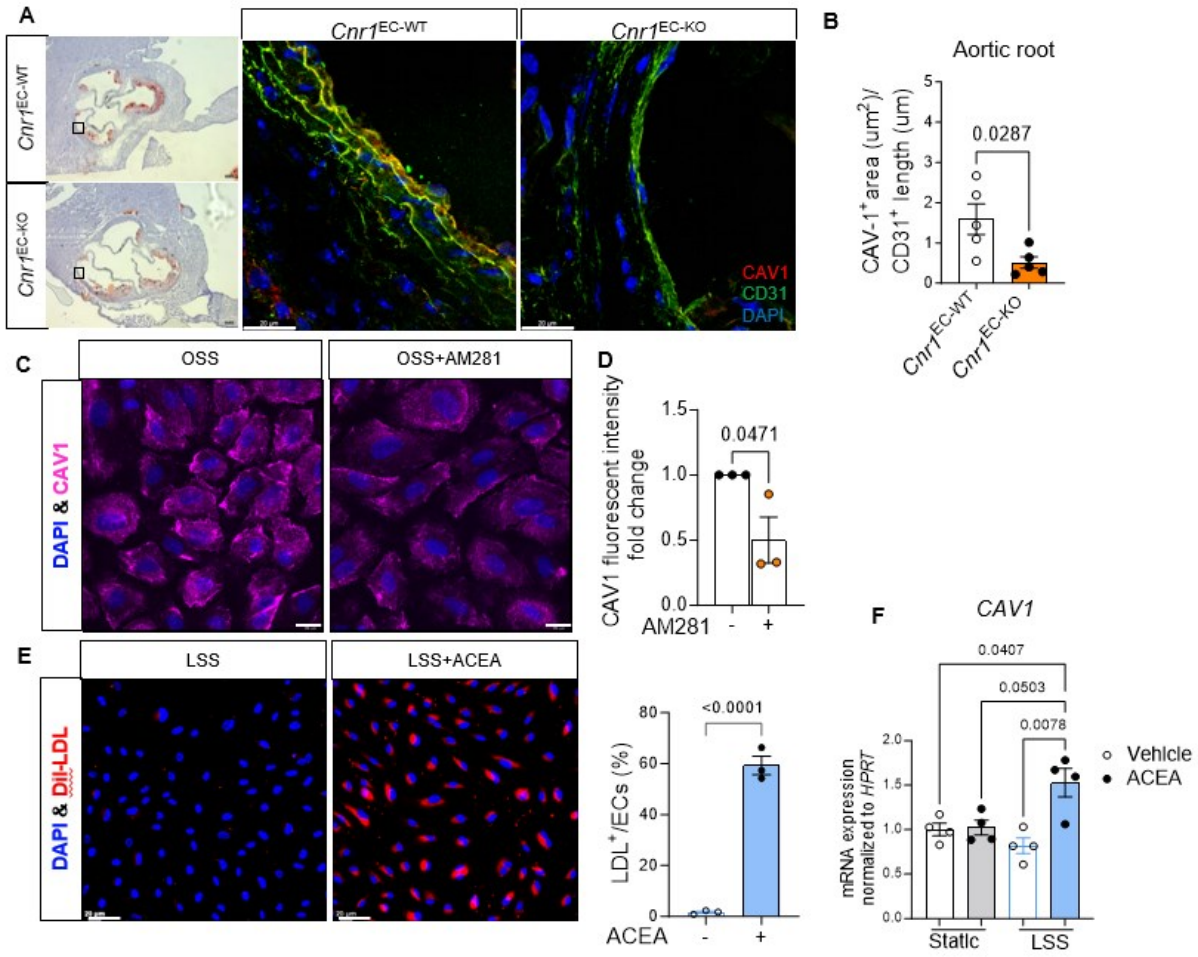

Figure 39. Cannabinoid receptor 1 (CB1) regulates endothelial low-density lipoprotein (LDL) transport during atherogenesis.
(A) Representative confocal images of caveolin-1 (CAV1, red) and CD31 (green) staining in aortic root sections of *Cnr1*$^{EC-KO}$ and *Cnr1*$^{EC-WT}$ mice after 4 weeks WD. Quantification of CAV1 expression is shown on the right **(B)** normalized to EC length. (n=5 mice) Scale bar, 20 µm. **(C)** HAoECs were preincubated with 1 µM AM281 or DMSO under OSS for 24 h followed with 1 µg/mL DiI LDL treatment for 30 min. Scale bar: 20 µm. **(D)**Quantification of CAV1 levels shown on the right. **(E)** HAoECs were preincubated with 1µM ACEA or vehicle buffer under LSS for 24 h followed with 1 µg/mL DiI LDL treatment for 90 min. Scale bar, 50 µm. **(F)** QPCR analysis of *CAV1* mRNA expression on HAoECs subjected to different treatments. The data were displayed as mean ± s.e.m., and each dot on the graph represented an individual experiment. P values were calculated through an unpaired Student's t-test or two-way ANOVA followed by a post-hoc Tukey multi-comparison test by GraphPad Prism.

5.7 Endothelial CB1 signalling regulates LDL uptake through cAMP-PKA dependent CAV1 modulation

5.7.1 Endothelial CB1 signalling affects the cyclic adenosine monophosphate (cAMP) formation

Protein kinase A (PKA) is known as a cAMP (cyclic adenosine monophosphate)-dependent enzyme. It becomes activated upon binding of cAMP to its regulatory catalytic subunits.[201] To validate whether CB1, described as a G_i-protein-coupled receptor in various cell lines,[202-204] affects cAMP formation, a reporter cell line was used.

A transgenic HEK293 FlpIn-TRex cell line stably transfected with a cAMP-luciferase reporter plasmid and the human *CNR1* cDNA (kindly provided by Professor Alexander Faussner) was employed to measure intracellular cAMP levels in response to CB1 activation or antagonism, respectively.[205] The CB1 antagonist AM281 elicited a significant increase in intracellular cAMP levels, whereas the CB1 agonist ACEA reduced intracellular cAMP concentration in a dose-dependent manner compared to the HBSS control. The synthetic cannabinoid CP55,940 and highly potent non-selective CB1 agonist also decreased intracellular cAMP levels at nanomolar concentrations. For inducing maximum intracellular cAMP levels, the potent adenyl cyclase activator forskolin was added shortly after agonist or antagonist administration (Figure 40A). In HAoECs, endogenous cAMP levels were measured via ELISA, revealing that AM281 under static conditions increased intracellular cAMP levels in a dose-dependent manner, while ACEA showed only a modest decrease of endogenous cAMP levels, possibly due to intrinsic activation of CB1 by endocannabinoids in basal condition (Figure 40B). Collectively, these data confirm that pharmacological inhibition of endothelial CB1 signalling leads to an increase of intracellular cAMP levels.

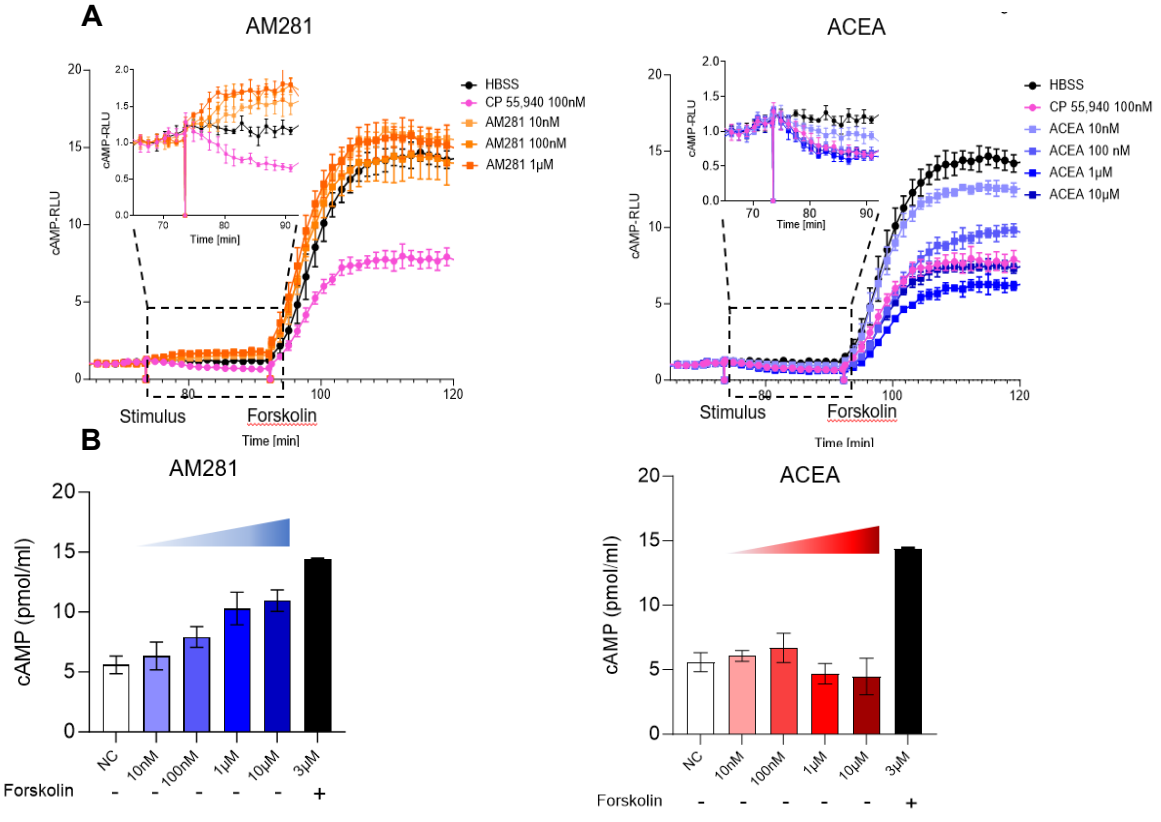

Figure 40. Cannabinoid receptor 1 (CB1) regulates cyclic adenosine monophosphate (cAMP) formation.
(A) Glosensor cAMP reporter assay in HEK293 FlpIn-TRex cell line stably expressing the cAMP-luciferase plasmid and a tetracyclin-inducible *CNR1* vector. **(B)** ELISA-based measurement of cAMP levels in HAoECs after 20 min stimulation with AM281 or ACEA (N=2). Data presented as mean ± s.e.m.

5.7.2 Endothelial CB1 signaling mediates LDL uptake via PKA-dependent CAV1 modulation

It has been previously reported that the activation of PKA leads to a reduction in CAV1 expression in Chinese hamster ovary cells.[206] Given that CB1 is a GPCR coupled to $G_{i/o}$, which inhibits adenyl cyclase (AC) activity, this inhibition results in decreased formation of cAMP. As a result, the activity of its effector PKA is reduced.[207] This knowledge led to the hypothesis that CAV1 expression is regulated by endothelial CB1 signaling in a cAMP-PKA-dependent manner. To verify this, HoEAC cells were treated with KT5720, a PKA inhibitor, before adding AM281 under OSS conditions. Consistent with previous experiments, the reduction in endothelial CAV1 expression was reproduced with AM281 treatment alone (Figure 41). Notably, the reduction in CAV1 levels and LDL uptake caused by AM281 was prevented by the pretreatment with the PKA inhibitor KT5720, suggesting that the decrease in CAV1 required PKA activation in ECs.

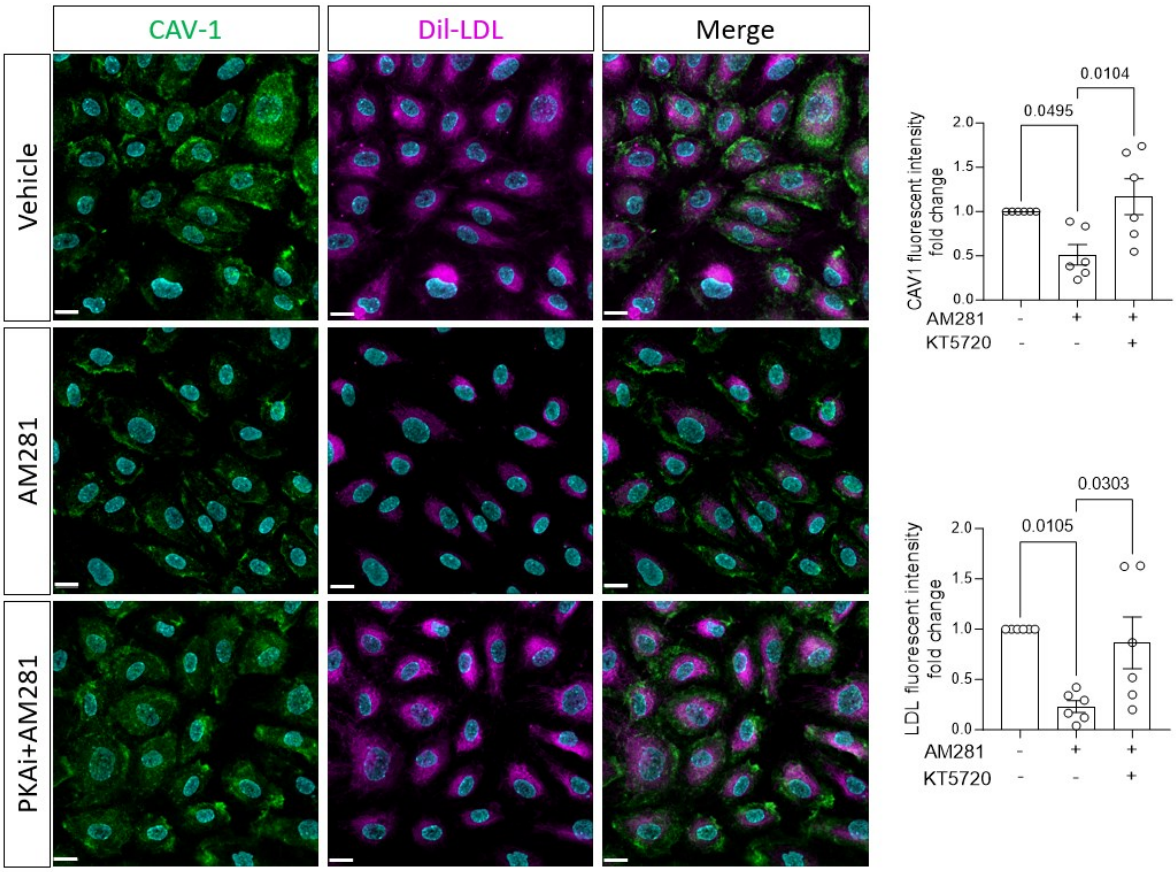

Figure 41. Endothelial CB1 signaling mediates LDL uptake via PKA-dependent CAV1 signalling. Representative immunofluorescence analysis of CAV1 expression and Dil-LDL uptake in HAoECs treated with 1 µM AM281 alone or in the presence of 1 µM PKA inhibitor (KT5720) under OSS for 24 h. An equal concentration of DMSO was added to the medium as a vehicle control. Scale bar, 20 µm. (n=6 independent experiments) Data are shown as mean ± s.e.m. P values were calculated by RM one-way ANOVA with Tukey correction in GraphPad Prism.

5.8 Impact of chronic peripheral CB1 antagonism on plaque progression and endothelial inflammation

5.8.1 Metabolic parameters after peripheral antagonist treatment

The peripheral CB1 antagonist JD5037 has been reported to exhibit potent metabolic benefits, as previously reported with global CB1 antagonists, but without showing neuropsychiatric side effects, which occur when interfering with CB1 signalling in the CNS.[208] To clarify whether JD5037 would reproduce the atheroprotective phenotype achieved by endothelial *Cnr1* deficiency, the *Ldlr*$^{-/-}$ atherosclerotic mouse model was chosen for a therapeutic study because the cholesterol profile in these mice is more comparable to humans. *Ldlr*$^{-/-}$ mice were subjected to a Western diet for 8 weeks to induce atherosclerotic lesions, followed by an additional 8-week JD5037 treatment in parallel to continuous WD feeding (Figure 42A). Consistent with previous studies,[167, 209] chronic administration of the peripheral CB1 antagonist JD5037 led to notable body weight reduction without changes in total plasma cholesterol and triglyceride levels after 16 weeks WD in both males and females (Figure 42B-D).

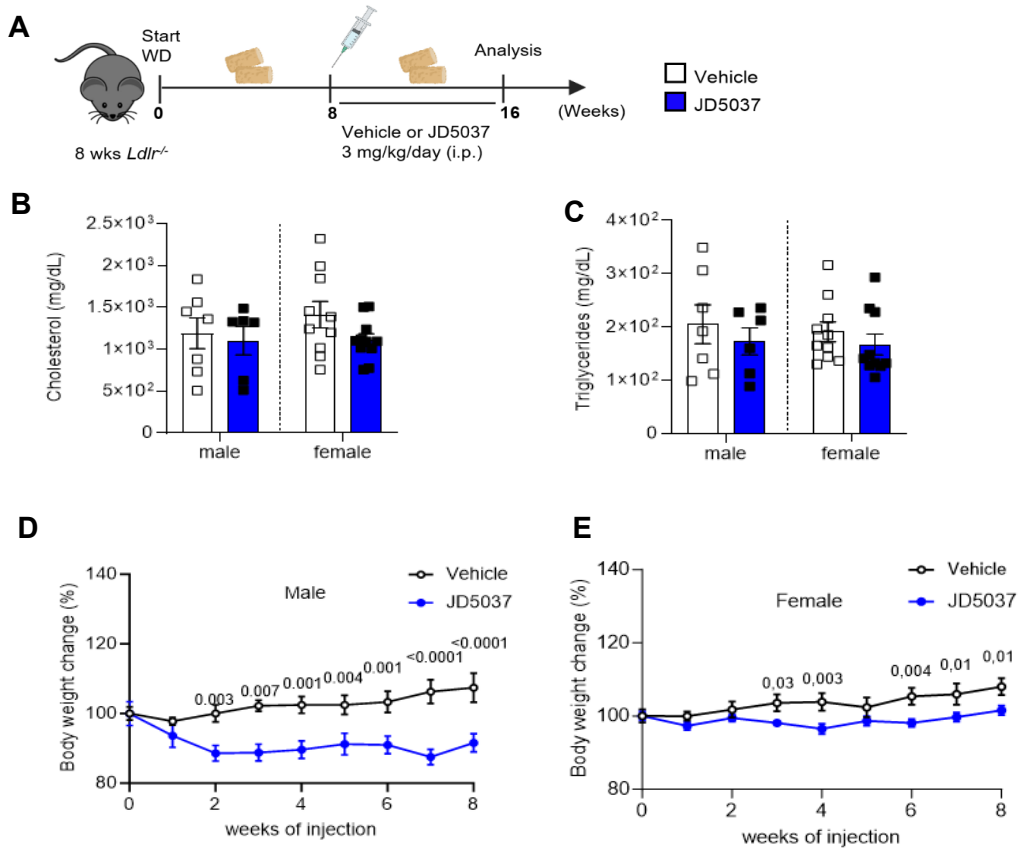

Figure 42. Peripheral CB1 antagonist JD5037 improves metabolic parameters.
(A) Scheme of experimental design. *Ldlr*$^{-/-}$ mice were fed with WD for 16 weeks. In the final 8 weeks of the study, the mice received daily intraperitoneal injections of JD5037 (3 mg/kg) or a corresponding vehicle. **(B)** Plasma cholesterol and **(C)** triglyceride levels in male and female *Ldlr*$^{-/-}$ mice (n=6-8) at the end point. Body weights change in male **(D)** and female **(E)** Ldlr$^{-/-}$ mice (n=6-8) during the 8 weeks of treatment. Two-sided unpaired Student's t-tests were conducted separately for males and females, and exact P values are indicated.

5.8.2 Effect of peripheral antagonism on atherosclerotic plaque progression

Subsequently, the progression of plaques in the mice treated with vehicle or JD5037 was assessed in cross-sections of the aortic roots (Figure 43A) and longitudinal sections of aortic arches (Figure 43B). No significant alterations in plaque sizes were observed in the aortic root when comparing the effects of JD5037 treatment to the corresponding sex-matched vehicle group (Figure 43C). Interestingly, a reduction in plaque progression in the aortic arch was noted in female *Ldlr*$^{-/-}$ mice treated with JD5037, whereas this effect was not achieved in male mice (Figure 43D). The aortic arch, an atheroprone site, is known for its preferential accumulation of lipid deposits.[210] Nevertheless, there were no notable changes in lesion size within the descending aorta, known as atheroresistant region, between JD5037 and vehicle-treated mice (Figure 43E and 43F).

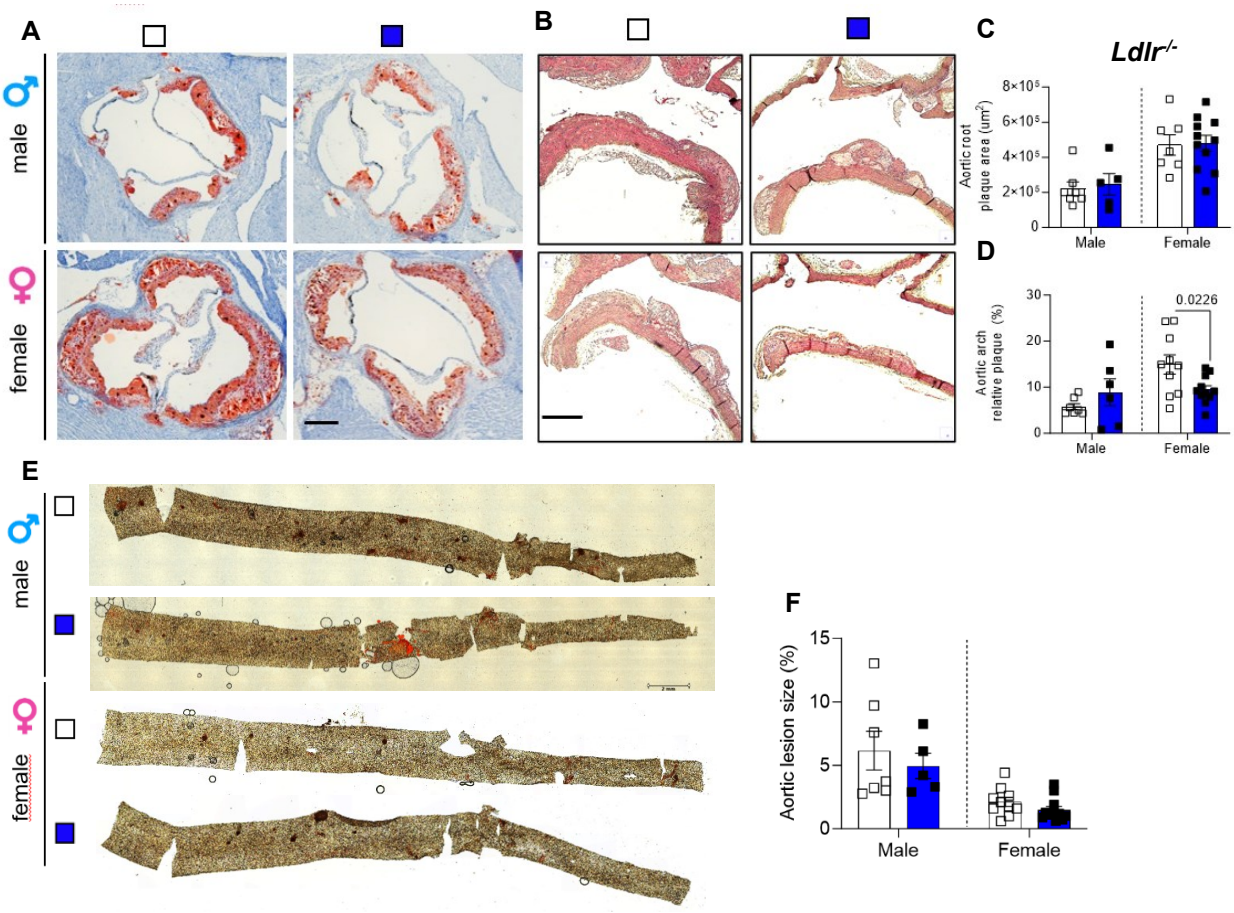

Figure 43. Peripheral CB1 antagonist JD5037 affects plaque progression in female *Ldlr*$^{-/-}$ mice. **(A)** Representative ORO stained images of aortic root cross-sections from the mice. Scale bar: 500 µm. **(B)** Representative images of H&E-stained aortic arch longitudinal sections. Quantification of absolute lesion area within **(C)** aortic roots sections (n=5-9 mice) and in **(D)** aortic arch sections (n=7-10). **(E)** En face preparations stained with ORO were used to determine the percentage of plaque in the descending thoracoabdominal aorta, relative to the total vessel area **(F)** Quantification of aortic lesions. Exact P-values are indicated for two-sided unpaired Student's t-tests conducted separately for males and females.

5.8.3 Vascular endothelial inflammation and CAV1 expression with JD5037 treatment

In agreement with previous observations in *Cnr1*$^{EC-KO}$ mice, the reduced plaque accumulation in female JD5037-treated mice was accompanied by diminished levels of CAV1, ICAM1, and VCAM1 in endothelial cells. Yet, a significant reduction in endothelial ICAM1 and VCAM1 levels in endothelial cells was also observed in male JD5037-treated mice compared to the vehicle group (Figure 44A-44D). These relevant observations, together with the elevated expression of CB1 in atheroprone regions, imply that endothelial CB1 contributes to alterations of endothelial CAV1 and lipid uptake, specifically in aortic areas exposed to disturbed flow, which are more susceptible to atherosclerotic lesion development.

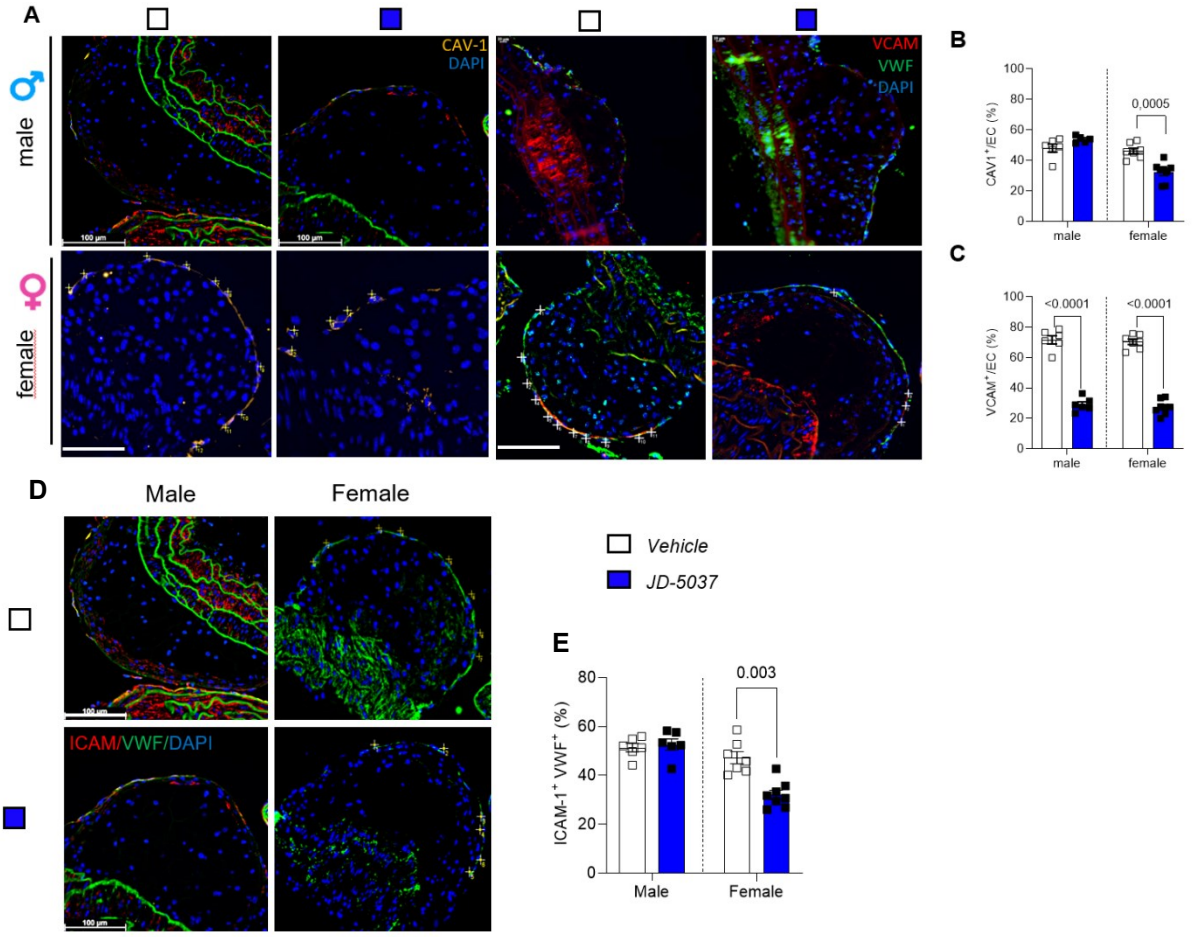

Figure 44 Impact of peripheral CB1 antagonist JD5037 on vascular endothelial inflammation and CAV1 expression.
(A) Representative images of CAV1 (yellow), VCAM (red) and vWF (green) in aortic arch plaques from *Ldlr*$^{-/-}$ mice treated with JD5037 or vehicle; nuclei were counterstained with Hoechst 33342. **(B-C)** Quantification of CAV1 and VCAM1 positive endothelial cells, using 4 sections per animal. **(D)** Double immunostaining and **(E)** quantification of ICAM1 (red) and VWF (green) -positive endothelial cells in aortic arch lesions of male and female *Ldlr*$^{-/-}$ mice (n=6-8) treated with vehicle or JD5037. Nuclei were counterstained with Hoechst 33342 (blue). Scale bar: 100 µm. Each data point on the graph signifies a biologically independent mouse sample, and all data are expressed as mean ± s.e.m. P values were obtained using an unpaired Student's t-test. Males and females were analysed independently.

6. DISCUSSION

CB1 belongs to the endocannabinoid system and plays prominent roles in the central nervous system and peripheral tissues by regulating pain, appetite, and metabolism, amongst many other physiological functions. In the cardiovascular system, past research has unveiled an upregulated CB1 expression in vulnerable human coronary artery plaques and in patients diagnosed with unstable angina pectoris.[158] Although diverse biological pathways are regulated by CB1, such as angiogenesis,[211] inflammation,[151] and apoptosis,[212] according to numerous *in vitro* and *in vivo* studies, the cell-specific role of CB1 has not been fully addressed, especially in the context of atherosclerosis. Unpublished human plaque single-cell RNA seq data from collaborators at the Technical University in Munich (Prof. Lars Maegdefessel) revealed that *CNR1* is particularly expressed in plaque endothelial cells (ECs). These findings support a central role for endothelial CB1 in atherosclerosis and have raised interest in exploring the role of endothelial CB1 in atherosclerosis. The current study used a transgenic mouse line (Bmx-CreERT2)[187] for the specific and inducible inactivation of the *Cnr1* gene in endothelial cells, thereby overcoming previously observed limitations using global knockouts or cell lines with pharmacological CB1 modulation.

This work provides unprecedented evidence for endothelial CB1 in regulating endothelial lipid uptake and responding to mechanical shear stress *in vivo* and *in vitro*. The specific deletion of endothelial *Cnr1* in *Apoe*$^{-/-}$ mice, or the application of a pharmacological blocking approach targeting peripheral CB1 in *Ldlr*$^{-/-}$ mice, reduced atherosclerotic lesion development in female mice, which is likely due to the attenuation of endothelial LDL uptake, vascular inflammation, and improved systemic metabolic function. The question of why *Cnr1* deficiency in ECs exhibits more beneficial properties in female compared to male mice remains to be elucidated in further studies. Endothelial *Cnr1* deficiency impeded LDL entry into lesions, highlighting the significant influence of CB1 signalling on endothelial lipid uptake, despite the presence of dyslipidaemia. The intimal accumulation of circulating LDL within the arterial wall is a crucial step in the development of atherosclerosis, which entails its passive penetration through a compromised endothelial barrier at lesion-prone sites, which exhibit elevated levels of endothelial senescence and apoptosis, as well as reduced capacity for proliferation and repair.[213] The current study provides evidence that endothelial CB1 plays a significant role in endothelial LDL uptake by regulating caveolae signalling. The regulation is also observed upon pharmacological treatment with the selective peripheral CB1 antagonist JD5037, thereby highlighting novel biological implications for endocannabinoid signalling in this relevant cellular process.

6.1 Endothelial CB1 expression is affected by shear stress

Shear stress, resulting from blood flow patterns, has been long recognized as a significant regulator of endothelial function.[214] In the current study, endothelial CB1 expression within two distinct regions of the arterial tree in *Apoe*$^{-/-}$ mice were examined: the aortic arch, where ECs are exposed to OSS, and the descending thoracic aorta, where ECs are subjected to LSS.[215] A significantly higher *Cnr1* expression level in the aortic arch compared to the descending thoracic aorta was observed, aligning with the prevailing understanding that OSS exacerbates atherosclerotic lesion development.[16] This suggests a potential link between endothelial *Cnr1* and atherogenic processes. Consistently, the *in vitro* flow assay with HAoECs revealed a significant upregulation of endothelial *CNR1* expression in response to OSS. These findings further highlight the dynamic nature of endothelial CB1 signalling and its capacity to adapt to varying mechanical forces. Whether endothelial CB1 itself may serve as a mechanosensitive element on the cell surface, responding to changes in shear stress patterns remains unknown. It is also conceivable that *CNR1* is a downstream target of mechanosensitive transcription factors, which requires further investigation. Moreover, the GO analysis from the transcriptomic profiling of murine aortic endothelial cells indicates that *Cnr1* is associated with the regulation of endothelial membrane raft and actin filament structures. Given that shear stress response and regulating ECs alignment depend on both the extracellular fibronectin matrix and intracellular cytoskeletal F-actin,[216] it is likely that endothelial CB1 through actin filament signalling regulation affects the endothelial morphology in response to the blood flow. The precise molecular mechanisms underlying this regulation remain to be fully elucidated.

6.2 Regulation of endothelial permeability by CB1

Endothelial actin filaments closely cooperate with the VE-cadherin–catenin complex, which forms the molecular basis of the adherence junctions.[217] These adherence junctions are specialized cell-cell connections that heavily rely on cadherins to provide the mechanical strength necessary for maintaining endothelial integrity. The upregulation of endothelial CB1 by OSS led to an investigation into whether adherence junctions and adhesion molecules in ECs are regulated by CB1 in response to hemodynamic forces. Endothelial *Cnr1* deficient mice exhibit minor, non-significant VE-cadherin levels compared to control mice, indicating that the structural integrity of adherence junctions may not be substantially affected by CB1 depletion. Though, ECs lacking the CB1 receptor exhibited a more elongated morphology, although again non-significant (likely due to the small sample size), accompanied by a reduction in the key adhesion molecules ICAM1 expression. The reduced ICAM1 expression was also observed upon *CNR1* siRNA-mediated knockdown *in vitro*, indicating a direct influence of endothelial CB1 on the expression of inflammatory mediators and adhesion molecules in ECs. These observations imply a potential role for CB1 in modulating the shape and adhesion properties

of ECs. ICAM molecules are critical for the adhesion and transmigration of leukocytes across endothelial barriers.[197] Previous studies have demonstrated that activation of ECs by disturbed flow or inflammatory mediators upregulates the production of adhesion molecules and cytokines, which in turn leads to leukocyte transmigration, increased vascular permeability, matrix degradation, and angiogenesis (Figure 47).[218, 219] The reduced ICAM1 expression by CB1 depletion can lead to a decrease in immune cell adhesiveness to the endothelium, thereby impacting the regulation of immune responses and inflammation within the vasculature. As a result, the study revealed that depletion of endothelial CB1 led to a reduction of endothelial permeability in the aorta under atherogenic conditions. These findings connect integrity and vascular inflammation to the expression of endothelial CB1.

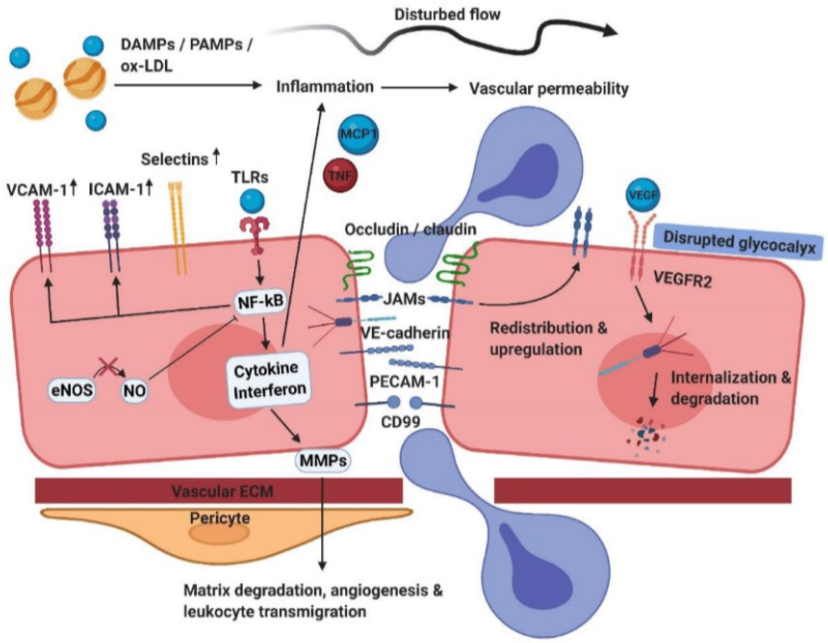

Figure 45. The endothelium under disturbed flow.
ECs can be activated in response to disturbed flow or inflammatory mediators. The junctions of ECs are vulnerable to disruption when ECs are activated. Figure adapted from Thijs J. Sluiter *et al.*[218]
DAMPs: damage-associated molecular patterns; PAMPs: pathogen-associated molecular patterns; ECM: extracellular matrix; JAMs: junctional adhesion molecules; TLR: Toll-like receptor; PECAM-1: Platelet endothelial cell adhesion molecule; VEGF: vascular endothelial growth factor.

6.3 Regulation of vascular inflammation by CB1

In previous studies, CB1 has been involved in the regulation of inflammation and immune cell extravasation, although compared to the cannabinoid CB2 receptor, its expression on immune cells is much lower.[209, 220] In skeletal muscle cells, the activation of cannabinoid CB1 receptors induced proinflammatory IL-6 mRNA expression.[221] In endothelial cells, the soybean isoflavone genistein was recently identified as a CB1 antagonist reported to inhibit plant cannabinoid-mediated inflammation and oxidative stress.[222] Jehle *et al.* showed that the endocannabinoid 2-arachidonoylglycerol (2-AG) inhibits endothelial repair and proliferation of human coronary

artery endothelial cells (HCAEC) while promoting the adhesion of leukocytes to ECs through CB1 signalling.[223] Interestingly, both alcoholic and non-alcoholic fatty liver disease (NAFLD) mouse models showed upregulated CB1 expression in the liver, and hepatocyte-specific CB1 depletion in mice resulted in reduced proinflammatory cytokines in the serum, along with reduced inflammatory cell infiltration and focal necrosis in the livers.[212] Additionally, in the diet-induced obesity (DIO) mouse model, the treatment of mice with a cannabinoid receptor 1 (CB1) antagonist attenuated inflammation and improved gut microbiota homeostasis.[224] In line with previous studies, it is intriguing that the EC-specific genetic *Cnr1* deficiency model resulted in the downregulation of several proinflammatory cytokines and chemokine receptors (e.g., *Il-6, Ccl2, Cxcr12, Ackr3*…), as revealed by transcriptional profiling. The functional role of endothelial CB1 in cell adhesion was further confirmed in this study through a monocyte adhesion assay conducted under flow conditions in HAoECs. These results indicate an inflammatory role of CB1 in ECs, as increased monocyte adhesion to ECs was observed after CB1 agonist ACEA stimulation. Recent studies by Yvonne Döring´s group demonstrated that specific depletion of CXCL12 or its receptor ACKR3 in arterial ECs reduces atherosclerotic lesions,[225, 226] while the depletion of endothelial CXCR4 increases plaque burden.[227] In their studies, they disclosed that arterial endothelial ACKR3 promotes atherosclerosis by mediating endothelial-immune cell adhesion without affecting vascular integrity. Moreover, they revealed that downregulated inflammation by endothelial *Ackr3* deficiency is associated with decreased NF-κB activity. The GSEA analysis of the current study indicates that inflammatory signalling regulated by CB1 is associated with the NF-κB pathway, although such causality is not validated further in this study. These findings, together with previous data, indicate that endothelial CB1 possibly serves as an upstream regulator of chemokine receptors ACKR3 and CXCL12, thereby modulating vascular inflammation in an NF-κB-dependent manner.

Another intriguing observation is that CB1 activation in HAoECs resulted in decreased anti-inflammatory transcription factor, *KLF2* and the KLF2-dependent gene NOS3 expression, which is induced by LSS.[228] Meanwhile, LSS-downregulated adhesion molecules ICAM1, VCAM1 and glycolysis enzyme PFKFB3 expression are enhanced upon CB1 activation. In fact, previous studies already demonstrated that the CB1 antagonist rimonabant improved aortic endothelium-dependent vasodilation and decreased aortic ROS production *in vivo*.[165] In cultured white adipocytes, rimonabant treatment increased the eNOS expression and mitochondrial DNA content,[229] whereas the selective CB1 agonist ACEA impaired eNOS production in mouse white adipose tissue cells.[230] Nonetheless, this direct role of CB1 on *KLF2* and *NOS3* has never been addressed in aortic ECs before, especially in the context of shear stress. Furthermore, the current study showed a downregulation of adhesion molecules and pro-inflammatory chemokine receptors mediated by CB1 silencing, together with a decrease in TNFα-induced ROS production. The uncoupling of eNOS from L-arginine leads to ROS

production, thereby accelerating the pathogenesis of atherosclerosis through the initiation of oxidative damage within arterial walls.[231] Collectively, these data suggest that there is a delicate balance of pro- and antioxidative stress signalling regulated by endothelial CB1.

6.4 The absence of endothelial *Cnr1* affects cardiac function and blood flow velocity

Previous studies have indicated that chronic use of marijuana causes a prolonged reduction in both blood pressure and heart rate, whereas acute use increases heart rate without affecting blood pressure.[232, 233] The echocardiographic assessment of cardiac function parameters in the described mouse model revealed that the absence of endothelial *Cnr1* resulted in improved cardiac function, characterized by preserved ejection fraction and fractional shortening after atherogenic diet feeding (unpublished data from Anna Kaltenbach, not presented in this thesis). Notably, this effect was observed without affecting the heart rate, suggesting that endothelial CB1 could potentially influence cardiac function. In anaesthetized animals, Δ9-tetrahydrocannabidiol (THC), its synthetic analogue HU-210, and anandamide induce bradycardia by decreasing cardiac contractility through the activation of CB1 receptors.[155] Cannabinoid receptors localized at central and presynaptic autonomic nerve terminals modulate neurotransmitter release, playing a crucial role in modulating sympathetic outflow and contributing to the constant control of cardiovascular function.[234, 235] Peripheral CB1 receptors appear to be involved in specific vasodilatory responses to cannabinoids; these effects may also be influenced by other receptors (such as TRPV1, GPR55, and unidentified ones).[236-238] Nonetheless, the prevailing evidence indicates that in healthy individuals under normal conditions, endocannabinoids play a limited or negligible role in regulating the cardiovascular system.[239, 240]

Besides, the echocardiographic assessment (unpublished data from Anna Kaltenbach, not presented in this thesis) revealed that the absence of endothelial CB1 increases flow velocity in atheroprone sites of the aorta, thereby sharing a similar phenotype with *Cav1* deficient mice.[115] In this regard, it was previously demonstrated that elevated flow velocity correlates with increased LDL uptake *ex vivo*.[241] In another study, increased LDL accumulation was observed when vascular ECs were exposed to low-shear stress conditions as compared to high-shear stress conditions in the presence of filtration flow.[242] However, the connection between flow velocity and atherogenesis is complicated and not well understood. Despite the higher velocity found in the atheroprone regions of endothelial *Cnr1*-deficient mice, a significant reduction in LDL infiltration was also observed in the *ex vivo* carotid artery model.

6.5 Endothelial CB1 regulates systemic metabolic function

The regulation of CB1 in adipose tissue and its impact on systemic metabolic function has been extensively studied.[159, 243] Recent findings indicate a marked increase in CB1 receptor expression detected in human cirrhotic liver ECs, indicating that CB1 in ECs of peripheral organs may be actively involved in systemic metabolic function.[244, 245] Here, the absence of endothelial CB1 displayed reduced white adipocytes mass and increased lipolysis in BAT, protecting against WD-induced body weight gain and metabolic disturbances. The enhanced lipolysis observed in *Cnr1*$^{EC\text{-}KO}$ mice was associated with an upregulation of *Gpihbp1* expression, thereby facilitating the entry of LpL into capillaries. Previous studies have shown that ECs maintain metabolic homeostasis by engaging in crosstalk with adipocytes through the secretion of extracellular vesicles (EVs).[246, 247] Erika Monelli and colleagues identified that local production of polyamines by ECs stimulates adipocyte lipolysis, mediated by mTORC1-dependent signalling, which in turn supported endothelial cell oxidative metabolism and reduced adiposity.[248, 249] Moreover, *Cnr1*$^{EC\text{-}KO}$ mice showed upregulated *Prdm16* expression, which is an important transcriptional regulator mediating beige adipocyte differentiation. This might hint at the regulation of mitochondrial respiration and ATP biosynthesis by endothelial CB1, which is also supported by the transcriptomic signature of BAT ECs from *Cnr1*$^{EC\text{-}KO}$ mice. Other factors may also contribute to the striking phenotypes observed in *Cnr1*$^{EC\text{-}KO}$ mice, including reduced lipid accumulation, enhanced insulin sensitivity and liver β-oxidation in the liver. These findings suggest that endothelial CB1 regulates adipose tissue and liver homeostasis in mice associated with insulin resistance and metabolic disorders. Despite these metabolic observations in the *Cnr1*$^{EC\text{-}KO}$ mice, the functional characteristics of ECs vary significantly depending on their location within vessels and tissues.[250] Hence, the tissue-specific mechanisms of endothelial CB1 in different organs and vascular beds deserve to be studied in more detail.

Despite an improved adipose tissue and liver metabolism, the endothelial *Cnr1*-deficient had more elevated plasma cholesterol levels, as previously reported in *Cav1*$^{-/-}$ mice.[251] A common phenotype of endothelial *Cav1* and *Cnr1* deficiency is the reduced LDL infiltration to the aorta and reduced lesion progression.[252] The systemic effects on plasma cholesterol levels were only observed in the *Apoe*$^{-/-}$ background, but not the *Ldlr*$^{-/-}$ model when treating mice chronically with the peripheral CB1 antagonist, indicating a potential clinical benefit without undesired side effects such as elevated plasma cholesterol levels.

6.6 Endothelial CB1 regulates LDL uptake in endothelial cells

It has long been believed that endothelial dysfunction typically begins at atheroprone sites, where the endothelium becomes more permeable to LDL. The accumulation of LDL within the

intima locally triggers inflammation and lipid buildup, ultimately resulting in the development of atherosclerotic lesions.[253] Sagamura and collegues[158] have previously reported upregulated CB1 expression in vulnerable human coronary artery plaques characterised by higher amounts of lipids and macrophages, indicating a regulatory role of CB1 in lipid metabolism. The GSEA findings indicate that signalling of CB1 is involved in the regulation of membrane raft and caveola, which are the major lipid uptake domains of endothelial cells.[108, 254] The reduced lipid content observed within the plaques of *Cnr1*$^{EC\text{-}KO}$ mice supports the *in vivo* role of EC-CB1 in regulating the cavaolae-mediated uptake of circulating LDL into the artery wall. While classical lipid receptors such as LDLR, SRB1, and LOX-1 remain unaffected by endothelial CB1 depletion, CAV1, and ALK-1, which are associated with caveola signalling, are downregulated in *Cnr1*$^{\Delta EC}$ mice. In fact, previous reports have shown that LDL can traverse the endothelial cell layer through specific transcytosis pathways that are independent of LDLR. Depletion of endothelial CAV1 or ALK-1 leads to impaired LDL uptake.[113, 121, 252] The current findings provided compelling evidence that CB1 agonist and antagonist treatment under flow conditions directly modulate CAV1 expression in human ECs, consequently regulating the uptake of LDL. Activation of CB1, a G protein-coupled receptor, has been reported to elicit G_i protein-dependent inhibition of adenyl cyclase (AC), resulting in a reduction of intracellular cyclic AMP production, which controls PKA activity.[202, 203] Inhibition of CB1 signalling, as observed in this study, restores adenylyl cyclase activity, leading to an increase in cAMP in both HEK293 FlpIn-Trex and HAoECs. Interestingly, previous studies showed that stimulation of cAMP signalling by forskolin, an adenyl cyclase activator, resulted in a decrease of *Cav1* mRNA expression in smooth muscle cells.[206, 255] Based on this evidence, it was speculated that the downregulation of CAV1 expression in ECs was due to increased cAMP levels and, consequently, enhanced PKA activity in the absence of CB1. In support of this hypothesis, *Cav1* expression was restored in AM281-treated HAoECs upon preincubation with the PKA inhibitor KT5720, which binds and inactivates the catalytic subunit of PKA. Thus, the modulation of PKA activity by the CB1 receptor may influence CAV1-mediated LDL trafficking, ultimately leading to altered LDL entry into the artery wall, which in turn affects the development of atherosclerosis. Furthermore, c-Jun emerged as one of the prominent transcription factor binding sites in the *CAV1* gene promoter (https://www.genecards.org/cgi-bin/carddisp.pl?gene=CAV1),[256] which was linked to the endothelial CB1-regulated transcriptomic signature in this study, according to the prediction of top transcription factor co-regulatory networks controlled by endothelial *Cnr1*. Recent research has also shown that the CB1 receptor couples with the stress-activated protein kinase, c-Jun N-terminal kinase (JNK), in cultured cells.[257, 258] In addition to the proposed cAMP-PKA- and c-JUN-dependent regulation of CAV1, it is possible that additional molecular mechanisms may be involved.

6.7 Peripheral CB1 antagonist administration suppresses endothelial CAV1 and adhesion molecular expression

Previous studies comparing the metabolic effects of the peripherally restricted CB1 inverse agonist JD5037 and its brain-penetrating parent compound found equal benefits in alleviating daily food consumption, body weight, and adiposity in DIO mice.[167] Of note, chronic treatment of *Ldlr*$^{-/-}$ mice with JD5037 not only reproduced the expected effects on body weight gain mitigation in atherogenic diet conditions but also inhibited the progression of atherosclerotic plaques. Although potential anti-atherogenic effects mediated by other cell types can not be ruled out, JD5037 administration notably improved endothelial function by decreasing endothelial CAV1 and adhesion molecules, as observed in the endothelial cell-specific genetic *Cnr1* deficiency model. The observed atheroprotective properties of the peripheral CB1 antagonist appear to be less relevant in male mice. The sex-specific CB1 signalling in atherosclerosis still remains to be studied in greater detail in order to further elucidate these findings.

6.8 Limitations of this study

It has been demonstrated that CB1 receptors, located on the neuronal mitochondrial membranes, engage a cAMP-PKA pathway to reduce respiration.[259] However, a limitation of this study is the unavailability of a CB1-specific antibody for detection at the protein level, which restricts the precise location of the CB1 receptor at the outer or mitochondrial cell membrane and the exploration of potential colocalization between CAV1 and CB1. A lentiviral vector for transgenic expression of a CB1 reporter fusion protein (e.g. CB1-GFP) in endothelial cells might help to clarify these remaining questions. CAV1 inactivation has been reported to inhibit ICAM1 and VCAM1 expression and decrease endothelial permeability,[115, 260] which is similar to the endothelial cell-specific genetic *Cnr1* deficiency phenotype. Further studies using CAV1 knockout mice or *CAV1* silencing in endothelial cells could provide insights whether the reduced vascular inflammation observed in *Cnr1*$^{EC\text{-}KO}$ mice is a consequence of *Cav1* downregulation. In addition, the endocannabinoid system is synthesized in regions of the hypothalamus responsible for hormone production, which is a critical modulator of female reproductive processes, implying the presence of sexual dimorphism in the endocannabinoid system.[261] A review on sex-dependent effects of cannabinoid compounds on emotion and cognition suggested that males have a greater abundance of brain CB1 receptor binding sites compared to females, while females appear to have more efficient CB1 receptors based on G protein receptor activation responses in various brain regions.[262] It is somewhat unclear how solid the experimental evidence is to support this assumption, given the limitations for detecting endogenous CB1 protein levels or receptor activity, respectively, and whether such findings can be extrapolated to other tissues and cells. In the present study, aortic ECs isolated from

female mouse aortas exhibited higher levels of *Cnr1* gene expression compared to male ECs, even though circulating endocannabinoid levels were comparable in male and female mice. Additional investigation is required to explore the sex-specific differences of endothelial CB1 signalling and underlying molecular mechanisms, which may involve both sex hormone-dependent and independent effects.

6.9 Conclusion and future perspectives

In summary, endothelial CB1 expression is upregulated by atheroprone oscillatory shear stress. Genetic deficiency or pharmacological inhibition of endothelial CB1 signalling conferred an atheroprotective phenotype in mice with improved metabolic function, reduced vascular inflammation and diminished LDL entry into the artery wall. Results from human aortic endothelial cells reinforced the anti-inflammatory signalling associated with CB1 receptor silencing or antagonist treatment, while CB1 activation induced a proinflammatory phenotype, monocyte adhesion and EC LDL uptake. The regulation of endothelial LDL uptake by CB1 involves a cAMP-PKA-dependent modulation of CAV1 regulation. In conclusion, peripheral CB1 antagonists may hold promise as an effective therapeutic strategy for treating atherosclerosis and related metabolic disorders.

7. REFERENCES

[1]. Shaito, A.; Aramouni, K.; Assaf, R.; Parenti, A.; Orekhov, A.; Yazbi, A. E.; Pintus, G.; Eid, A. H. Oxidative Stress-Induced Endothelial Dysfunction in Cardiovascular Diseases. Frontiers in Bioscience-Landmark 2022, 27 (3), 0105. DOI: 10.31083/j.fbl2703105.

[2]. Roth, G. A.; Abate, D.; Abate, K. H.; Abay, S. M.; Abbafati, C.; Abbasi, N.; Abbastabar, H.; Abd-Allah, F.; Abdela, J.; Abdelalim, A.; et al. Global, regional, and national age-sex-specific mortality for 282 causes of death in 195 countries and territories, 1980–2017: a systematic analysis for the Global Burden of Disease Study 2017. The Lancet 2018, 392 (10159), 1736-1788. DOI: 10.1016/s0140-6736(18)32203-7.

[3]. Vikramaditya, B.; Satija, M.; Chaudhary, A.; Sharma, S.; Girdhar, S.; Bansal, P. A community based cross-sectional study to estimate total cardiovascular risk in rural Punjab. Int J Community Med Public Health 2017, 4, 1295-1302.

[4]. Vaduganathan, M.; Mensah, G. A.; Turco, J. V.; Fuster, V.; Roth, G. A. The Global Burden of Cardiovascular Diseases and Risk. Journal of the American College of Cardiology 2022, 80 (25), 2361-2371. DOI: 10.1016/j.jacc.2022.11.005.

[5]. Welsh, P.; Grassia, G.; Botha, S.; Sattar, N.; Maffia, P. Targeting inflammation to reduce cardiovascular disease risk: a realistic clinical prospect? British Journal of Pharmacology 2017, 174 (22), 3898-3913. DOI: 10.1111/bph.13818.

[6]. Balta, S. Endothelial Dysfunction and Inflammatory Markers of Vascular Disease. Curr Vasc Pharmacol 2021, 19 (3), 243-249. DOI: 10.2174/1570161118666200421142542.

[7]. Xu, S.; Ilyas, I.; Little, P. J.; Li, H.; Kamato, D.; Zheng, X.; Luo, S.; Li, Z.; Liu, P.; Han, J.; et al. Endothelial Dysfunction in Atherosclerotic Cardiovascular Diseases and Beyond: From Mechanism to Pharmacotherapies. Pharmacological Reviews 2021, 73 (3), 924-967. DOI: 10.1124/pharmrev.120.000096.

[8]. Fan, J.; Watanabe, T. Atherosclerosis: Known and unknown. Pathology International 2022, 72 (3), 151-160. DOI: 10.1111/pin.13202.

[9]. Libby, P. The changing landscape of atherosclerosis. Nature 2021, 592 (7855), 524-533. DOI: 10.1038/s41586-021-03392-8.

[10]. Tabas, I.; García-Cardeña, G.; Owens, G. K. Recent insights into the cellular biology of atherosclerosis. Journal of Cell Biology 2015, 209 (1), 13-22. DOI: 10.1083/jcb.201412052.

[11]. Zhu, Y.; Xian, X.; Wang, Z.; Bi, Y.; Chen, Q.; Han, X.; Tang, D.; Chen, R. Research Progress on the Relationship between Atherosclerosis and Inflammation. Biomolecules 2018, 8 (3), 80. DOI: 10.3390/biom8030080.

[12]. Badimon, L.; Vilahur, G. Thrombosis formation on atherosclerotic lesions and plaque rupture. J Intern Med 2014, 276 (6), 618-632. DOI: 10.1111/joim.12296.

[13]. Kong, P.; Cui, Z.-Y.; Huang, X.-F.; Zhang, D.-D.; Guo, R.-J.; Han, M. Inflammation and atherosclerosis: signaling pathways and therapeutic intervention. Signal Transduction and Targeted Therapy 2022, 7 (1). DOI: 10.1038/s41392-022-00955-7.

[14]. Lutgens, E.; Atzler, D.; Döring, Y.; Duchene, J.; Steffens, S.; Weber, C. Immunotherapy for cardiovascular disease. Eur Heart J 2019, 40 (48), 3937-3946. DOI: 10.1093/eurheartj/ehz283.

[15]. Ridker, P. M.; Everett, B. M.; Thuren, T.; Macfadyen, J. G.; Chang, W. H.; Ballantyne, C.; Fonseca, F.; Nicolau, J.; Koenig, W.; Anker, S. D.; et al. Antiinflammatory Therapy with Canakinumab for Atherosclerotic Disease. New England Journal of Medicine 2017, 377 (12), 1119-1131. DOI: 10.1056/nejmoa1707914.

[16]. Cheng, C.; Tempel, D.; van Haperen, R.; van der Baan, A.; Grosveld, F.; Daemen, M. J.; Krams, R.; de Crom, R. Atherosclerotic lesion size and vulnerability are determined by

patterns of fluid shear stress. Circulation 2006, 113 (23), 2744-2753. DOI: 10.1161/circulationaha.105.590018.

[17]. Roy, P.; Orecchioni, M.; Ley, K. How the immune system shapes atherosclerosis: roles of innate and adaptive immunity. Nature Reviews Immunology 2022, 22 (4), 251-265. DOI: 10.1038/s41577-021-00584-1.

[18]. McAlpine, C. S.; Kiss, M. G.; Rattik, S.; He, S.; Vassalli, A.; Valet, C.; Anzai, A.; Chan, C. T.; Mindur, J. E.; Kahles, F. Sleep modulates haematopoiesis and protects against atherosclerosis. Nature 2019, 566 (7744), 383-387.

[19]. Incalza, M. A.; D'Oria, R.; Natalicchio, A.; Perrini, S.; Laviola, L.; Giorgino, F. Oxidative stress and reactive oxygen species in endothelial dysfunction associated with cardiovascular and metabolic diseases. Vascul Pharmacol 2018, 100, 1-19. DOI: 10.1016/j.vph.2017.05.005.

[20]. Liao, J. K. Linking endothelial dysfunction with endothelial cell activation. The Journal of clinical investigation 2013, 123 (2), 540-541.

[21]. Duchene, J.; von Hundelshausen, P. Platelet-derived chemokines in atherosclerosis. Hämostaseologie 2015, 35 (02), 137-141.

[22]. Galkina, E.; Ley, K. Leukocyte influx in atherosclerosis. Current drug targets 2007, 8 (12), 1239-1248.

[23]. Björkegren, J. L.; Lusis, A. J. Atherosclerosis: recent developments. Cell 2022.

[24]. Koltsova, E. K.; Ley, K. How dendritic cells shape atherosclerosis. Trends Immunol 2011, 32 (11), 540-547. DOI: 10.1016/j.it.2011.07.001.

[25]. Getz, G. S.; Reardon, C. A. Do the Apoe−/− and Ldlr−/–mice yield the same insight on atherogenesis? Arteriosclerosis, thrombosis, and vascular biology 2016, 36 (9), 1734-1741.

[26]. Orecchioni, M.; Meyer, M. A.; Hedrick, C. C.; Ley, K. Flow Cytometry and Mass Cytometry Mass cytometry for Measuring the Immune Cell Immune cells Infiltrate in Atherosclerotic Arteries. In Atherosclerosis: Methods and Protocols, Springer, 2022; pp 779-800.

[27]. Jaffer, F. A.; Calfon, M. A.; Rosenthal, A.; Mallas, G.; Razansky, R. N.; Mauskapf, A.; Weissleder, R.; Libby, P.; Ntziachristos, V. Two-dimensional intravascular near-infrared fluorescence molecular imaging of inflammation in atherosclerosis and stent-induced vascular injury. Journal of the American College of Cardiology 2011, 57 (25), 2516-2526.

[28]. Li, J.; Wang, K.; Pan, W.; Li, N.; Tang, B. Targeted imaging in atherosclerosis. Analytical Chemistry 2022, 94 (36), 12263-12273.

[29]. Moore, K. J.; Sheedy, F. J.; Fisher, E. A. Macrophages in atherosclerosis: a dynamic balance. Nature Reviews Immunology 2013, 13 (10), 709-721.

[30]. Serbina, N. V.; Pamer, E. G. Monocyte emigration from bone marrow during bacterial infection requires signals mediated by chemokine receptor CCR2. Nature immunology 2006, 7 (3), 311-317.

[31]. Rahman, K.; Vengrenyuk, Y.; Ramsey, S. A.; Vila, N. R.; Girgis, N. M.; Liu, J.; Gusarova, V.; Gromada, J.; Weinstock, A.; Moore, K. J. Inflammatory Ly6C hi monocytes and their conversion to M2 macrophages drive atherosclerosis regression. The Journal of clinical investigation 2017, 127 (8), 2904-2915.

[32]. Hamers, A. A.; Dinh, H. Q.; Thomas, G. D.; Marcovecchio, P.; Blatchley, A.; Nakao, C. S.; Kim, C.; McSkimming, C.; Taylor, A. M.; Nguyen, A. T. Human monocyte heterogeneity as revealed by high-dimensional mass cytometry. Arteriosclerosis, thrombosis, and vascular biology 2019, 39 (1), 25-36.

[33]. Schober, A.; Zernecke, A.; Liehn, E. A.; Von Hundelshausen, P.; Knarren, S.; Kuziel, W. A.; Weber, C. Crucial role of the CCL2/CCR2 axis in neointimal hyperplasia after arterial injury in hyperlipidemic mice involves early monocyte recruitment and CCL2 presentation on platelets. Circulation research 2004, 95 (11), 1125-1133.

[34]. Yan, Y.; Thakur, M.; van der Vorst, E. P.; Weber, C.; Döring, Y. Targeting the chemokine network in atherosclerosis. Atherosclerosis 2021, 330, 95-106.

[35]. Živković, L.; Asare, Y.; Bernhagen, J.; Dichgans, M.; Georgakis, M. K. Pharmacological targeting of the CCL2/CCR2 Axis for atheroprotection: a meta-analysis of preclinical studies. Arteriosclerosis, Thrombosis, and Vascular Biology 2022, 42 (5), e131-e144.

[36]. Feria, M.; Díaz-González, F. The CCR2 receptor as a therapeutic target. Expert Opinion on Therapeutic Patents 2006, 16 (1), 49-57.

[37]. Moore, K. J.; Tabas, I. Macrophages in the pathogenesis of atherosclerosis. Cell 2011, 145 (3), 341-355. DOI: 10.1016/j.cell.2011.04.005.

[38]. Tabas, I.; Lichtman, A. H. Monocyte-macrophages and T cells in atherosclerosis. Immunity 2017, 47 (4), 621-634.

[39]. Moore, K. J.; Kunjathoor, V. V.; Koehn, S. L.; Manning, J. J.; Tseng, A. A.; Silver, J. M.; McKee, M.; Freeman, M. W. Loss of receptor-mediated lipid uptake via scavenger receptor A or CD36 pathways does not ameliorate atherosclerosis in hyperlipidemic mice. J Clin Invest 2005, 115 (8), 2192-2201. DOI: 10.1172/jci24061.

[40]. Kim, K.; Shim, D.; Lee, J. S.; Zaitsev, K.; Williams, J. W.; Kim, K.-W.; Jang, M.-Y.; Seok Jang, H.; Yun, T. J.; Lee, S. H. Transcriptome analysis reveals nonfoamy rather than foamy plaque macrophages are proinflammatory in atherosclerotic murine models. Circulation research 2018, 123 (10), 1127-1142.

[41]. Spann, N. J.; Garmire, L. X.; McDonald, J. G.; Myers, D. S.; Milne, S. B.; Shibata, N.; Reichart, D.; Fox, J. N.; Shaked, I.; Heudobler, D. Regulated accumulation of desmosterol integrates macrophage lipid metabolism and inflammatory responses. Cell 2012, 151 (1), 138-152.

[42]. Klinke, A.; Nussbaum, C.; Kubala, L.; Friedrichs, K.; Rudolph, T. K.; Rudolph, V.; Paust, H.-J.; Schröder, C.; Benten, D.; Lau, D. Myeloperoxidase attracts neutrophils by physical forces. Blood, The Journal of the American Society of Hematology 2011, 117 (4), 1350-1358.

[43]. Ionita, M. G.; van den Borne, P.; Catanzariti, L. M.; Moll, F. L.; de Vries, J. P.; Pasterkamp, G.; Vink, A.; de Kleijn, D. P. High neutrophil numbers in human carotid atherosclerotic plaques are associated with characteristics of rupture-prone lesions. Arterioscler Thromb Vasc Biol 2010, 30 (9), 1842-1848. DOI: 10.1161/atvbaha.110.209296.

[44]. Rotzius, P.; Thams, S.; Soehnlein, O.; Kenne, E.; Tseng, C. N.; Björkström, N. K.; Malmberg, K. J.; Lindbom, L.; Eriksson, E. E. Distinct infiltration of neutrophils in lesion shoulders in ApoE-/- mice. Am J Pathol 2010, 177 (1), 493-500. DOI: 10.2353/ajpath.2010.090480.

[45]. Jonasson, L.; Holm, J.; Skalli, O.; Gabbiani, G.; Hansson, G. K. Expression of class II transplantation antigen on vascular smooth muscle cells in human atherosclerosis. J Clin Invest 1985, 76 (1), 125-131. DOI: 10.1172/jci111934.

[46]. Saigusa, R.; Winkels, H.; Ley, K. T cell subsets and functions in atherosclerosis. Nature Reviews Cardiology 2020, 17 (7), 387-401.

[47]. Zhou, X.; Nicoletti, A.; Elhage, R.; Hansson, G. K. Transfer of CD4(+) T cells aggravates atherosclerosis in immunodeficient apolipoprotein E knockout mice. Circulation 2000, 102 (24), 2919-2922. DOI: 10.1161/01.cir.102.24.2919.

[48]. Huber, S. A.; Sakkinen, P.; David, C.; Newell, M. K.; Tracy, R. P. T helper-cell phenotype regulates atherosclerosis in mice under conditions of mild hypercholesterolemia. Circulation 2001, 103 (21), 2610-2616. DOI: 10.1161/01.cir.103.21.2610.

[49]. Elhage, R.; Gourdy, P.; Brouchet, L.; Jawien, J.; Fouque, M. J.; Fiévet, C.; Huc, X.; Barreira, Y.; Couloumiers, J. C.; Arnal, J. F.; Bayard, F. Deleting TCR alpha beta+ or CD4+ T lymphocytes leads to opposite effects on site-specific atherosclerosis in female apolipoprotein E-deficient mice. Am J Pathol 2004, 165 (6), 2013-2018. DOI: 10.1016/s0002-9440(10)63252-x.

[50]. Sage, A. P.; Tsiantoulas, D.; Binder, C. J.; Mallat, Z. The role of B cells in atherosclerosis. Nature Reviews Cardiology 2019, 16 (3), 180-196.

[51]. Kyaw, T.; Tipping, P.; Toh, B. H.; Bobik, A. Current understanding of the role of B cell subsets and intimal and adventitial B cells in atherosclerosis. Curr Opin Lipidol 2011, 22 (5), 373-379. DOI: 10.1097/MOL.0b013e32834adaf3.

[52]. Ketelhuth, D. F.; Hansson, G. K. Adaptive response of T and B cells in atherosclerosis. Circulation research 2016, 118 (4), 668-678.

[53]. Tsiantoulas, D.; Diehl, C. J.; Witztum, J. L.; Binder, C. J. B cells and humoral immunity in atherosclerosis. Circulation research 2014, 114 (11), 1743-1756.

[54]. Caligiuri, G.; Nicoletti, A.; Poirier, B.; Hansson, G. K. Protective immunity against atherosclerosis carried by B cells of hypercholesterolemic mice. The Journal of clinical investigation 2002, 109 (6), 745-753.

[55]. Morris-Rosenfeld, S.; Perry, H. M.; Srikakulapu, P.; McSkimming, C.; Gonen, A.; Prohaska, T. A.; Tsimikas, S.; Witztum, J. L.; Bender, T. P.; Taylor, A. B-1b Cells Secrete Atheroprotective IgM and Attenuate Atherosclerosis. Arteriosclerosis, Thrombosis, and Vascular Biology 2015, 35 (suppl_1), A21-A21.

[56]. Kyaw, T.; Tay, C.; Krishnamurthi, S.; Kanellakis, P.; Agrotis, A.; Tipping, P.; Bobik, A.; Toh, B.-H. B1a B lymphocytes are atheroprotective by secreting natural IgM that increases IgM deposits and reduces necrotic cores in atherosclerotic lesions. Circulation research 2011, 109 (8), 830-840.

[57]. Lewis, M. J.; Malik, T. H.; Ehrenstein, M. R.; Boyle, J. J.; Botto, M.; Haskard, D. O. Immunoglobulin M is required for protection against atherosclerosis in low-density lipoprotein receptor-deficient mice. Circulation 2009, 120 (5), 417-426. DOI: 10.1161/circulationaha.109.868158.

[58]. Kyaw, T.; Tay, C.; Khan, A.; Dumouchel, V.; Cao, A.; To, K.; Kehry, M.; Dunn, R.; Agrotis, A.; Tipping, P. Conventional B2 B cell depletion ameliorates whereas its adoptive transfer aggravates atherosclerosis. The Journal of Immunology 2010, 185 (7), 4410-4419.

[59]. Ait-Oufella, H.; Herbin, O.; Bouaziz, J.-D.; Binder, C. J.; Uyttenhove, C.; Laurans, L.; Taleb, S.; Van Vré, E.; Esposito, B.; Vilar, J. B cell depletion reduces the development of atherosclerosis in mice. Journal of Experimental Medicine 2010, 207 (8), 1579-1587.

[60]. Nus, M.; Sage, A. P.; Lu, Y.; Masters, L.; Lam, B. Y.; Newland, S.; Weller, S.; Tsiantoulas, D.; Raffort, J.; Marcus, D. Marginal zone B cells control the response of follicular helper T cells to a high-cholesterol diet. Nature medicine 2017, 23 (5), 601-610.

[61]. Gimbrone, M. A.; García-Cardeña, G. Endothelial Cell Dysfunction and the Pathobiology of Atherosclerosis. Circulation Research 2016, 118 (4), 620-636. DOI: 10.1161/circresaha.115.306301.

[62]. Mitchell, J. A.; Ali, F.; Bailey, L.; Moreno, L.; Harrington, L. S. Role of nitric oxide and prostacyclin as vasoactive hormones released by the endothelium. Exp Physiol 2008, 93 (1), 141-147. DOI: 10.1113/expphysiol.2007.038588.

[63]. Cai, H.; Harrison, D. G. Endothelial dysfunction in cardiovascular diseases: the role of oxidant stress. Circ Res 2000, 87 (10), 840-844. DOI: 10.1161/01.res.87.10.840.

[64]. Souilhol, C.; Serbanovic-Canic, J.; Fragiadaki, M.; Chico, T. J.; Ridger, V.; Roddie, H.; Evans, P. C. Endothelial responses to shear stress in atherosclerosis: a novel role for developmental genes. Nat Rev Cardiol 2020, 17 (1), 52-63. DOI: 10.1038/s41569-019-0239-5.

[65]. Kim, J.-a.; Montagnani, M.; Chandrasekran, S.; Quon, M. J. Role of lipotoxicity in endothelial dysfunction. Heart failure clinics 2012, 8 (4), 589-607.

[66]. Gimbrone, M. A., Jr.; Topper, J. N.; Nagel, T.; Anderson, K. R.; Garcia-Cardeña, G. Endothelial dysfunction, hemodynamic forces, and atherogenesis. Ann N Y Acad Sci 2000, 902, 230-239; discussion 239-240. DOI: 10.1111/j.1749-6632.2000.tb06318.x.

[67]. Bonetti, P. O.; Lerman, L. O.; Lerman, A. Endothelial Dysfunction. Arteriosclerosis, Thrombosis, and Vascular Biology 2003, 23 (2), 168-175. DOI: 10.1161/01.atv.0000051384.43104.fc.

[68]. Stone, P. H.; Saito, S.; Takahashi, S.; Makita, Y.; Nakamura, S.; Kawasaki, T.; Takahashi, A.; Katsuki, T.; Nakamura, S.; Namiki, A.; et al. Prediction of Progression of Coronary Artery Disease and Clinical Outcomes Using Vascular Profiling of Endothelial Shear Stress and Arterial Plaque Characteristics. Circulation 2012, 126 (2), 172-181. DOI: 10.1161/circulationaha.112.096438.

[69]. Harris, N. R.; Carter, P. R.; Lee, S.; Watts, M. N.; Zhang, S.; Grisham, M. B. Association between blood flow and inflammatory state in a T-cell transfer model of inflammatory bowel disease in mice. Inflammatory Bowel Diseases 2010, 16 (5), 776-782. DOI: 10.1002/ibd.21126.

[70]. Cybulsky, M. I.; Marsden, P. A. Effect of Disturbed Blood Flow on Endothelial Cell Gene Expression. Arteriosclerosis, Thrombosis, and Vascular Biology 2014, 34 (9), 1806-1808. DOI: 10.1161/atvbaha.114.304099.

[71]. Samyn, M. M.; Ladisa, J. F. Novel Applications of Cardiovascular Magnetic Resonance Imaging-Based Computational Fluid Dynamics Modeling in Pediatric Cardiovascular and Congenital Heart Disease. InTech, 2016.

[72]. Tamargo, I. A.; Baek, K. I.; Kim, Y.; Park, C.; Jo, H. Flow-induced reprogramming of endothelial cells in atherosclerosis. Nat Rev Cardiol 2023, 1-16. DOI: 10.1038/s41569-023-00883-1.

[73]. Passerini, A. G.; Polacek, D. C.; Shi, C.; Francesco, N. M.; Manduchi, E.; Grant, G. R.; Pritchard, W. F.; Powell, S.; Chang, G. Y.; Stoeckert, C. J., Jr.; Davies, P. F. Coexisting proinflammatory and antioxidative endothelial transcription profiles in a disturbed flow region of the adult porcine aorta. Proc Natl Acad Sci U S A 2004, 101 (8), 2482-2487. DOI: 10.1073/pnas.0305938101.

[74]. Serbanovic-Canic, J.; de Luca, A.; Warboys, C.; Ferreira, P. F.; Luong, L. A.; Hsiao, S.; Gauci, I.; Mahmoud, M.; Feng, S.; Souilhol, C.; et al. Zebrafish Model for Functional Screening of Flow-Responsive Genes. Arterioscler Thromb Vasc Biol 2017, 37 (1), 130-143. DOI: 10.1161/atvbaha.116.308502.

[75]. Butcher, J. T.; Tressel, S.; Johnson, T.; Turner, D.; Sorescu, G.; Jo, H.; Nerem, R. M. Transcriptional profiles of valvular and vascular endothelial cells reveal phenotypic differences: influence of shear stress. Arterioscler Thromb Vasc Biol 2006, 26 (1), 69-77. DOI: 10.1161/01.ATV.0000196624.70507.0d.

[76]. Björck, H. M.; Renner, J.; Maleki, S.; Nilsson, S. F.; Kihlberg, J.; Folkersen, L.; Karlsson, M.; Ebbers, T.; Eriksson, P.; Länne, T. Characterization of shear-sensitive genes in the normal rat aorta identifies Hand2 as a major flow-responsive transcription factor. PLoS One 2012, 7 (12), e52227. DOI: 10.1371/journal.pone.0052227.

[77]. Dekker, R. J.; van Thienen, J. V.; Rohlena, J.; de Jager, S. C.; Elderkamp, Y. W.; Seppen, J.; de Vries, C. J.; Biessen, E. A.; van Berkel, T. J.; Pannekoek, H. Endothelial KLF2 links local arterial shear stress levels to the expression of vascular tone-regulating genes. The American journal of pathology 2005, 167 (2), 609-618.

[78]. van Thienen, J. V.; Fledderus, J. O.; Dekker, R. J.; Rohlena, J.; van Ijzendoorn, G. A.; Kootstra, N. A.; Pannekoek, H.; Horrevoets, A. J. Shear stress sustains atheroprotective endothelial KLF2 expression more potently than statins through mRNA stabilization. Cardiovasc Res 2006, 72 (2), 231-240. DOI: 10.1016/j.cardiores.2006.07.008.

[79]. Hamik, A.; Lin, Z.; Kumar, A.; Balcells, M.; Sinha, S.; Katz, J.; Feinberg, M. W.; Gerzsten, R. E.; Edelman, E. R.; Jain, M. K. Kruppel-like factor 4 regulates endothelial inflammation. J Biol Chem 2007, 282 (18), 13769-13779. DOI: 10.1074/jbc.M700078200.

[80]. Schrimpf, C.; Koppen, T.; Duffield, J. S.; Böer, U.; David, S.; Ziegler, W.; Haverich, A.; Teebken, O. E.; Wilhelmi, M. TIMP3 is Regulated by Pericytes upon Shear Stress Detection Leading to a Modified Endothelial Cell Response. Eur J Vasc Endovasc Surg 2017, 54 (4), 524-533. DOI: 10.1016/j.ejvs.2017.07.002.

[81]. Boo, Y. C.; Jo, H. Flow-dependent regulation of endothelial nitric oxide synthase: role of protein kinases. Am J Physiol Cell Physiol 2003, 285 (3), C499-508. DOI: 10.1152/ajpcell.00122.2003.

[82]. DeVerse, J. S.; Sandhu, A. S.; Mendoza, N.; Edwards, C. M.; Sun, C.; Simon, S. I.; Passerini, A. G. Shear stress modulates VCAM-1 expression in response to TNF-α and dietary lipids via interferon regulatory factor-1 in cultured endothelium. American Journal of Physiology-Heart and Circulatory Physiology 2013, 305 (8), H1149-H1157.

[83]. Magid, R.; Murphy, T. J.; Galis, Z. S. Expression of matrix metalloproteinase-9 in endothelial cells is differentially regulated by shear stress. Role of c-Myc. J Biol Chem 2003, 278 (35), 32994-32999. DOI: 10.1074/jbc.M304799200.

[84]. Sorescu, G. P.; Sykes, M.; Weiss, D.; Platt, M. O.; Saha, A.; Hwang, J.; Boyd, N.; Boo, Y. C.; Vega, J. D.; Taylor, W. R. Bone morphogenic protein 4 produced in endothelial cells by oscillatory shear stress stimulates an inflammatory response. Journal of Biological Chemistry 2003, 278 (33), 31128-31135.

[85]. Lu, Q.; Meng, Q.; Qi, M.; Li, F.; Liu, B. Shear-Sensitive lncRNA AF131217.1 Inhibits Inflammation in HUVECs via Regulation of KLF4. Hypertension 2019, 73 (5), e25-e34. DOI: 10.1161/hypertensionaha.118.12476.

[86]. Sun, X.; Feinberg, M. W. Regulation of endothelial cell metabolism: just go with the flow. Arterioscler Thromb Vasc Biol 2015, 35 (1), 13-15. DOI: 10.1161/atvbaha.114.304869.

[87]. Ni, C. W.; Qiu, H.; Rezvan, A.; Kwon, K.; Nam, D.; Son, D. J.; Visvader, J. E.; Jo, H. Discovery of novel mechanosensitive genes in vivo using mouse carotid artery endothelium exposed to disturbed flow. Blood 2010, 116 (15), e66-73. DOI: 10.1182/blood-2010-04-278192.

[88]. Sorescu, G. P.; Sykes, M.; Weiss, D.; Platt, M. O.; Saha, A.; Hwang, J.; Boyd, N.; Boo, Y. C.; Vega, J. D.; Taylor, W. R.; Jo, H. Bone morphogenic protein 4 produced in endothelial cells by oscillatory shear stress stimulates an inflammatory response. J Biol Chem 2003, 278 (33), 31128-31135. DOI: 10.1074/jbc.M300703200.

[89]. Chang, K.; Weiss, D.; Suo, J.; Vega, J. D.; Giddens, D.; Taylor, W. R.; Jo, H. Bone morphogenic protein antagonists are coexpressed with bone morphogenic protein 4 in endothelial cells exposed to unstable flow in vitro in mouse aortas and in human coronary arteries: role of bone morphogenic protein antagonists in inflammation and atherosclerosis. Circulation 2007, 116 (11), 1258-1266. DOI: 10.1161/circulationaha.106.683227.

[90]. Fledderus, J. O.; van Thienen, J. V.; Boon, R. A.; Dekker, R. J.; Rohlena, J.; Volger, O. L.; Bijnens, A. P.; Daemen, M. J.; Kuiper, J.; van Berkel, T. J.; et al. Prolonged shear

stress and KLF2 suppress constitutive proinflammatory transcription through inhibition of ATF2. Blood 2007, 109 (10), 4249-4257. DOI: 10.1182/blood-2006-07-036020.

[91]. Lee, J. S.; Yu, Q.; Shin, J. T.; Sebzda, E.; Bertozzi, C.; Chen, M.; Mericko, P.; Stadtfeld, M.; Zhou, D.; Cheng, L.; et al. Klf2 is an essential regulator of vascular hemodynamic forces in vivo. Dev Cell 2006, 11 (6), 845-857. DOI: 10.1016/j.devcel.2006.09.006.

[92]. Lin, Z.; Kumar, A.; SenBanerjee, S.; Staniszewski, K.; Parmar, K.; Vaughan, D. E.; Gimbrone, M. A., Jr.; Balasubramanian, V.; García-Cardeña, G.; Jain, M. K. Kruppel-like factor 2 (KLF2) regulates endothelial thrombotic function. Circ Res 2005, 96 (5), e48-57. DOI: 10.1161/01.RES.0000159707.05637.a1.

[93]. Huang, J.; Pu, Y.; Zhang, H.; Xie, L.; He, L.; Zhang, C. L.; Cheng, C. K.; Huo, Y.; Wan, S.; Chen, S.; et al. KLF2 Mediates the Suppressive Effect of Laminar Flow on Vascular Calcification by Inhibiting Endothelial BMP/SMAD1/5 Signaling. Circ Res 2021, 129 (4), e87-e100. DOI: 10.1161/circresaha.120.318690.

[94]. Chen, B. P.; Li, Y. S.; Zhao, Y.; Chen, K. D.; Li, S.; Lao, J.; Yuan, S.; Shyy, J. Y.; Chien, S. DNA microarray analysis of gene expression in endothelial cells in response to 24-h shear stress. Physiol Genomics 2001, 7 (1), 55-63. DOI: 10.1152/physiolgenomics.2001.7.1.55.

[95]. Feng, S.; Bowden, N.; Fragiadaki, M.; Souilhol, C.; Hsiao, S.; Mahmoud, M.; Allen, S.; Pirri, D.; Ayllon, B. T.; Akhtar, S.; et al. Mechanical Activation of Hypoxia-Inducible Factor 1α Drives Endothelial Dysfunction at Atheroprone Sites. Arterioscler Thromb Vasc Biol 2017, 37 (11), 2087-2101. DOI: 10.1161/atvbaha.117.309249.

[96]. Akhtar, S.; Hartmann, P.; Karshovska, E.; Rinderknecht, F. A.; Subramanian, P.; Gremse, F.; Grommes, J.; Jacobs, M.; Kiessling, F.; Weber, C.; et al. Endothelial Hypoxia-Inducible Factor-1α Promotes Atherosclerosis and Monocyte Recruitment by Upregulating MicroRNA-19a. Hypertension 2015, 66 (6), 1220-1226. DOI: 10.1161/hypertensionaha.115.05886.

[97]. Cooley, B. C.; Nevado, J.; Mellad, J.; Yang, D.; St Hilaire, C.; Negro, A.; Fang, F.; Chen, G.; San, H.; Walts, A. D.; et al. TGF-β signaling mediates endothelial-to-mesenchymal transition (EndMT) during vein graft remodeling. Sci Transl Med 2014, 6 (227), 227ra234. DOI: 10.1126/scitranslmed.3006927.

[98]. Gonzalez, D. M.; Medici, D. Signaling mechanisms of the epithelial-mesenchymal transition. Sci Signal 2014, 7 (344), re8. DOI: 10.1126/scisignal.2005189.

[99]. Mittal, M.; Siddiqui, M. R.; Tran, K.; Reddy, S. P.; Malik, A. B. Reactive oxygen species in inflammation and tissue injury. Antioxid Redox Signal 2014, 20 (7), 1126-1167. DOI: 10.1089/ars.2012.5149.

[100]. Schiffrin, E. L. Oxidative stress, nitric oxide synthase, and superoxide dismutase: a matter of imbalance underlies endothelial dysfunction in the human coronary circulation. Hypertension 2008, 51 (1), 31-32. DOI: 10.1161/hypertensionaha.107.103226.

[101]. Touyz, R. M.; Montezano, A. C. Vascular Nox4: a multifarious NADPH oxidase. Circ Res 2012, 110 (9), 1159-1161. DOI: 10.1161/circresaha.112.269068.

[102]. Yang, K. C.; Kyle, J. W.; Makielski, J. C.; Dudley, S. C., Jr. Mechanisms of sudden cardiac death: oxidants and metabolism. Circ Res 2015, 116 (12), 1937-1955. DOI: 10.1161/CIRCRESAHA.116.304691 Medline.

[103]. Eelen, G.; de Zeeuw, P.; Treps, L.; Harjes, U.; Wong, B. W.; Carmeliet, P. Endothelial cell metabolism. Physiological reviews 2018, 98 (1), 3-58.

[104]. De Bock, K.; Georgiadou, M.; Schoors, S.; Kuchnio, A.; Wong, B. W.; Cantelmo, A. R.; Quaegebeur, A.; Ghesquiere, B.; Cauwenberghs, S.; Eelen, G. Role of PFKFB3-driven glycolysis in vessel sprouting. Cell 2013, 154 (3), 651-663.

[105]. Schoors, S.; Bruning, U.; Missiaen, R.; Queiroz, K. C.; Borgers, G.; Elia, I.; Zecchin, A.; Cantelmo, A. R.; Christen, S.; Goveia, J. Fatty acid carbon is essential for dNTP synthesis in endothelial cells. Nature 2015, 520 (7546), 192-197.

[106]. Son, N.-H.; Basu, D.; Samovski, D.; Pietka, T. A.; Peche, V. S.; Willecke, F.; Fang, X.; Yu, S.-Q.; Scerbo, D.; Chang, H. R. Endothelial cell CD36 optimizes tissue fatty acid uptake. The Journal of clinical investigation 2018, 128 (10), 4329-4342.

[107]. Tabas, I.; Williams, K. J.; Borén, J. Subendothelial lipoprotein retention as the initiating process in atherosclerosis: update and therapeutic implications. Circulation 2007, 116 (16), 1832-1844. DOI: 10.1161/circulationaha.106.676890.

[108]. Filippini, A.; D'Alessio, A. Caveolae and Lipid Rafts in Endothelium: Valuable Organelles for Multiple Functions. Biomolecules 2020, 10 (9). DOI: 10.3390/biom10091218.

[109]. Pol, A.; Martin, S.; Fernandez, M. A.; Ingelmo-Torres, M.; Ferguson, C.; Enrich, C.; Parton, R. G. Cholesterol and fatty acids regulate dynamic caveolin trafficking through the Golgi complex and between the cell surface and lipid bodies. Mol Biol Cell 2005, 16 (4), 2091-2105. DOI: 10.1091/mbc.e04-08-0737.

[110]. Williams, P. T.; Superko, H. R.; Haskell, W. L.; Alderman, E. L.; Blanche, P. J.; Holl, L. G.; Krauss, R. M. Smallest LDL particles are most strongly related to coronary disease progression in men. Arterioscler Thromb Vasc Biol 2003, 23 (2), 314-321. DOI: 10.1161/01.atv.0000053385.64132.2d.

[111]. Komarova, Y. A.; Kruse, K.; Mehta, D.; Malik, A. B. Protein Interactions at Endothelial Junctions and Signaling Mechanisms Regulating Endothelial Permeability. Circ Res 2017, 120 (1), 179-206. DOI: 10.1161/circresaha.116.306534.

[112]. Armstrong, S. M.; Sugiyama, M. G.; Fung, K. Y.; Gao, Y.; Wang, C.; Levy, A. S.; Azizi, P.; Roufaiel, M.; Zhu, S. N.; Neculai, D.; et al. A novel assay uncovers an unexpected role for SR-BI in LDL transcytosis. Cardiovasc Res 2015, 108 (2), 268-277. DOI: 10.1093/cvr/cvv218.

[113]. Zhang, X.; Fernandez-Hernando, C. Transport of LDLs into the arterial wall: impact in atherosclerosis. Curr Opin Lipidol 2020, 31 (5), 279-285. DOI: 10.1097/MOL.0000000000000701 Medline.

[114]. Parton, R. G. Caveolae: Structure, Function, and Relationship to Disease. Annu Rev Cell Dev Biol 2018, 34, 111-136. DOI: 10.1146/annurev-cellbio-100617-062737.

[115]. Ramirez, C. M.; Zhang, X.; Bandyopadhyay, C.; Rotllan, N.; Sugiyama, M. G.; Aryal, B.; Liu, X.; He, S.; Kraehling, J. R.; Ulrich, V.; et al. Caveolin-1 Regulates Atherogenesis by Attenuating Low-Density Lipoprotein Transcytosis and Vascular Inflammation Independently of Endothelial Nitric Oxide Synthase Activation. Circulation 2019, 140 (3), 225-239. DOI: 10.1161/CIRCULATIONAHA.118.038571 Medline.

[116]. Zhang, X.; Ramírez, C. M.; Aryal, B.; Madrigal-Matute, J.; Liu, X.; Diaz, A.; Torrecilla-Parra, M.; Suárez, Y.; Cuervo, A. M.; Sessa, W. C.; Fernández-Hernando, C. Cav-1 (Caveolin-1) Deficiency Increases Autophagy in the Endothelium and Attenuates Vascular Inflammation and Atherosclerosis. Arterioscler Thromb Vasc Biol 2020, 40 (6), 1510-1522. DOI: 10.1161/atvbaha.120.314291.

[117]. Zhang, X.; Sessa, W. C.; Fernández-Hernando, C. Endothelial Transcytosis of Lipoproteins in Atherosclerosis. Front Cardiovasc Med 2018, 5, 130. DOI: 10.3389/fcvm.2018.00130.

[118]. Kraehling, J. R.; Chidlow, J. H.; Rajagopal, C.; Sugiyama, M. G.; Fowler, J. W.; Lee, M. Y.; Zhang, X.; Ramírez, C. M.; Park, E. J.; Tao, B. Genome-wide RNAi screen reveals ALK1 mediates LDL uptake and transcytosis in endothelial cells. Nature communications 2016, 7 (1), 13516.

[119]. Huang, L.; Chambliss, K. L.; Gao, X.; Yuhanna, I. S.; Behling-Kelly, E.; Bergaya, S.; Ahmed, M.; Michaely, P.; Luby-Phelps, K.; Darehshouri, A.; et al. SR-B1 drives endothelial cell LDL transcytosis via DOCK4 to promote atherosclerosis. Nature 2019, 569 (7757), 565-569. DOI: 10.1038/s41586-019-1140-4.

[120]. He, J.; Cui, Z.; Zhu, Y. The role of caveolae in endothelial dysfunction. Medical Review 2021, 1 (1), 78-91.

[121]. Lee, S.; Schleer, H.; Park, H.; Jang, E.; Boyer, M.; Tao, B.; Gamez-Mendez, A.; Singh, A.; Folta-Stogniew, E.; Zhang, X.; et al. Genetic or therapeutic neutralization of ALK1 reduces LDL transcytosis and atherosclerosis in mice. Nature Cardiovascular Research 2023, 2 (5), 438-448. DOI: 10.1038/s44161-023-00266-2.

[122]. Frühbeck, G.; Becerril, S.; Sáinz, N.; Garrastachu, P.; García-Velloso, M. J. BAT: a new target for human obesity? Trends in pharmacological sciences 2009, 30 (8), 387-396.

[123]. Cannon, B.; Nedergaard, J. Brown adipose tissue: function and physiological significance. Physiol Rev 2004, 84 (1), 277-359. DOI: 10.1152/physrev.00015.2003.

[124]. Wu, J.; Boström, P.; Sparks, L. M.; Ye, L.; Choi, J. H.; Giang, A. H.; Khandekar, M.; Virtanen, K. A.; Nuutila, P.; Schaart, G.; et al. Beige adipocytes are a distinct type of thermogenic fat cell in mouse and human. Cell 2012, 150 (2), 366-376. DOI: 10.1016/j.cell.2012.05.016.

[125]. Arner, P.; Bernard, S.; Salehpour, M.; Possnert, G.; Liebl, J.; Steier, P.; Buchholz, B. A.; Eriksson, M.; Arner, E.; Hauner, H.; et al. Dynamics of human adipose lipid turnover in health and metabolic disease. Nature 2011, 478 (7367), 110-113. DOI: 10.1038/nature10426.

[126]. Lee, M. K.; Lee, B.; Kim, C. Y. Natural Extracts That Stimulate Adipocyte Browning and Their Underlying Mechanisms. Antioxidants (Basel) 2021, 10 (2). DOI: 10.3390/antiox10020308.

[127]. Bartelt, A.; Bruns, O. T.; Reimer, R.; Hohenberg, H.; Ittrich, H.; Peldschus, K.; Kaul, M. G.; Tromsdorf, U. I.; Weller, H.; Waurisch, C.; et al. Brown adipose tissue activity controls triglyceride clearance. Nat Med 2011, 17 (2), 200-205. DOI: 10.1038/nm.2297.

[128]. Khedoe, P. P.; Hoeke, G.; Kooijman, S.; Dijk, W.; Buijs, J. T.; Kersten, S.; Havekes, L. M.; Hiemstra, P. S.; Berbée, J. F.; Boon, M. R.; Rensen, P. C. Brown adipose tissue takes up plasma triglycerides mostly after lipolysis. J Lipid Res 2015, 56 (1), 51-59. DOI: 10.1194/jlr.M052746.

[129]. Berbée, J. F.; Boon, M. R.; Khedoe, P. P.; Bartelt, A.; Schlein, C.; Worthmann, A.; Kooijman, S.; Hoeke, G.; Mol, I. M.; John, C.; et al. Brown fat activation reduces hypercholesterolaemia and protects from atherosclerosis development. Nat Commun 2015, 6, 6356. DOI: 10.1038/ncomms7356.

[130]. Yoneshiro, T.; Aita, S.; Matsushita, M.; Kayahara, T.; Kameya, T.; Kawai, Y.; Iwanaga, T.; Saito, M. Recruited brown adipose tissue as an antiobesity agent in humans. J Clin Invest 2013, 123 (8), 3404-3408. DOI: 10.1172/jci67803.

[131]. Young, S. G.; Fong, L. G.; Beigneux, A. P.; Allan, C. M.; He, C.; Jiang, H.; Nakajima, K.; Meiyappan, M.; Birrane, G.; Ploug, M. GPIHBP1 and lipoprotein lipase, partners in plasma triglyceride metabolism. Cell metabolism 2019, 30 (1), 51-65.

[132]. Fong, L. G.; Young, S. G.; Beigneux, A. P.; Bensadoun, A.; Oberer, M.; Jiang, H.; Ploug, M. GPIHBP1 and Plasma Triglyceride Metabolism. Trends Endocrinol Metab 2016, 27 (7), 455-469. DOI: 10.1016/j.tem.2016.04.013.

[133]. Beigneux, A. P.; Miyashita, K.; Ploug, M.; Blom, D. J.; Ai, M.; Linton, M. F.; Khovidhunkit, W.; Dufour, R.; Garg, A.; McMahon, M. A.; et al. Autoantibodies against GPIHBP1 as a Cause of Hypertriglyceridemia. N Engl J Med 2017, 376 (17), 1647-1658. DOI: 10.1056/NEJMoa1611930.

[134]. Finn, D. P.; Haroutounian, S.; Hohmann, A. G.; Krane, E.; Soliman, N.; Rice, A. S. Cannabinoids, the endocannabinoid system and pain: a review of preclinical studies. Pain 2021, 162 (Suppl 1), S5.

[135]. dos Santos, N. A.; Romão, W. Cannabis-a state of the art about the millenary plant: Part I. Forensic Chemistry 2023, 100470.

[136]. Pertwee, R. G. Pharmacology of cannabinoid CB1 and CB2 receptors. Pharmacology & therapeutics 1997, 74 (2), 129-180.

[137]. Di Marzo, V. Endocannabinoids: synthesis and degradation. Reviews of Physiology Biochemistry and Pharmacology 2008, 1-24.

[138]. Munro, S.; Thomas, K. L.; Abu-Shaar, M. Molecular characterization of a peripheral receptor for cannabinoids. Nature 1993, 365 (6441), 61-65.

[139]. Rajesh, M.; Bátkai, S.; Kechrid, M.; Mukhopadhyay, P.; Lee, W.-S.; Horváth, B.; Holovac, E.; Cinar, R.; Liaudet, L.; Mackie, K. Cannabinoid 1 receptor promotes cardiac dysfunction, oxidative stress, inflammation, and fibrosis in diabetic cardiomyopathy. Diabetes 2012, 61 (3), 716-727.

[140]. Mukhopadhyay, P.; Bátkai, S.; Rajesh, M.; Czifra, N.; Harvey-White, J.; Haskó, G.; Zsengeller, Z.; Gerard, N. P.; Liaudet, L.; Kunos, G. Pharmacological inhibition of CB1cannabinoid receptor protects against doxorubicin-induced cardiotoxicity. Journal of the American College of Cardiology 2007, 50 (6), 528-536.

[141]. Zhao, Y.; Yuan, Z.; Liu, Y.; Xue, J.; Tian, Y.; Liu, W.; Zhang, W.; Shen, Y.; Xu, W.; Liang, X. Activation of cannabinoid CB2 receptor ameliorates atherosclerosis associated with suppression of adhesion molecules. Journal of cardiovascular pharmacology 2010, 55 (3), 292-298.

[142]. Hoyer, F. F.; Steinmetz, M.; Zimmer, S.; Becker, A.; Lütjohann, D.; Buchalla, R.; Zimmer, A.; Nickenig, G. Atheroprotection via cannabinoid receptor-2 is mediated by circulating and vascular cells in vivo. Journal of molecular and cellular cardiology 2011, 51 (6), 1007-1014.

[143]. Guillamat-Prats, R.; Hering, D.; Derle, A.; Rami, M.; Härdtner, C.; Santovito, D.; Rinne, P.; Bindila, L.; Hristov, M.; Pagano, S. GPR55 in B cells limits atherosclerosis development and regulates plasma cell maturation. Nature cardiovascular research 2022, 1 (11), 1056-1071.

[144]. Morales, P.; Lago-Fernandez, A.; Hurst, D. P.; Sotudeh, N.; Brailoiu, E.; Reggio, P. H.; Abood, M. E.; Jagerovic, N. Therapeutic exploitation of GPR18: beyond the cannabinoids? Miniperspective. Journal of medicinal chemistry 2020, 63 (23), 14216-14227.

[145]. Qian, Y.; Wang, J.; Yang, L.; Liu, Y.; Wang, L.; Liu, W.; Lin, Y.; Yang, H.; Ma, L.; Ye, S. Activation and signaling mechanism revealed by GPR119-Gs complex structures. Nature Communications 2022, 13 (1), 7033.

[146]. Yien, R. M. K.; Gomes, A. C. C.; Goetze Fiorot, R.; Miranda, A. L. P.; Neves, G. A.; Andrade, B. d. S.; Costa, F. N.; Tributino, J. L. M.; Simas, N. K. Alkylamides from Acmella oleracea: Antinociceptive effect and molecular docking with cannabinoid and TRPV1 receptors. Natural Product Research 2023, 37 (18), 3136-3144.

[147]. Horn, H.; Böhme, B.; Dietrich, L.; Koch, M. Endocannabinoids in Body Weight Control. Pharmaceuticals (Basel) 2018, 11 (2). DOI: 10.3390/ph11020055.

[148]. Steffens, S.; Veillard, N. R.; Arnaud, C.; Pelli, G.; Burger, F.; Staub, C.; Karsak, M.; Zimmer, A.; Frossard, J. L.; Mach, F. Low dose oral cannabinoid therapy reduces progression of atherosclerosis in mice. Nature 2005, 434 (7034), 782-786. DOI: 10.1038/nature03389.

[149]. Zhao, Y.; Yuan, Z.; Liu, Y.; Xue, J.; Tian, Y.; Liu, W.; Zhang, W.; Shen, Y.; Xu, W.; Liang, X.; Chen, T. Activation of cannabinoid CB2 receptor ameliorates atherosclerosis associated with suppression of adhesion molecules. J Cardiovasc Pharmacol 2010, 55 (3), 292-298. DOI: 10.1097/FJC.0b013e3181d2644d.

[150]. Wei, T.-T.; Chandy, M.; Nishiga, M.; Zhang, A.; Kumar, K. K.; Thomas, D.; Manhas, A.; Rhee, S.; Justesen, J. M.; Chen, I. Y.; et al. Cannabinoid receptor 1 antagonist genistein attenuates marijuana-induced vascular inflammation. Cell 2022, 185 (10), 1676-1693.e1623. DOI: 10.1016/j.cell.2022.04.005.

[151]. Yang, L.; Tian, L.; Zhang, Z.; Zhou, X.; Ji, X.; Liu, F.; Dong, C.; Hou, L.; Zhao, X.; Chang, N.; et al. Cannabinoid Receptor 1/miR-30b-5p Axis Governs Macrophage NLRP3 Expression and Inflammasome Activation in Liver Inflammatory Disease. Molecular Therapy - Nucleic Acids 2020, 20, 725-738. DOI: 10.1016/j.omtn.2020.04.010.

[152]. Rorabaugh, B. R.; Guindon, J.; Morgan, D. J. Role of cannabinoid signaling in cardiovascular function and ischemic injury. Journal of Pharmacology and Experimental Therapeutics 2023, 387 (3), 265-276.

[153]. Greiner, B.; Sommerfeld, M.; Kintscher, U.; Unger, T.; Kappert, K.; Kaschina, E. Differential Regulation of MMPs, Apoptosis and Cell Proliferation by the Cannabinoid Receptors CB1 and CB2 in Vascular Smooth Muscle Cells and Cardiac Myocytes. Biomedicines 2022, 10 (12), 3271.

[154]. Malinowska, B.; Kwolek, G.; Göthert, M. Anandamide and methanandamide induce both vanilloid VR1- and cannabinoid CB1 receptor-mediated changes in heart rate and blood pressure in anaesthetized rats. Naunyn Schmiedebergs Arch Pharmacol 2001, 364 (6), 562-569. DOI: 10.1007/s00210-001-0498-6.

[155]. Rajesh, M.; Mukhopadhyay, P.; Haskó, G.; Liaudet, L.; Mackie, K.; Pacher, P. Cannabinoid-1 receptor activation induces reactive oxygen species-dependent and -independent mitogen-activated protein kinase activation and cell death in human coronary artery endothelial cells. Br J Pharmacol 2010, 160 (3), 688-700. DOI: 10.1111/j.1476-5381.2010.00712.x.

[156]. Mukhopadhyay, P.; Rajesh, M.; Batkai, S.; Patel, V.; Kashiwaya, Y.; Liaudet, L.; Evgenov, O. V.; Mackie, K.; Haskó, G.; Pacher, P. CB1 cannabinoid receptors promote oxidative stress and cell death in murine models of doxorubicin-induced cardiomyopathy and in human cardiomyocytes. Cardiovascular research 2010, 85 (4), 773-784.

[157]. Cappellano, G.; Uberti, F.; Caimmi, P. P.; Pietronave, S.; Mary, D. A.; Dianzani, C.; Micalizzi, E.; Melensi, M.; Boldorini, R.; Nicosia, G.; et al. Different expression and function of the endocannabinoid system in human epicardial adipose tissue in relation to heart disease. Can J Cardiol 2013, 29 (4), 499-509. DOI: 10.1016/j.cjca.2012.06.003.

[158]. Sugamura, K.; Sugiyama, S.; Nozaki, T.; Matsuzawa, Y.; Izumiya, Y.; Miyata, K.; Nakayama, M.; Kaikita, K.; Obata, T.; Takeya, M.; Ogawa, H. Activated endocannabinoid system in coronary artery disease and antiinflammatory effects of cannabinoid 1 receptor blockade on macrophages. Circulation 2009, 119 (1), 28-36. DOI: 10.1161/circulationaha.108.811992.

[159]. Ruiz de Azua, I.; Mancini, G.; Srivastava, R. K.; Rey, A. A.; Cardinal, P.; Tedesco, L.; Zingaretti, C. M.; Sassmann, A.; Quarta, C.; Schwitter, C.; et al. Adipocyte cannabinoid receptor CB1 regulates energy homeostasis and alternatively activated macrophages. J Clin Invest 2017, 127 (11), 4148-4162. DOI: 10.1172/jci83626.

[160]. Van Gaal, L. F.; Rissanen, A. M.; Scheen, A. J.; Ziegler, O.; Rössner, S. Effects of the cannabinoid-1 receptor blocker rimonabant on weight reduction and cardiovascular risk factors in overweight patients: 1-year experience from the RIO-Europe study. The Lancet 2005, 365 (9468), 1389-1397.

[161]. Després, J.-P.; Golay, A.; Sjöström, L. Effects of rimonabant on metabolic risk factors in overweight patients with dyslipidemia. New England Journal of Medicine 2005, 353 (20), 2121-2134.

[162]. Nissen, S. E.; Nicholls, S. J.; Wolski, K.; Rodés-Cabau, J.; Cannon, C. P.; Deanfield, J. E.; Després, J.-P.; Kastelein, J. J.; Steinhubl, S. R.; Kapadia, S. Effect of rimonabant on progression of atherosclerosis in patients with abdominal obesity and coronary artery disease: the STRADIVARIUS randomized controlled trial. Jama 2008, 299 (13), 1547-1560.

[163]. Henness, S.; Robinson, D. M.; Lyseng-Williamson, K. A. Rimonabant. Drugs 2006, 66 (16), 2109-2119. DOI: 10.2165/00003495-200666160-00006.

[164]. Dol-Gleizes, F.; Paumelle, R.; Visentin, V.; Marés, A. M.; Desitter, P.; Hennuyer, N.; Gilde, A.; Staels, B.; Schaeffer, P.; Bono, F. Rimonabant, a selective cannabinoid CB1 receptor antagonist, inhibits atherosclerosis in LDL receptor-deficient mice. Arterioscler Thromb Vasc Biol 2009, 29 (1), 12-18. DOI: 10.1161/atvbaha.108.168757.

[165]. Tiyerili, V.; Zimmer, S.; Jung, S.; Wassmann, K.; Naehle, C. P.; Lütjohann, D.; Zimmer, A.; Nickenig, G.; Wassmann, S. CB1 receptor inhibition leads to decreased vascular AT1 receptor expression, inhibition of oxidative stress and improved endothelial function. Basic Res Cardiol 2010, 105 (4), 465-477. DOI: 10.1007/s00395-010-0090-7.

[166]. Wang, Y.; Li, G.; Chen, B.; Shakir, G.; Volz, M.; Vorst, E. P. C. v. d.; Maas, S. L.; Li, Z.; Maegdefessel, L.; Hristov, M.; et al. Loss of myeloid cannabinoid CB1 receptor confers atheroprotection by reducing macrophage proliferation and immunometabolic reprogramming. bioRxiv 2023, 2023.2004.2006.535832. DOI: 10.1101/2023.04.06.535832.

[167]. Tam, J.; Cinar, R.; Liu, J.; Godlewski, G.; Wesley, D.; Jourdan, T.; Szanda, G.; Mukhopadhyay, B.; Chedester, L.; Liow, J. S.; et al. Peripheral cannabinoid-1 receptor inverse agonism reduces obesity by reversing leptin resistance. Cell Metab 2012, 16 (2), 167-179. DOI: 10.1016/j.cmet.2012.07.002.

[168]. Tam, J.; Vemuri, V. K.; Liu, J.; Bátkai, S.; Mukhopadhyay, B.; Godlewski, G.; Osei-Hyiaman, D.; Ohnuma, S.; Ambudkar, S. V.; Pickel, J.; et al. Peripheral CB1 cannabinoid receptor blockade improves cardiometabolic risk in mouse models of obesity. J Clin Invest 2010, 120 (8), 2953-2966. DOI: 10.1172/jci42551.

[169]. Marsicano, G.; Goodenough, S.; Monory, K.; Hermann, H.; Eder, M.; Cannich, A.; Azad, S. C.; Cascio, M. G.; Gutiérrez, S. O.; van der Stelt, M.; et al. CB1 cannabinoid receptors and on-demand defense against excitotoxicity. Science 2003, 302 (5642), 84-88. DOI: 10.1126/science.1088208.

[170]. Ehling, M.; Adams, S.; Benedito, R.; Adams, R. H. Notch controls retinal blood vessel maturation and quiescence. Development 2013, 140 (14), 3051-3061. DOI: 10.1242/dev.093351.

[171]. Tan, S.; Liu, H.; Ke, B.; Jiang, J.; Wu, B. The peripheral CB1 receptor antagonist JD5037 attenuates liver fibrosis via a CB1 receptor/β-arrestin1/Akt pathway. British journal of pharmacology 2020, 177 (12), 2830-2847.

[172]. Ishibashi, S.; Brown, M. S.; Goldstein, J. L.; Gerard, R. D.; Hammer, R. E.; Herz, J. Hypercholesterolemia in low density lipoprotein receptor knockout mice and its reversal by adenovirus-mediated gene delivery. The Journal of clinical investigation 1993, 92 (2), 883-893.

[173]. Chen, P. Y.; Qin, L.; Simons, M. Imaging and Analysis of Oil Red O-Stained Whole Aorta Lesions in an Aneurysm Hyperlipidemia Mouse Model. J Vis Exp 2022, (183). DOI: 10.3791/61277.

[174]. Ko, K. A.; Fujiwara, K.; Krishnan, S.; Abe, J. I. En Face Preparation of Mouse Blood Vessels. J Vis Exp 2017, (123). DOI: 10.3791/55460.

[175]. Natarelli, L.; Geißler, C.; Csaba, G.; Wei, Y.; Zhu, M.; di Francesco, A.; Hartmann, P.; Zimmer, R.; Schober, A. miR-103 promotes endothelial maladaptation by targeting lncWDR59. Nature communications 2018, 9 (1), 2645.

[176]. van der Vorst, E. P. C.; Maas, S. L.; Ortega-Gomez, A.; Hameleers, J. M. M.; Bianchini, M.; Asare, Y.; Soehnlein, O.; Döring, Y.; Weber, C.; Megens, R. T. A. Functional ex-vivo Imaging of Arterial Cellular Recruitment and Lipid Extravasation. Bio Protoc 2017, 7 (12). DOI: 10.21769/BioProtoc.2344.

[177]. Aldrich, J. L.; Long, D. S. In situ fixation and subsequent collection of cultured endothelial cells in a shear flow. MethodsX 2019, 6, 1164-1173.

[178]. Kang, S.-A.; Bajana, S.; Tanaka, T. In vitro flow adhesion assay for analyzing shear-resistant adhesion of metastatic cancer cells to endothelial cells. Bio-protocol 2016, 6 (4), e1731-e1731.

[179]. ibidi. Cell Culture Under Flow. ibidi Application Guide 2019.

[180]. Love, M.; Anders, S.; Huber, W. Differential analysis of count data–the DESeq2 package. Genome Biol 2014, 15 (550), 10-1186.

[181]. Love, M. I.; Huber, W.; Anders, S. Moderated estimation of fold change and dispersion for RNA-seq data with DESeq2. Genome biology 2014, 15 (12), 1-21.

[182]. Yu, G.; He, Q.-Y. ReactomePA: an R/Bioconductor package for reactome pathway analysis and visualization. Molecular BioSystems 2016, 12 (2), 477-479.

[183]. Keenan, A. B.; Torre, D.; Lachmann, A.; Leong, A. K.; Wojciechowicz, M. L.; Utti, V.; Jagodnik, K. M.; Kropiwnicki, E.; Wang, Z.; Ma'ayan, A. ChEA3: transcription factor enrichment analysis by orthogonal omics integration. Nucleic acids research 2019, 47 (W1), W212-W224.

[184]. Subramanian, A.; Tamayo, P.; Mootha, V. K.; Mukherjee, S.; Ebert, B. L.; Gillette, M. A.; Paulovich, A.; Pomeroy, S. L.; Golub, T. R.; Lander, E. S. Gene set enrichment analysis: a knowledge-based approach for interpreting genome-wide expression profiles. Proceedings of the National Academy of Sciences 2005, 102 (43), 15545-15550.

[185]. Luo, W.; Friedman, M. S.; Shedden, K.; Hankenson, K. D.; Woolf, P. J. GAGE: generally applicable gene set enrichment for pathway analysis. BMC bioinformatics 2009, 10, 1-17.

[186]. Davies, P. F. Hemodynamic shear stress and the endothelium in cardiovascular pathophysiology. Nat Clin Pract Cardiovasc Med 2009, 6 (1), 16-26. DOI: 10.1038/ncpcardio1397.

[187]. Ehling, M.; Adams, S.; Benedito, R.; Adams, R. H. Notch controls retinal blood vessel maturation and quiescence. Development 2013, 140 (14), 3051-3061.

[188]. Wang, F.; Wang, Z.; Pu, J.; Xie, X.; Gao, X.; Gu, Y.; Chen, S.; Zhang, J. Oscillating flow promotes inflammation through the TLR2–TAK1–IKK2 signalling pathway in human umbilical vein endothelial cell (HUVECs). Life sciences 2019, 224, 212-221.

[189]. Cockcroft, N. Y.; Oke, O.; Cunningham, F.; Bishop, E.; Fearon, I. M.; Zantl, R.; Gaça, M. D. An in vitro perfusion system to examine the responses of endothelial cells to simulated flow and inflammatory stimulation. Alternatives to Laboratory Animals 2009, 37 (6), 657-669.

[190]. Helmlinger, G.; Geiger, R.; Schreck, S.; Nerem, R. Effects of pulsatile flow on cultured vascular endothelial cell morphology. 1991.

[191]. Breen, L. T.; McHugh, P. E.; Murphy, B. P. HUVEC ICAM-1 and VCAM-1 synthesis in response to potentially athero-prone and athero-protective mechanical and nicotine chemical stimuli. Annals of biomedical engineering 2010, 38, 1880-1892.

[192]. Gomez, I.; Ward, B.; Souilhol, C.; Recarti, C.; Ariaans, M.; Johnston, J.; Burnett, A.; Mahmoud, M.; Luong, L. A.; West, L. Neutrophil microvesicles drive atherosclerosis by delivering miR-155 to atheroprone endothelium. Nature communications 2020, 11 (1), 214.

[193]. Wilhelm, D. L. Mechanisms responsible for increased vascular permeability in acute inflammation. Agents Actions 1973, 3 (5), 297-306. DOI: 10.1007/bf01986484.

[194]. Craps, S.; Van Wauwe, J.; De Moudt, S.; De Munck, D.; Leloup, A. J. A.; Boeckx, B.; Vervliet, T.; Dheedene, W.; Criem, N.; Geeroms, C.; et al. Prdm16 Supports Arterial Flow Recovery by Maintaining Endothelial Function. Circ Res 2021, 129 (1), 63-77. DOI: 10.1161/circresaha.120.318501.

[195]. Sager, H. B.; Dutta, P.; Dahlman, J. E.; Hulsmans, M.; Courties, G.; Sun, Y.; Heidt, T.; Vinegoni, C.; Borodovsky, A.; Fitzgerald, K. RNAi targeting multiple cell adhesion molecules reduces immune cell recruitment and vascular inflammation after myocardial infarction. Science translational medicine 2016, 8 (342), 342ra380-342ra380.

[196]. Ye, N.; Ding, Y.; Wild, C.; Shen, Q.; Zhou, J. Small molecule inhibitors targeting activator protein 1 (AP-1). J Med Chem 2014, 57 (16), 6930-6948. DOI: 10.1021/jm5004733.

[197]. Schnitzler, J. G.; Hoogeveen, R. M.; Ali, L.; Prange, K. H. M.; Waissi, F.; van Weeghel, M.; Bachmann, J. C.; Versloot, M.; Borrelli, M. J.; Yeang, C.; et al. Atherogenic Lipoprotein(a) Increases Vascular Glycolysis, Thereby Facilitating Inflammation and Leukocyte Extravasation. Circ Res 2020, 126 (10), 1346-1359. DOI: 10.1161/circresaha.119.316206.

[198]. Di Marzo, V.; Piscitelli, F.; Mechoulam, R. Cannabinoids and endocannabinoids in metabolic disorders with focus on diabetes. Handb Exp Pharmacol 2011, (203), 75-104. DOI: 10.1007/978-3-642-17214-4_4.

[199]. Zhang, L.; Keung, W.; Samokhvalov, V.; Wang, W.; Lopaschuk, G. D. Role of fatty acid uptake and fatty acid beta-oxidation in mediating insulin resistance in heart and skeletal muscle. Biochim Biophys Acta 2010, 1801 (1), 1-22. DOI: 10.1016/j.bbalip.2009.09.014.

[200]. Santibanez, J. F.; Blanco, F. J.; Garrido-Martin, E. M.; Sanz-Rodriguez, F.; Del Pozo, M. A.; Bernabeu, C. Caveolin-1 interacts and cooperates with the transforming growth factor-β type I receptor ALK1 in endothelial caveolae. Cardiovascular research 2008, 77 (4), 791-799.

[201]. Caza, M.; Kronstad, J. W. The cAMP/Protein Kinase a Pathway Regulates Virulence and Adaptation to Host Conditions in Cryptococcus neoformans. Front Cell Infect Microbiol 2019, 9, 212. DOI: 10.3389/fcimb.2019.00212.

[202]. Pacher, P.; Bátkai, S.; Kunos, G. The endocannabinoid system as an emerging target of pharmacotherapy. Pharmacol Rev 2006, 58 (3), 389-462. DOI: 10.1124/pr.58.3.2.

[203]. Pagano Zottola, A. C.; Severi, I.; Cannich, A.; Ciofi, P.; Cota, D.; Marsicano, G.; Giordano, A.; Bellocchio, L. Expression of Functional Cannabinoid Type-1 (CB(1)) Receptor in Mitochondria of White Adipocytes. Cells 2022, 11 (16). DOI: 10.3390/cells11162582.

[204]. Alonso, B.; Bartolomé-Martín, D.; Ferrero, J. J.; Ramírez-Franco, J.; Torres, M.; Sánchez-Prieto, J. CB 1 receptors down-regulate a cAMP/Epac2/PLC pathway to silence the nerve terminals of cerebellar granule cells. Journal of Neurochemistry 2017, 142 (3), 350-364.

[205]. Faussner, A.; Deininger, M. M.; Weber, C.; Steffens, S. Direct addition of poly-lysine or poly-ethylenimine to the medium: A simple alternative to plate pre-coating. PLOS ONE 2022, 17 (7), e0260173. DOI: 10.1371/journal.pone.0260173.

[206]. Engelman, J. A.; Zhang, X. L.; Razani, B.; Pestell, R. G.; Lisanti, M. P. p42/44 MAP Kinase-dependent and -independent Signaling Pathways Regulate Caveolin-1 Gene Expression. Journal of Biological Chemistry 1999, 274 (45), 32333-32341. DOI: 10.1074/jbc.274.45.32333.

[207]. Sassone-Corsi, P. The cyclic AMP pathway. Cold Spring Harb Perspect Biol 2012, 4 (12). DOI: 10.1101/cshperspect.a011148.

[208]. Cinar, R.; Iyer, M. R.; Kunos, G. The therapeutic potential of second and third generation CB(1)R antagonists. Pharmacol Ther 2020, 208, 107477. DOI: 10.1016/j.pharmthera.2020.107477.

[209]. Cinar, R.; Godlewski, G.; Liu, J.; Tam, J.; Jourdan, T.; Mukhopadhyay, B.; Harvey-White, J.; Kunos, G. Hepatic cannabinoid-1 receptors mediate diet-induced insulin resistance by increasingde novosynthesis of long-chain ceramides. Hepatology 2014, 59 (1), 143-153.

[210]. Bobryshev, Y. V.; Lord, R. S. Accumulation of co-localised unesterified cholesterol and neutral lipids within vacuolised elastin fibres in athero-prone areas of the human aorta. Atherosclerosis 1999, 142 (1), 121-131.

[211]. Pisanti, S.; Picardi, P.; Prota, L.; Proto, M. C.; Laezza, C.; McGuire, P. G.; Morbidelli, L.; Gazzerro, P.; Ziche, M.; Das, A.; Bifulco, M. Genetic and pharmacologic inactivation of cannabinoid CB1 receptor inhibits angiogenesis. Blood 2011, 117 (20), 5541-5550. DOI: 10.1182/blood-2010-09-307355.

[212]. Kim, Y.; Gautam, S.; Aseer, K. R.; Kim, J.; Chandrasekaran, P.; Mazucanti, C. H.; Ghosh, P.; O'Connell, J. F.; Doyle, M. E.; Appleton, A.; et al. Hepatocyte cannabinoid 1 receptor nullification alleviates toxin-induced liver damage via NF-κB signaling. Cell Death Dis 2020, 11 (12), 1044. DOI: 10.1038/s41419-020-03261-8.

[213]. Abumrad, N. A.; Cabodevilla, A. G.; Samovski, D.; Pietka, T.; Basu, D.; Goldberg, I. J. Endothelial Cell Receptors in Tissue Lipid Uptake and Metabolism. Circulation Research 2021, 128 (3), 433-450. DOI: 10.1161/circresaha.120.318003.

[214]. Trimm, E.; Red-Horse, K. Vascular endothelial cell development and diversity. Nat Rev Cardiol 2023, 20 (3), 197-210. DOI: 10.1038/s41569-022-00770-1.

[215]. Wang, L.; Luo, J. Y.; Li, B.; Tian, X. Y.; Chen, L. J.; Huang, Y.; Liu, J.; Deng, D.; Lau, C. W.; Wan, S.; et al. Integrin-YAP/TAZ-JNK cascade mediates atheroprotective effect of unidirectional shear flow. Nature 2016, 540 (7634), 579-582. DOI: 10.1038/nature20602.

[216]. Gong, X.; Zhao, X.; Li, B.; Sun, Y.; Liu, M.; Huang, Y.; Jia, X.; Ji, J.; Fan, Y. Quantitative Studies of Endothelial Cell Fibronectin and Filamentous Actin (F-Actin) Coalignment in Response to Shear Stress. Microsc Microanal 2017, 23 (5), 1013-1023. DOI: 10.1017/s1431927617012454.

[217]. Cao, J.; Schnittler, H. Putting VE-cadherin into JAIL for junction remodeling. J Cell Sci 2019, 132 (1). DOI: 10.1242/jcs.222893.

[218]. Sluiter, T. J.; van Buul, J. D.; Huveneers, S.; Quax, P. H. A.; de Vries, M. R. Endothelial Barrier Function and Leukocyte Transmigration in Atherosclerosis. Biomedicines 2021, 9 (4). DOI: 10.3390/biomedicines9040328.

[219]. Jaipersad, A. S.; Lip, G. Y.; Silverman, S.; Shantsila, E. The role of monocytes in angiogenesis and atherosclerosis. J Am Coll Cardiol 2014, 63 (1), 1-11. DOI: 10.1016/j.jacc.2013.09.019.

[220]. Ibsen, M. S.; Connor, M.; Glass, M. Cannabinoid CB1 and CB2 receptor signaling and bias. Cannabis and cannabinoid research 2017, 2 (1), 48-60.

[221]. Haddad, M. The Impact of CB1 Receptor on Inflammation in Skeletal Muscle Cells. J Inflamm Res 2021, 14, 3959-3967. DOI: 10.2147/jir.S322247.

[222]. Wei, T. T.; Chandy, M.; Nishiga, M.; Zhang, A.; Kumar, K. K.; Thomas, D.; Manhas, A.; Rhee, S.; Justesen, J. M.; Chen, I. Y.; et al. Cannabinoid receptor 1 antagonist genistein attenuates marijuana-induced vascular inflammation. Cell 2022, 185 (10), 1676-1693.e1623. DOI: 10.1016/j.cell.2022.04.005.

[223]. Jehle, J.; Eich, L.; Danisch, M.; Bagheri, S.; Avraamidou, E.; Pfeifer, P.; Tiyerili, V.; Bindila, L.; Lutz, B.; Nickenig, G. The endocannabinoid 2-arachidonoylglycerol inhibits endothelial function and repair. International Journal of Cardiology 2021, 323, 243-250.

[224]. Mehrpouya-Bahrami, P.; Chitrala, K. N.; Ganewatta, M. S.; Tang, C.; Murphy, E. A.; Enos, R. T.; Velazquez, K. T.; McCellan, J.; Nagarkatti, M.; Nagarkatti, P. Blockade of CB1 cannabinoid receptor alters gut microbiota and attenuates inflammation and diet-induced obesity. Sci Rep 2017, 7 (1), 15645. DOI: 10.1038/s41598-017-15154-6.

[225]. Gencer, S.; Döring, Y.; Jansen, Y.; Bayasgalan, S.; Yan, Y.; Bianchini, M.; Cimen, I.; Müller, M.; Peters, L. J. F.; Megens, R. T. A.; et al. Endothelial ACKR3 drives atherosclerosis by promoting immune cell adhesion to vascular endothelium. Basic Res Cardiol 2022, 117 (1), 30. DOI: 10.1007/s00395-022-00937-4.

[226]. Döring, Y.; van der Vorst, E. P. C.; Duchene, J.; Jansen, Y.; Gencer, S.; Bidzhekov, K.; Atzler, D.; Santovito, D.; Rader, D. J.; Saleheen, D.; Weber, C. CXCL12 Derived From Endothelial Cells Promotes Atherosclerosis to Drive Coronary Artery Disease. Circulation 2019, 139 (10), 1338-1340. DOI: 10.1161/circulationaha.118.037953.

[227]. Döring, Y.; Noels, H.; van der Vorst, E. P. C.; Neideck, C.; Egea, V.; Drechsler, M.; Mandl, M.; Pawig, L.; Jansen, Y.; Schröder, K.; et al. Vascular CXCR4 Limits Atherosclerosis by Maintaining Arterial Integrity: Evidence From Mouse and Human Studies. Circulation 2017, 136 (4), 388-403. DOI: 10.1161/circulationaha.117.027646.

[228]. Coon, B. G.; Timalsina, S.; Astone, M.; Zhuang, Z. W.; Fang, J.; Han, J.; Themen, J.; Chung, M.; Yang-Klingler, Y. J.; Jain, M.; et al. A mitochondrial contribution to anti-inflammatory shear stress signaling in vascular endothelial cells. J Cell Biol 2022, 221 (7). DOI: 10.1083/jcb.202109144.

[229]. Tedesco, L.; Valerio, A.; Cervino, C.; Cardile, A.; Pagano, C.; Vettor, R.; Pasquali, R.; Carruba, M. O.; Marsicano, G.; Lutz, B.; et al. Cannabinoid type 1 receptor blockade promotes mitochondrial biogenesis through endothelial nitric oxide synthase expression in white adipocytes. Diabetes 2008, 57 (8), 2028-2036. DOI: 10.2337/db07-1623.

[230]. Tedesco, L.; Valerio, A.; Dossena, M.; Cardile, A.; Ragni, M.; Pagano, C.; Pagotto, U.; Carruba, M. O.; Vettor, R.; Nisoli, E. Cannabinoid receptor stimulation impairs mitochondrial biogenesis in mouse white adipose tissue, muscle, and liver: the role of eNOS, p38 MAPK, and AMPK pathways. Diabetes 2010, 59 (11), 2826-2836. DOI: 10.2337/db09-1881.

[231]. Xu, J.; Xie, Z.; Reece, R.; Pimental, D.; Zou, M. H. Uncoupling of endothelial nitric oxidase synthase by hypochlorous acid: role of NAD(P)H oxidase-derived superoxide and peroxynitrite. Arterioscler Thromb Vasc Biol 2006, 26 (12), 2688-2695. DOI: 10.1161/01.Atv.0000249394.94588.82.

[232]. Gorelick, D. A.; Heishman, S. J.; Preston, K. L.; Nelson, R. A.; Moolchan, E. T.; Huestis, M. A. The cannabinoid CB1 receptor antagonist rimonabant attenuates the hypotensive effect of smoked marijuana in male smokers. Am Heart J 2006, 151 (3), 754.e751-754.e755. DOI: 10.1016/j.ahj.2005.11.006.

[233]. Pacher, P.; Bátkai, S.; Kunos, G. Cardiovascular Pharmacology of Cannabinoids. Springer-Verlag, pp 599-625.

[234]. Varga, K.; Lake, K. D.; Huangfu, D.; Guyenet, P. G.; Kunos, G. Mechanism of the hypotensive action of anandamide in anesthetized rats. Hypertension 1996, 28 (4), 682-686.

[235]. Niederhoffer, N.; Szabo, B. Effect of the cannabinoid receptor agonist WIN55212‐2 on sympathetic cardiovascular regulation. British journal of pharmacology 1999, 126 (2), 457-466.

[236]. Pacher, P.; Batkai, S.; Kunos, G. Cardiovascular pharmacology of cannabinoids. Cannabinoids 2005, 599-625.

[237]. Johns, D.; Behm, D.; Walker, D.; Ao, Z.; Shapland, E.; Daniels, D.; Riddick, M.; Dowell, S.; Staton, P.; Green, P. The novel endocannabinoid receptor GPR55 is activated by atypical cannabinoids but does not mediate their vasodilator effects. British journal of pharmacology 2007, 152 (5), 825-831.

[238]. Zygmunt, P. M.; Petersson, J.; Andersson, D. A.; Chuang, H.-h.; Sørgård, M.; Di Marzo, V.; Julius, D.; Högestätt, E. D. Vanilloid receptors on sensory nerves mediate the vasodilator action of anandamide. Nature 1999, 400 (6743), 452-457.

[239]. Bátkai, S.; Pacher, P.; Osei-Hyiaman, D.; Radaeva, S.; Liu, J.; Harvey-White, J.; Offertáler, L.; Mackie, K.; Rudd, M. A.; Bukoski, R. D. Endocannabinoids acting at cannabinoid-1 receptors regulate cardiovascular function in hypertension. Circulation 2004, 110 (14), 1996-2002.

[240]. Bátkai, S.; Pacher, P.; Járai, Z.; Wagner, J. A.; Kunos, G. Cannabinoid antagonist SR-141716 inhibits endotoxic hypotension by a cardiac mechanism not involving CB1 or CB2 receptors. American Journal of Physiology-Heart and Circulatory Physiology 2004, 287 (2), H595-H600.

[241]. Warty, V. S.; Calvo, W. J.; Berceli, S. A.; Pham, S. M.; Durham, S. J.; Tanksale, S. K.; Klein, E. C.; Herman, I. M.; Borovetz, H. S. Hemodynamics alter arterial low-density lipoprotein metabolism. J Vasc Surg 1989, 10 (4), 392-399. DOI: 10.1067/mva.1989.13732.

[242]. Sakai, J.; Karino, T.; Niwa, K. Flow-dependent accumulation of LDL in co-cultures of endothelial and smooth muscle cells in the presence of filtration flow through the cell layer. Clin Hemorheol Microcirc 2008, 38 (4), 245-256.

[243]. Matias, I.; Gonthier, M. P.; Orlando, P.; Martiadis, V.; De Petrocellis, L.; Cervino, C.; Petrosino, S.; Hoareau, L.; Festy, F.; Pasquali, R.; et al. Regulation, function, and dysregulation of endocannabinoids in models of adipose and beta-pancreatic cells and in obesity and hyperglycemia. J Clin Endocrinol Metab 2006, 91 (8), 3171-3180. DOI: 10.1210/jc.2005-2679.

[244]. Bátkai, S.; Járai, Z.; Wagner, J. A.; Goparaju, S. K.; Varga, K.; Liu, J.; Wang, L.; Mirshahi, F.; Khanolkar, A. D.; Makriyannis, A. Endocannabinoids acting at vascular CB1 receptors mediate the vasodilated state in advanced liver cirrhosis. Nature medicine 2001, 7 (7), 827-832.

[245]. Bátkai, S.; Pacher, P. Endocannabinoids and cardiac contractile function: pathophysiological implications. Pharmacol Res 2009, 60 (2), 99-106. DOI: 10.1016/j.phrs.2009.04.003.

[246]. Isaac, R.; Reis, F. C. G.; Ying, W.; Olefsky, J. M. Exosomes as mediators of intercellular crosstalk in metabolism. Cell Metab 2021, 33 (9), 1744-1762. DOI: 10.1016/j.cmet.2021.08.006.

[247]. Li, C. J.; Fang, Q. H.; Liu, M. L.; Lin, J. N. Current understanding of the role of Adipose-derived Extracellular Vesicles in Metabolic Homeostasis and Diseases: Communication from the distance between cells/tissues. Theranostics 2020, 10 (16), 7422-7435. DOI: 10.7150/thno.42167.

[248]. Monelli, E.; Villacampa, P.; Zabala-Letona, A.; Martinez-Romero, A.; Llena, J.; Beiroa, D.; Gouveia, L.; Chivite, I.; Zagmutt, S.; Gama-Perez, P.; et al. Angiocrine polyamine production regulates adiposity. Nat Metab 2022, 4 (3), 327-343. DOI: 10.1038/s42255-022-00544-6.

[249]. Rudnicki, M.; Haas, T. L. Adipose tissue lipolysis controlled by endothelial cells. Nat Rev Endocrinol 2022, 18 (7), 397-398. DOI: 10.1038/s41574-022-00695-2.

[250]. Paik, D. T.; Tian, L.; Williams, I. M.; Rhee, S.; Zhang, H.; Liu, C.; Mishra, R.; Wu, S. M.; Red-Horse, K.; Wu, J. C. Single-Cell RNA Sequencing Unveils Unique Transcriptomic Signatures of Organ-Specific Endothelial Cells. Circulation 2020, 142 (19), 1848-1862. DOI: 10.1161/circulationaha.119.041433.

[251]. Razani, B.; Combs, T. P.; Wang, X. B.; Frank, P. G.; Park, D. S.; Russell, R. G.; Li, M.; Tang, B.; Jelicks, L. A.; Scherer, P. E.; Lisanti, M. P. Caveolin-1-deficient mice are lean, resistant to diet-induced obesity, and show hypertriglyceridemia with adipocyte abnormalities. J Biol Chem 2002, 277 (10), 8635-8647. DOI: 10.1074/jbc.M110970200.

[252]. Fernández-Hernando, C.; Yu, J.; Suárez, Y.; Rahner, C.; Dávalos, A.; Lasunción, M. A.; Sessa, W. C. Genetic evidence supporting a critical role of endothelial caveolin-1 during the progression of atherosclerosis. Cell Metab 2009, 10 (1), 48-54. DOI: 10.1016/j.cmet.2009.06.003.

[253]. Bentzon, J. F.; Otsuka, F.; Virmani, R.; Falk, E. Mechanisms of plaque formation and rupture. Circ Res 2014, 114 (12), 1852-1866. DOI: 10.1161/circresaha.114.302721.

[254]. Fridolfsson, H. N.; Roth, D. M.; Insel, P. A.; Patel, H. H. Regulation of intracellular signaling and function by caveolin. Faseb j 2014, 28 (9), 3823-3831. DOI: 10.1096/fj.14-252320.

[255]. Yamamoto, M.; Okumura, S.; Oka, N.; Schwencke, C.; Ishikawa, Y. Downregulation of caveolin expression by cAMP signal. Life Sci 1999, 64 (15), 1349-1357. DOI: 10.1016/s0024-3205(99)00070-3.

[256]. Samak, G.; Narayanan, D.; Jaggar, J. H.; Rao, R. CaV1.3 channels and intracellular calcium mediate osmotic stress-induced N-terminal c-Jun kinase activation and disruption of tight junctions in Caco-2 CELL MONOLAYERS. J Biol Chem 2011, 286 (34), 30232-30243. DOI: 10.1074/jbc.M111.240358.

[257]. Rueda, D.; Galve-Roperh, I.; Haro, A.; Guzmán, M. The CB(1) cannabinoid receptor is coupled to the activation of c-Jun N-terminal kinase. Mol Pharmacol 2000, 58 (4), 814-820. DOI: 10.1124/mol.58.4.814.

[258]. Liu, J.; Gao, B.; Mirshahi, F.; Sanyal, A. J.; Khanolkar, A. D.; Makriyannis, A.; Kunos, G. Functional CB1 cannabinoid receptors in human vascular endothelial cells. Biochem J 2000, 346 Pt 3 (Pt 3), 835-840.

[259]. Bénard, G.; Massa, F.; Puente, N.; Lourenço, J.; Bellocchio, L.; Soria-Gómez, E.; Matias, I.; Delamarre, A.; Metna-Laurent, M.; Cannich, A.; et al. Mitochondrial CB_1 receptors regulate neuronal energy metabolism. Nat Neurosci 2012, 15 (4), 558-564. DOI: 10.1038/nn.3053.

[260]. Pavlides, S.; Gutierrez-Pajares, J. L.; Iturrieta, J.; Lisanti, M. P.; Frank, P. G. Endothelial caveolin-1 plays a major role in the development of atherosclerosis. Cell Tissue Res 2014, 356 (1), 147-157. DOI: 10.1007/s00441-013-1767-7.

[261]. Walker, O. L. S.; Holloway, A. C.; Raha, S. The role of the endocannabinoid system in female reproductive tissues. Journal of Ovarian Research 2019, 12 (1), 3. DOI: 10.1186/s13048-018-0478-9.

[262]. Rubino, T.; Parolaro, D. Sexually dimorphic effects of cannabinoid compounds on emotion and cognition. Front Behav Neurosci 2011, 5, 64. DOI: 10.3389/fnbeh.2011.00064.

8. ACKNOWLEDGEMENTS

"*The most incomprehensible thing about the world is that it is at all comprehensible.*"

- Albert Einstein

Time flies, I can hardly believe it, but this is the end of my doctorate. As the journey neared its close, time seemed to flutter away, leaving me with the opportunity to look back at this remarkable 4.5 years, a chapter filled with moments of challenges and profound value. At this moment, I would like to extend deep gratitude to the companions who have shared this path with me over the past few years.

First, I wish to express my gratitude to my supervisor, Prof. Dr. Sabine Steffens, who gave me this opportunity to join this excellent group at IPEK to explore lipid signalling in cardiovascular disease. The work could not have been done without her continuous support, guidance and advice. She always encourages us to present our research at conferences and actively engage in enlightening workshops, providing us with a conducive scholarly environment. Her passion for research and critical thinking has consistently influenced me, transforming me from a student into a passionate scientist. She has been more than just a supervisor; She has been a trusted mentor and a friend. Her approachability, patience, and genuine interest in my growth and well-being have made this journey not only productive but also enjoyable. I am truly fortunate to have had the opportunity to work with someone who not only provided invaluable professional guidance but also created a warm and encouraging atmosphere.

My special thanks go to Dr. Raquel Guillamat Prats, who not only imparted invaluable knowledge and techniques but also took the time to work side by side with me during experiments and skill-building. It is through her exceptional guidance, hands-on teaching, and friendship that I have grown both professionally and personally. Thank you, Raquel, for your remarkable mentorship and the friendship that has made my journey truly exceptional.

Many thanks to Prof. Dr. Stephan Herzig for his invaluable contribution as a member of my thesis advisory committee. His profound expertise in metabolic regulation and disorders has not only enriched my research but also provided me with profound inspiration for my future academic pursuits.

I extend my heartfelt appreciation to Prof. Dr. Alexander Faussner and Dr. Sarah-Lena Puhl, for their invaluable insights, expertise, and the memorable moments we shared at coffee breaks, team activities, and beer on Fridays... and Dr. Martina Rami for her kind guidance when I first arrived the lab. Each of them has left an indelible mark on my professional journey, and I am sincerely thankful for the profound influence they've had on my work and my life.

I would like to express my sincere gratitude to my fellow PhD students for their help on my project. I would like to thank Yong Wang, George Shakir, Anna Kaltenbach and Yi Xuan Shia for their unwavering helpfulness, encouragement, and significant contributions to various facets of this project. I extend my heartfelt appreciation to Guo Li for her pivotal role in conducting the bioinformatic analysis for this research. Special thanks to Aishvaryaa Prabhu, who has been involved in the project since her master's thesis study and has made significant contributions by providing essential data. She not only contributed to the project but also enriched our academic environment with her inquisitiveness and unwavering motivation.

Furthermore, I would like express my sincere gratitude to Dr. Lucia Natarelli for her contribution to the *in situ* hybridization experiment, Dr. Remco Megens for his continuous support and expertise in advanced microscopic imaging, and Dr. Xinyu Di for performing the endocannabinoid measurement.

I would also like to thank Srishti Ramanathan, Martina Geiger, Yvonne Jansen, Soyolmaa Bayasgalan, Diana Wagner, Silviya Wolkerstorfer, and Rodrigo Carrasco. Their expertise, hard work, and unwavering commitment to ensuring the smooth execution of experiments and data collection were instrumental. Without their invaluable contributions, this research would not have been possible. I am deeply grateful for their professionalism and support.

Furthermore, I would like to convey my sincere appreciation to Spela Barbic, Anna Polla, Emmanuel Sebastien, Marleen Stremlau and Emma Buller for their outstanding contributions during their internship in our team. I am confident that their experience in our lab has been a valuable part of their professional development, and I wish them all the best in their future endeavors.

I also really appreciate the China Scholarship Council (CSC) for providing funding throughout my doctoral studies, which made it possible for me to embark on and complete this research endeavor.

Last but not least, I would like to express my love and gratitude to my family, my friend Jin Yan, and especially my husband, Jian Wu. Their endless patience, encouragement, and unwavering belief in me have sustained me throughout this long and challenging process. To my dear grandparents, your love and wisdom have been a guiding light in my life, and I cherish the values and spirit you instilled in me.

I would like to end with the wise words of our former PhD student, Dr. Martina Rami:

„Wird es einfach sein? NEIN. Wird es das wert sein? ABSOLUT! “

Confirmation of congruency

LMU LUDWIG-MAXIMILIANS-UNIVERSITÄT MÜNCHEN

Promotionsbüro
Medizinische Fakultät

MMRS

Confirmation of congruency between printed and electronic version of the doctoral thesis

Chen Bingni

Surname, first name

Pettenkoferstraße 8a und 9, 80336 München,Germany

Address

I hereby declare, that the submitted thesis entitled:

Role of peripheral CB1 cannabinoid receptors in atherosclerosis and metabolism

is congruent with the printed version both in content and format.

München , 07.05.2024

Place, date

Bingni Chen

Signature doctoral candidate

LMU LUDWIG-MAXIMILIANS-UNIVERSITÄT MÜNCHEN

Promotionsbüro
Medizinische Fakultät

MMRS

Affidavit

Chen Bingni

Surname, first name

Pettenkoferstraße 8a und 9, 80336 München,Germany

Address

I hereby declare, that the submitted thesis entitled:

Role of peripheral CB1 cannabinoid receptors in atherosclerosis and metabolism

is my own work. I have only used the sources indicated and have not made unauthorised use of services of a third party. Where the work of others has been quoted or reproduced, the source is always given.
I further declare that the dissertation presented here has not been submitted in the same or similar form to any other institution for the purpose of obtaining an academic degree.

München , 07.05.2024

Place, date

Bingni Chen

Signature doctoral candidate